International Journal of Polymer Science

Chemicals, Materials, and Catalysts from Natural Renewable Lignocelluloses

Lead Guest Editor: Xiaofei Tian
Guest Editors: Zhibin He, Xuebing Zhao, and Shanghuan Feng

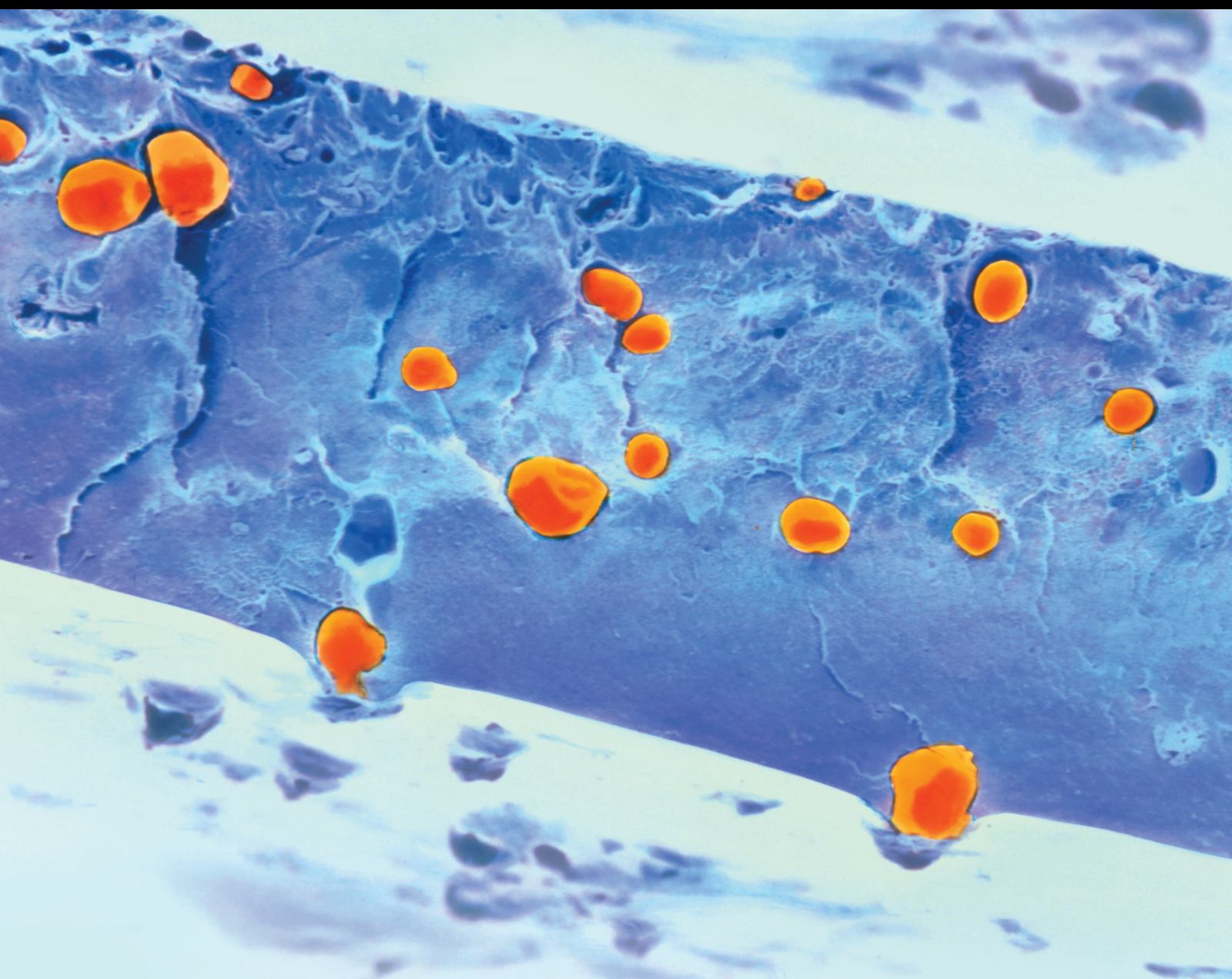

Chemicals, Materials, and Catalysts from Natural Renewable Lignocelluloses

International Journal of Polymer Science

Chemicals, Materials, and Catalysts from Natural Renewable Lignocelluloses

Lead Guest Editor: Xiaofei Tian
Guest Editors: Zhibin He, Xuebing Zhao, and Shanghuan Feng

Editorial Board

Contents

Hindawi
International Journal of Polymer Science
Volume 2018, Article ID 8742094, 2 pages
https://doi.org/10.1155/2018/8742094

Editorial

Chemicals, Materials, and Catalysts from Natural Renewable Lignocelluloses

Xiaofei Tian,[1] **Xuebing Zhao**,[2] **Zhibin He**,[3] **and Shanghuan Feng**[4]

[1]*School of Biology and Biological Engineering, South China University of Technology, Guangzhou 510006, China*
[2]*Department of Chemical Engineering, Tsinghua University, Beijing 100084, China*
[3]*Limerick Pulp and Paper Centre, University of New Brunswick, Fredericton, Canada E3B 5A3*
[4]*Department of Chemical and Biochemical Engineering, Faculty of Engineering, Western University, London, Canada N6A 3K7*

Correspondence should be addressed to Xiaofei Tian; xtien@scut.edu.cn

Received 13 August 2018; Accepted 13 August 2018; Published 2 September 2018

Lignocelluloses consist of the biopolymers of cellulose, hemicellulose, and lignin that form a natural structural matrix. Representing one of the most abundant renewable natural resources, the utilization of lignocelluloses does not necessarily impact the environment and land use. The substitution of traditional fossil resources by the three major biopolymers as sustainable feedstock has been extensively investigated for the manufacture of high value-added products including biofuels, commodity chemicals, biobased functional materials, and heterogeneous catalysts that could be directly applied for promoting the manufacturing processes. Effective separation and conversion techniques would play a significant role in economic viability of manufacturing these products from the lignocellulosic feedstock. Aiming at improving the conversion effectiveness or developing innovative techniques for new value-added products, this special issue was conceived for the collection of studies on state-of-art techniques developed specifically for producing chemicals, materials, and catalysts from the lignocellulosic feedstock.

In the natural source of cell walls, hemicellulose and lignin can be closely linked together in a homogeneous state to form the lignin-carbohydrate complexes (LCC). Recently, the great strength and good biocompatibility of the lignin composition, as well as the stimulation of the animal cell adsorption and growth by the containing galactose composition, were reported. In the study entitled "Lignin-Carbohydrate Complexes Based Spherical Biocarriers: Preparation, Characterization, and Biocompatibility," H. Zhao et al. prepared porous spherical carriers from the natural LCC isolated from the xylem of *Ginkgo biloba* L. with a high physical strength. Because it contains the galactose unit, the carriers are very biocompatible to human hepatocytes. It shows a good promise of the LCC to be introduced as a biomedical supporter in the tissue engineering.

Nanofibrillated celluloses (NFCs) are high value-added cellulosic materials for their high strength, high Young's modulus but low coefficient of thermal expansion and transparency. The NFCs were mechanically prepared from lignocellulosic biomass in the industry. However, the natural cellulose showed a strong resistance against the mechanical fibrillation. The low yield, high degradation, and low energy efficiency always challenge the current mechanical preparation of NFCs. In the study entitled "Ozone Oxidation of Kraft Bamboo Pulp for Preparation of Nanofibrillated Cellulose," M. Liu et al. developed a novel green approach for NFC production from the low-cost Kraft bamboo pulp. Results showed that the NFC product could be efficiently produce through the homogenization method combined with the advanced oxidation technique using ozone. The prepared NFC had a high aspect ratio of length (≥250 nm) versus width (10–20 nm). In the study entitled "Preparation and Characterization of Nanofibrillated Cellulose from Bamboo Fiber via Ultrasonication Assisted by Repulsive Effect," Z. Hu et al. reported an alternative process to efficiently isolate the NFCs from bamboo fiber using ultrasonic homogenization with the assistance of negatively charged entities. As the presence of the carboxyl groups attributed

to the ionic repulsion between the carboxylate groups of the cellulose chains, the number of carboxyl groups that had led to the addition of negative charge played a critical role in the dispersion of NFCs. Ultrasonic homogenization could contribute to a further augmentation of the surface charge by destroying the crystal structure of the cellulose composition.

Carbonaceous adsorbents derived from lignocellulosic biomass could be applied in removal of heavy metals from aqueous environments. In the study entitled "Valorizing Rice Straw and Its Anaerobically Digested Residues for Biochar to Remove Pb(II) from Aqueous Solution," both the rice straw and its anaerobically digested residues (ADR) were valorized to biochar through the pyrolysis approach. Results showed that the Pb(II) absorption capacities of biochar produced from the rice straw and its ADR at 500°C were 276.3 and 90.5 $mg \cdot g^{-1}$, respectively. Different adsorption mechanisms acted between the biochar produced from the two biomass resources. The biochar from the rice straw promised an efficient adsorbent for removal of the Pb(II) from aqueous solutions, in which the existence of the carbonates and carboxylates was considered to be responsible for the promoted adsorption efficiency.

Soybean straw is a renewable resource in agricultural byproducts. In the study entitled "Evaluation of Alkali-Pretreated Soybean Straw for Lignocellulosic Bioethanol Production," S. Kim tested the potential of the soybean straw to be used as the raw material for lignocellulosic bioethanol production. The results showed that the alkali-pretreatment with sodium hydroxide could remove the lignin and hemicellulose from the soybean straw effectively. The enzyme digestibility of the raw material was promoted leading an over 90% of the cellulose composition converted to fermentable sugars catalyzed by the commercial Cellic CTec2 enzyme cocktail. The ethanol yield was 0.305 g ethanol/g dry soybean straw through the simultaneous hydrolysis and fermentation process under the optimal condition. The ethanol productivity from soybean straw was greatly enhanced by the pretreatment using sodium hydroxide.

We hope all the work above in this special issue could provide useful information and shall technically contribute to further development of the biorefinery field.

Conflicts of Interest

The authors declare that they have no conflict of interest.

Acknowledgments

The editors sincerely appreciate all the authors and referees for their kind support and valuable contributions to this special issue.

Xiaofei Tian
Xuebing Zhao
Zhibin He
Shanghuan Feng

Hindawi
International Journal of Polymer Science
Volume 2018, Article ID 3452586, 7 pages
https://doi.org/10.1155/2018/3452586

Research Article

Ozone Oxidation of Kraft Bamboo Pulp for Preparation of Nanofibrillated Cellulose

Mingyou Liu,[1] Xia Chen,[1] and Xiaofei Tian[2,3]

[1]*School of Light Industry, South China University of Technology, Guangzhou 510006, China*
[2]*School of Biology and Biological Engineering, South China University of Technology, Guangzhou 510006, China*
[3]*Guangxi Key Laboratory of Clean Pulp & Papermaking and Pollution Control, College of Light Industry and Food Engineering, Guangxi University, Nanning 530004, China*

Correspondence should be addressed to Xiaofei Tian; xtien@scut.edu.cn

Received 9 March 2018; Revised 16 May 2018; Accepted 21 May 2018; Published 3 July 2018

Academic Editor: Marta Fernández-García

The influence of ozonation on the homogenization of Kraft bamboo pulp (KBP) for the production of nanofibrillated cellulose (NFC) was studied. Using optimized conditions for ozonation, that is, pulp consistency 35%, ozone dosage 0.87% (*v*/*w*), and pH = 2.5, the kappa number and viscosity of KBP decreased from 10.8 to 2.8 and from 1024 mL•g^{-1} to 258 mL•g^{-1}, respectively, while the crystallinity and carboxylate content increased from 36.2% to 48% and 0.93 mmol/g to 1.26 mmol/g, respectively. The ozonation-treated KPB was used as the substrate for NFC preparation through homogenization. With a width of 10–20 nm and length ≥ 250 nm, the prepared NFC had a high aspect ratio of length versus width. Ozonation can be used as an alternative approach to promote the efficient production of NFC from KBP.

1. Introduction

Cellulose is a natural, renewable material commonly used in the production of biocompatible or environmentally friendly product [1, 2]. It is also used as a low-cost filler for sustainable composite materials and, therefore, could be applied as a reinforcing element in polymer matrices [3]. In particular, bioderived, nanosized cellulose nanofillers have attracted great attention because they have a stronger reinforcing potential than individual cellulose fibers [4]. Nanofibrillated cellulose (NFC) is a common nanosized material for which at least one dimension is at the nanometer level. The diameters of NFC particles are usually below 100 nm. Furthermore, the high strength, high Young's modulus, low coefficient of thermal expansion, and transparency of NFC make it one of the most promising reinforcing elements to be used in a range of products.

NFC can be mechanically separated from woody biomass [5, 6]. The natural herbal fibers have a complex multilayer structure, which contributes to a complex aggregation of fibers. Moreover, there is a large extent of hydrogen bonding among the cellulose microfibrils. The natural cellulose material showed a strong resistance against mechanical fibrillation. Therefore, the mechanical preparation of NFC is a high-energy process that requires special equipment, which is not conducive to industrial production [7].

To improve the production efficiency of NFC, the raw materials are pretreated prior to mechanical shearing. Chemical pretreatment methods, including oxidation, acid hydrolysis, or organic solvent dissolution, are commonly applied to remove lignin and hemicellulose, to reduce the crystallinity of the cellulose, and to promote the hydrophilicity of the material. Besbes et al. [8] reported a TEMPO-(2,2,6,6-tetramethylpiperidine-1-oxyl radical-) mediated oxidation procedure, which assisted the defibrillation process by reducing the number of required passes and preventing the cellulose fibers from clogging in the homogenizer [9, 10]. Acid pretreatment is typically performed in a heated acidic solution (64% concentrated sulfuric acid) with ultrasound or mechanical stirring in order to hydrolyze

the cellulose fibers. Unfortunately, most chemical methods suffer from harsh reaction conditions and result in environmental pollution.

Ozone is a green oxidizing reagent that has been important in pulp bleaching because of its strong capacity for lignin removal. In addition, it could also efficiently perform ozonation (ozone oxidization) on the carbohydrate polymers in the fiber. While ozone is a strong oxidant, ozonation of cellulose leads to a minor oxidation reaction mostly at the C-6 position [11, 12]. The reaction could increase the number of negatively charged species on the fiber surface, similar to the TEMPO-mediated oxidation system, to promote fibrillation during the homogenization process. The ozonation could spur the development of new applications and markets for CNF with the advantages of low energy and low chemical requirement [13].

Bleached pulp from the pulping and paper industries has been extensively used as a raw material for the preparation of NFC [14, 15]. Although they are readily available and contain high-purity cellulose, bleached pulp and pure cellulose fibers are more expensive than unbleached pulp, especially when considering large-scale production. However, unbleached pulp has a high lignin content that should be removed from the fibers as much as possible before use. The retained fiber should also be broken down and turned into filaments before homogenization to avoid clogging the high-pressure homogenizer.

Considering the high efficiencies of delignification as well as good oxidizing selectivity, direct application of the ozonation method on the pretreatment of the unbleached Kraft pulp instead of pure cellulose fibers for the NFC preparation would be feasible. In this study, the effect of ozonation on the physical properties of Kraft bamboo pulp (KPB) for subsequent mechanical production of NFC was determined. The objective of this work is to demonstrate that the ozone oxidation could be applied in conjunction with mechanical homogenization for produce CNF from the Kraft pulps.

2. Experiments

2.1. Materials. The KBP sample was obtained from a local pulp mill (Sichuan, China). The kappa number, viscosity, and water consistency of the KBP were 10.1, 1024 mL•g^{-1}, and 33%, respectively. Before use, the KBP was activated via oxidation with oxygen at 100°C for 100 min. Then, 60 g (dry weight (DW)) of EKP was sealed in a 2 L reactor (Dawn Precision Instrument Co., Ltd, Shandong, China) with 700 mL of a solution containing 10% (*w*/*v*) NaOH, 1% (*w*/*v*) $MgSO_4$, and 30% (*v*/*v*) H_2O_2. The pressure in the reactor was 0.6 Mpa at 100°C.

2.2. NFC Preparation

2.2.1. PFI Refining. The KBP was adjusted to a 10% (*w*/*w*) oven-dried (OD) consistency with distilled water and dispersed evenly. According to QB/T 1463-2010, the pulp was loaded and mechanically sheared on a PFI refiner (Mark VI, Hamjern Maskin A/S, Hamar, Norway) for 1000 revolutions.

Table 1: Reaction conditions for the ozonation stage.

Condition	*A*	*Z*	*E*	*P*
Pulp consistency (*w*/*w*)	6.0	25–45	7.0	10
Temperature (°C)	60	RT	70	90
Time (min)	60	4–12	60	100
pH	NA	1.5–3.5	NA	NA
H_2SO_4 (*w*/*w*)	2.0	—	—	—
O_3 (*v*/*w*)	—	0.4–1.2	—	—
NaOH (*w*/*w*)	—	—	1.5	0.5
H_2O_2 (*w*/*w*)	—	—	—	2.5

RT: room temperature (25°C); NA: not available.

2.2.2. Ozonation. The ozonation process includes 4 stages: pretreatment with sulfuric acid (*A*), ozone oxidation (*Z*), alkali treatment with sodium hydroxide (*E*), and hydrogen peroxide treatment (*P*). Table 1 shows the reaction conditions applied in each of the 4 stages.

In the *A*, *E*, and *P* stages, the BKP was sealed in polyethylene bags and incubated at the designated temperature in a water bath. During the reaction, the BKP sample was mixed every 20 min by hand kneading the bags. After each stage of the reaction, the collected BKP samples were washed thoroughly with distilled water (5 times *w*/*v*) until the pH reached 7.

Before ozone oxidation, the washed pulp was dewatered and sealed in polyethylene bags for 12 h at room temperature to maintain consistent water content. Then, the sample was placed in a self-designed rotary reactor [16]. Ozone with a flow of 120 L/Nm^3 was pumped into a 2.5 L bleaching reactor through Teflon tubes at a flow rate of 800 mL/min. The ozone was produced by an ozone generator (KCF-SF100B, Koner, Jiangsu, China) using the compressed pure O_2 as the gas supply. The reactor was rotating at 60 r/min at 25°C.

2.2.3. Mechanical Homogenization. The disintegration of ozone-treated KBP pulp was performed using a high-pressure microfluidizer (Lab-scale, Nano DeBEE, USA) equipped with D5 and D10 nozzles. The KBP was dispersed in distilled water and diluted to a 0.1% (*w*/*w*) suspension. A 50 mL suspension was continuously homogenized for 3 times at 10,000 psi and then twice at 25,000 psi.

2.3. Characterization

2.3.1. Kappa Number and Viscosity. The kappa number and viscosity of the BKP were determined according to GB/T 1546-1989 and GB/T 1548-2016, respectively. The BKP sample that was collected after ozonation was recognized as the treated BKP.

2.3.2. Determination of the Degree of Crystallinity. The X-ray diffraction (XRD) patterns of the original and treated BKP were recorded using a Bruker X-ray diffractometer (D8 Advance, USA) equipped with Cu-Kα radiation ($\lambda = 0.154$ nm). The 2θ values were measured from 5° to 40° with a step

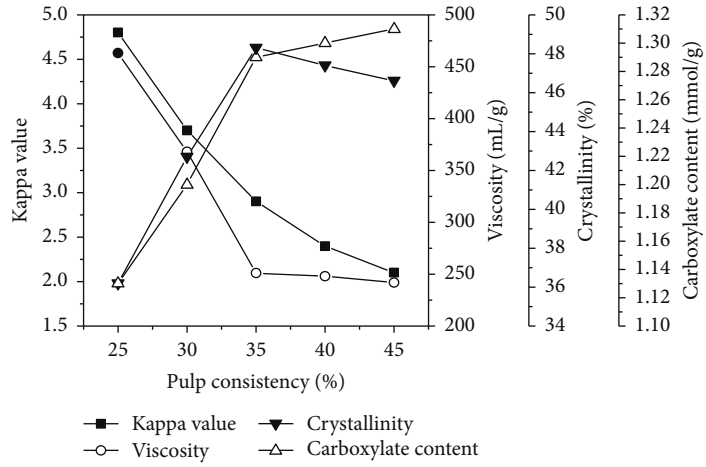

Figure 1: Effect of pulp consistency on kappa number, viscosity, crystallinity, and carboxylate content.

of 0.04° and 0.2 s. The crystallinity index (CrI) was calculated by formula [17] as follows:

$$\mathrm{Cr}\% = \left[\frac{I_{002} - I_{\mathrm{am}}}{I_{002}}\right] \times 100 \quad (1)$$

where I_{002} and I_{am} represent the intensity of the peaks that correlate to the 020 and $10\bar{1}$ lattice planes of cellulose I at 2 $\theta = 22.5°$ and 16.5°, respectively.

2.3.3. Carboxylate Content. The carboxylate content in BKP was determined using the conductometric-titration method. A 55 mL BKP suspension (0.55%, *w*/*w*) was prepared in deionized water. After adding 5 mL of 0.01 M NaCl, the pH was adjusted to 2.5 using 0.1 M HCl. The mixture was stirred well and titrated with 0.1 M NaOH. The total amount of carboxyl groups was calculated according to

$$C = \frac{(V_2 - V_1) \times C_{\mathrm{NaOH}}}{m}, \quad (2)$$

where C (mmol/g) is the carboxylate content, V_2 (mL) is the added volume of the NaOH solution when the titration curves reached their peak point, V_1 (mL) is the volume of HCl added to the mixture, C_{NaOH} (M) is the exact concentration of the NaOH solution, and m is the weight of the dried product (g).

2.3.4. Electron Microscopy. The surface of the treated BKP and the nanostructure of the NFC product were observed with a Carl Zeiss Evo 18 scanning electron microscope (SEM; Germany) and H-7650 HITACHI transmission electron microscope (TEM; Japan), respectively. Before observation, the treated BKP was freeze-dried and coated with a gold film. The NFC product was transferred into a 2 mL tube and centrifuged at 8000 r/min for 5 min using a centrifuge (Eppendorf Vertrieb GmbH, Germany). The liquid supernatant was diluted 50 times with distilled water, and 20 μL of the diluted supernatant was dropped on a copper sample disc and air dried. The SEM and TEM images were collected at an acceleration voltage of 5–15 kV and 150 kV, respectively.

Table 2: The relationship between the ozone dosage and treatment time.

Ozone dosage (%)	Time (min)
0.42	4
0.64	6
0.87	8
1.06	10
1.21	12

3. Results and Discussion

3.1. Ozonation of KBP. The selective oxidization of the hydroxymethyl groups on cellulose using a TEMPO-mediated system led to significant improvements in the efficiency of mechanical processing in the preparation of individual NFC suspensions [18–20], which suggests that a net increase in the negative surface charge of the nanofibers could facilitate mechanical peeling of the fibers. Ozone is a strong oxidant that could simultaneously react with the residual lignin and oxidize the groups, such as aromatic rings and -C=C- in the side chains, to improve the surface hydrophilicity of the fibers. In theory, ozone is a promising green reagent for pretreating unbleached pulp before the preparation of NFC; nevertheless, free radicals generated during ozonation could cause the degradation of the cellulose and carbohydrates. This potential problem can be combatted by controlling the intensity of the reaction.

In ozonation, pulp consistency, ozone consumption, and initial pH were considered as the key factors for an efficient oxidation process [21]. Their optimal levels were determined by single-factor experiments using the change in the KBP properties, that is, crystallinity, viscosity, kappa number, and carboxylate content, as the response factors.

3.1.1. Effect of Pulp Consistency. For the ozonation of high-consistency pulp, the optimal concentration of the pH and ozone dosage were 2-3 and 0.4–1.2%, respectively [22]. When the pulp consistency varied from 25% to 45%, the

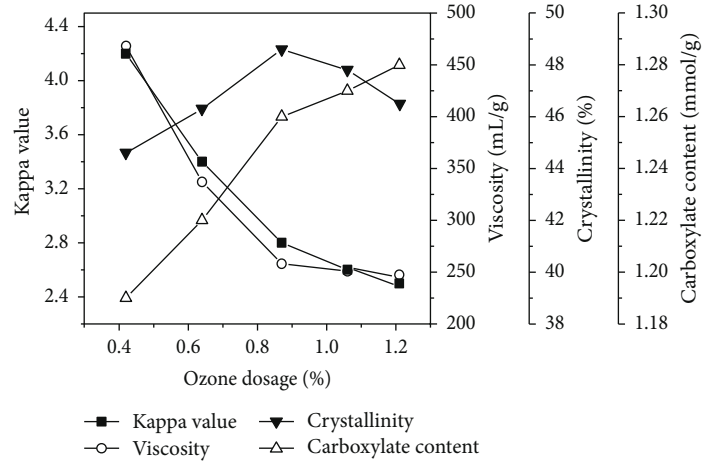

Figure 2: Effect of ozone dosage on kappa number, viscosity, crystallinity, and carboxylate content.

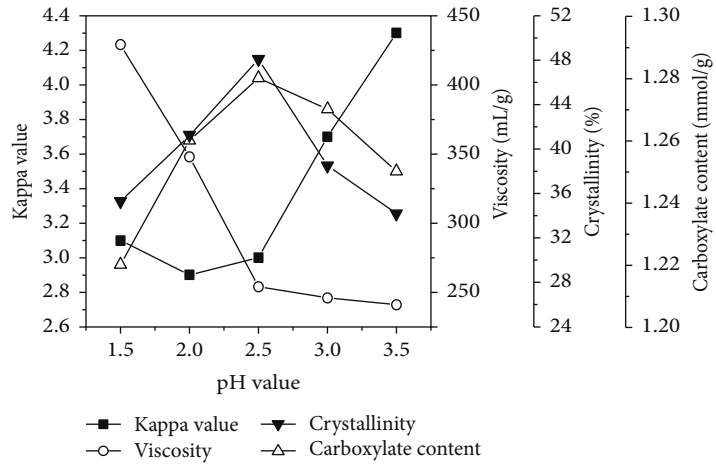

Figure 3: Effect of pH on kappa number, viscosity, crystallinity, and carboxylate content of the pulp.

Table 3: Change in the properties of the KBP.

	Original KBP	Treated KBP after ozonation
Kappa number	10.8	2.8
Viscosity ($mL \cdot g^{-1}$)	1024	258
Crystallinity degree (%)	36.2	48
Carboxylate content (mmol/g)	0.93	1.26

acquired experimental pH and ozone dosage were 2.5 and 0.87%, respectively.

Figure 1 shows the change in kappa number, viscosity, crystallinity, and carboxylate content for KBP when different pulp consistencies are used in the ozonation process. When the pulp consistency increased from 25% to 35%, the kappa number and viscosity decreased rapidly. This indicated accelerated delignification and degradation of the cellulose. Ozonation is recognized as a complex mass-transfer process including stages of both solid chemical absorption and gas-liquid mass transfer [23, 24]. Because ozone is nearly insoluble in water, the resistance of mass transfer was supposed to be generally dependent on the water film between the ozone and the surface of the BKP. With accelerated ozonation, the increased pulp consistency may have led to a thinner water film on the BKP. This is consistent with the measured increase in crystallinity and carboxylate content that was caused by the oxidization of the amorphous cellulose and hydroxyl groups, respectively. When the pulp consistency exceeded 35%, the rates of decrease in the Kappa number and viscosity, as well as the rate of increase in the carboxylate content, were slowed down. However, a decrease in crystallinity was observed. This indicated that the cellulose had an intense reaction with the ozone.

Based on these results, the critical level of pulp consistency for the ozonation reaction was 35%, and a 35% pulp consistency was applied to subsequent experiments.

3.1.2. Effect of Ozone Dosage. At a constant ozone composition (120 L/Nm^3) and gas flow rate (800 mL/min), the ozone dosage is mostly dependent on the amount of time the oxidation reaction is continued. In this experiment,

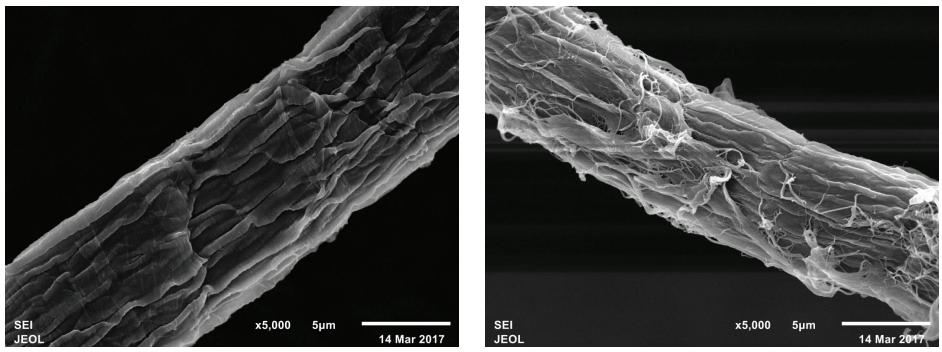

(a) (b)

Figure 4: The morphology of the BKP fiber and the prepared BKP fiber before (a) and after (b) ozonation.

different ozone dosages were applied in the ozonation process by controlling the reaction time (Table 2). The effect of the ozone dosage on the BKP properties was examined at pH = 2.5 and 35% pulp consistency.

As the ozone dosage increased, the kappa number and viscosity gradually decreased. The rate of decline decreased when the ozone dosage exceeded 0.87% (Figure 2). Conversely, the crystallinity and carboxylate content increased notably when the ozone dosage increased from 0.42% to 0.87%. When the ozone dosage was over 0.87%, the crystallinity started to decrease.

The reduction in the viscosity indicated the degradation of cellulose. This was correlated to the ozone-induced delignification reaction, which could generate a large number of free radicals. These free radicals could attack the chemical bonds within the carbohydrates and cause the degradation of cellulose in the BKP. Because the cellulose crystal structure is also impacted by the free radical attacks, the crystallinity of the cellulose decreased as the oxidation time increased. The increasing carboxylate content with increasing ozone dosage indicated the oxidation of hydroxyl groups to carboxyl groups by ozonation.

3.1.3. Effect of pH. The rate of ozone self-decomposition could be reduced by the proper H^+ concentration within the pulp. The effect of pH on the properties of the pulp was studied using a 35% pulp consistency and ozone dosage of 0.87%.

Figure 3 shows that the lowest kappa number and the highest crystallinity and carboxylate content were achieved when pH = 2.5. When pH < 2.5, the ozone decomposed less and the delignification rate increased, while the cellulose decomposition decreased. Higher pH led to lower viscosity but a higher kappa number, as intensive decomposition of the ozone could generate a large amount of hydroxyl radicals to oxidize the cellulose polymers. The overconsumption of ozone to produce hydroxyl radicals had a negative effect on delignification.

3.1.4. Preparation of the Substrate for NFC Production via Ozonation. Using the optimized conditions (35% pulp consistency, pH = 2.5, and ozone dosage of 0.87%), ozonation of the KBP was performed. After the ozonation, the kappa number and the viscosity of the KBP decreased by 74.1% and 74.8%, respectively, while the crystallinity and carboxylate content increased by 32.6% and 35.5%, respectively (Table 3). The size of the BKP fibers was not dramatically changed by the ozonation treatment and had an average diameter of 10 μm (Figures 4(a) and 4(b)). However, the distinct microfiber structure on the surface of the BKP fibers became less obvious due to the formation of fibrils and fragments.

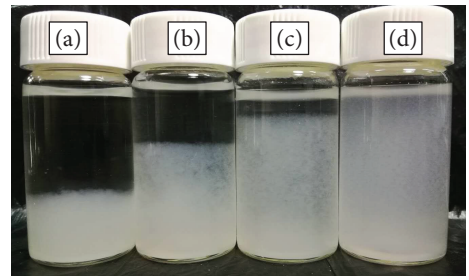

Figure 5: Appearance of the NFC product after standing still for 24 h. Samples before (a) and after 1 (b), 3 (c), and 5 (d) passes through the microfluidizer.

3.2. Defibrillation of the KBP and the NFC Morphology. The treated KBP was then homogenized for NFC production. The treated KBP could smoothly pass through the microfluidizer, and a suspension of the NFC product was stably suspended after 5 cycles (Figure 5). In contrast, the untreated KBP seriously clogged the nozzles of the microfluidizer, which caused the NFC preparation to fail. The prepared NFC from the visible suspension from the 5-cycle homogenization was observed using TEM (Figures 6(a) and 6(b)). The TEM images of the isolated NFC showed widths of 10–20 nm and lengths up to 250 nm. The high aspect ratio of the prepared NFC is consistent with the literature [25].

Ozone is an oxidizing agent with high oxidation potential. The ozonation treatment of KBP promoted fibrillation, which was advantageous for the preparation of NFC. This improved fibrillation can be explained by the decreased lignin composition and increased negative surface charge on the fibers. The ozone-induced delignification occurred via an electrophilic substitution reaction on the lignin units or

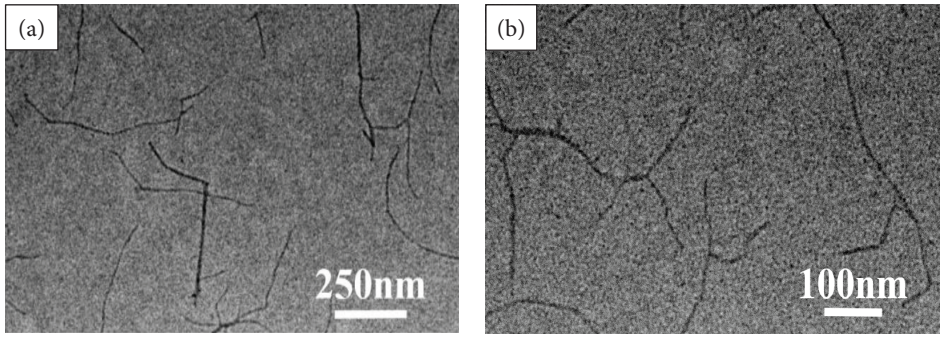

(a) (b)

Figure 6: Appearance of the NFC with the scale bar of 250 nm (a) and 100 nm (b).

side chains [26, 27]. Free radical reactions induced by the decomposition of ozone and lignin self-ozonation could also contribute to the improved delignification. Ozone could also enhance the hydrophilicity of the fibers, which may prevent the reformation of hydrogen bonds during mechanical defibrillation. In this study, ozone treatment of pulp had a similar effect as acid hydrolysis or TEMPO-mediated oxidation; however, the ozonation method is essentially free of environmental pollutants. The combination of ozone oxidation and high-pressure homogenization is an effective way to prepare nanocellulose.

4. Conclusion

NFC was successfully prepared from unbleached KBP using the combination of ozonation and high-pressure homogenization. The pulp consistency, pH value, and ozone dosage are important parameters in the ozonation of KBP. The ozonation treatment enabled the fibrillation of the KBP for the efficient preparation of NFC. The obtained NFC nanoparticles had a high aspect ratio.

Data Availability

The authors declare that all the supporting data for the results have been included in the submission.

Conflicts of Interest

The authors declare that they have no conflicts of interest.

Acknowledgments

The authors acknowledge the financial support of the National Science Foundation of China (31741023); Natural Science Foundation of Guangdong Province, China (2017A030310078); and Fundamental Research Funds for the Central Universities (D2172840) as well as the Opening Project of the Guangxi Key Laboratory of Clean Pulp & Papermaking and Pollution Control (KF201603).

References

[1] K. L. Tovar-Carrillo, M. Tagaya, and T. Kobayashi, "Biohydrogels interpenetrated with hydroxyethyl cellulose and wooden pulp for biocompatible materials," *Industrial & Engineering Chemistry Research*, vol. 53, no. 12, pp. 4650–4659, 2014.

[2] A. H. Basta, H. El-Saied, and V. F. Lotfy, "Performance of rice straw-based composites using environmentally friendly polyalcoholic polymers-based adhesive system," *Pigment & Resin Technology*, vol. 42, no. 1, pp. 24–33, 2013.

[3] J. Pang, X. Liu, X. Zhang, Y. Wu, and R. Sun, "Fabrication of cellulose film with enhanced mechanical properties in ionic liquid 1-allyl-3-methylimidaxolium chloride (AmimCl)," *Materials*, vol. 6, no. 4, pp. 1270–1284, 2013.

[4] S. K. Rahimi and J. U. Otaigbe, "Polyamide 6 nanocomposites incorporating cellulose nanocrystals prepared by *in situ* ring-opening polymerization: viscoelasticity, creep behavior, and melt rheological properties," *Polymer Engineering and Science*, vol. 56, no. 9, pp. 1045–1060, 2016.

[5] F. W. Herrick, R. L. Casebier, J. K. Hamilton, and K. R. Sandberg, "Microfibrillated cellulose: morphology and accessibility," *Journal of Applied Polymer Science: Applied Polymer Symposium*, vol. 37, pp. 797–813, 1983.

[6] A. F. Turbak, F. W. Snyder, and K. R. Sanberg, "Microfibrillated cellulose, a new cellulose product: properties, uses and commercial potential," *Journal of Applied Polymer Science: Applied Polymer Symposium*, vol. 37, pp. 815–827, 1983.

[7] I. Fatah, H. Khalil, M. Hossain et al., "Exploration of a chemo-mechanical technique for the isolation of nanofibrillated cellulosic fiber from oil palm empty fruit bunch as a reinforcing agent in composites materials," *Polymer*, vol. 6, no. 10, pp. 2611–2624, 2014.

[8] I. Besbes, S. Alila, and S. Boufi, "Nanofibrillated cellulose from TEMPO-oxidized eucalyptus fibres: effect of the carboxyl content," *Carbohydrate Polymers*, vol. 84, no. 3, pp. 975–983, 2011.

[9] W. Bai, J. Holbery, and K. Li, "A technique for production of nanocrystalline cellulose with a narrow size distribution," *Cellulose*, vol. 16, no. 3, pp. 455–465, 2009.

[10] P. Podsiadlo, S. Y. Choi, B. Shim, J. Lee, M. Cuddihy, and N. A. Kotov, "Molecularly engineered nanocomposites: layer-by-layer assembly of cellulose nanocrystals," *Biomacromolecules*, vol. 6, no. 6, pp. 2914–2918, 2005.

[11] K. Kato, V. N. Vasilets, M. N. Fursa, M. Meguro, Y. Ikada, and K. Nakamae, "Surface oxidation of cellulose fibers by vacuum

ultraviolet irradiation," *Journal of Polymer Science Part A: Polymer Chemistry*, vol. 37, no. 3, pp. 357–361, 1999.

[12] S. Lemeune, H. Jameel, H. M. Chang, and J. F. Kadla, "Effects of ozone and chlorine dioxide on the chemical properties of cellulose fibers," *Journal of Applied Polymer Science*, vol. 93, no. 3, pp. 1219–1223, 2004.

[13] I. B. Tabar, X. Zhang, J. P. Youngblood, and N. S. Mosier, "Production of cellulose nanofibers using phenolic enhanced surface oxidation," *Carbohydrate Polymers*, vol. 174, pp. 120–127, 2017.

[14] J. Zhang, H. Song, L. Lin, J. Zhuang, C. Pang, and S. Liu, "Microfibrillated cellulose from bamboo pulp and its properties," *Biomass & Bioenergy*, vol. 39, no. 8, pp. 78–83, 2012.

[15] N. Siddiqui, R. H. Mills, D. J. Gardner et al., "Production and characterization of cellulose nanofibers from wood pulp," *Journal of Science and Technology*, vol. 25, no. 6-7, pp. 709–721, 2011.

[16] T. He, M. Y. Liu, and X. Tian, "Kinetics of ozone bleaching of eucalyptus kraft pulp and factors affecting the properties of the bleached pulp," *BioResources*, vol. 13, no. 1, pp. 425–436, 2018.

[17] L. Segal, J. J. Creely, A. E. Martin Jr, and C. M. Conrad, "An empirical method for estimating the degree of crystallinity of native cellulose using the X-ray diffractometer," *Textile Research Journal*, vol. 29, no. 10, pp. 786–794, 1959.

[18] F. Bettaieb, O. Nechyporchuk, R. Khiari, M. F. Mhenni, A. Dufresne, and M. N. Belgacem, "Effect of the oxidation treatment on the production of cellulose nanofiber suspensions from Posidonia oceanica: the rheological aspect," *Carbohydrate Polymers*, vol. 134, pp. 664–672, 2015.

[19] A. Ämmälä, H. Liimatainen, C. Burmeister, and J. Niinimäki, "Effect of tempo and periodate-chlorite oxidized nanofibrils on ground calcium carbonate flocculation and retention in sheet forming and on the physical properties of sheets," *Cellulose*, vol. 20, no. 5, pp. 2451–2460, 2013.

[20] T. Saito, M. Hirota, N. Tamura et al., "Individualization of nano-sized plant cellulose fibrils by direct surface carboxylation using TEMPO catalyst under neutral conditions," *Biomacromolecules*, vol. 10, no. 7, pp. 1992–1996, 2009.

[21] N. Yaqoob, K. Stack, and K. L. Nguyen, "TCF bleaching of eucalypt kraft pulp with oxone," *Appita Journal*, vol. 63, no. 5, pp. 381–386, 2010.

[22] M. B. Roncero, M. A. Queral, J. F. Colom, and T. Vidal, "Why acid pH increases the selectivity of the ozone bleaching processes," *Ozone Science & Engineering*, vol. 25, no. 6, pp. 523–534, 2003.

[23] S. Perincek, M. İ. Bahtiyari, A. E. Körlü, and K. Duran, "Ozone bleaching of jute fabrics," *AATCC Review*, vol. 7, no. 3, pp. 34–39, 2007.

[24] A. Seisto, K. Poppius-Levlin, and A. Fuhrmann, "Effect of ozone bleaching on the fibre properties of pine and birch kraft pulp," *Cellulosic Pulps, Fibres and Materials*, pp. 137–147, 2000.

[25] J. Xu, L. Tan, S. A. Baig, D. Wu, X. Lv, and X. Xu, "Dechlorination of 2,4-dichlorophenol by nanoscale magnetic Pd/Fe particles: effects of pH, temperature, common dissolved ions and humic acid," *Chemical Engineering Journal*, vol. 231, no. 17, pp. 26–35, 2013.

[26] E. Gilli, F. Schmied, S. Diebald, A. T. Horvath, C. Teichert, and R. Schennach, "Analysis of lignin precipitates on ozone treated kraft pulp by FTIR and AFM," *Cellulose*, vol. 19, no. 1, pp. 249–256, 2012.

[27] A. N. Mitrofanova, A. G. Khudoshin, and V. V. Lunin, "The ozonization of model lignin compounds in aqueous solutions catalyzed by Mn(II) ions," *Russian Journal of Physical Chemistry A*, vol. 84, no. 7, pp. 1141–1146, 2010.

Hindawi
International Journal of Polymer Science
Volume 2018, Article ID 5241748, 7 pages
https://doi.org/10.1155/2018/5241748

Research Article

Evaluation of Alkali-Pretreated Soybean Straw for Lignocellulosic Bioethanol Production

Seonghun Kim

Jeonbuk Branch Institute, Korea Research Institute of Bioscience and Biotechnology, 181 Ipsin-gil, Jeongeup 56212, Republic of Korea

Correspondence should be addressed to Seonghun Kim; seonghun@kribb.re.kr

Received 17 December 2017; Revised 27 February 2018; Accepted 18 March 2018; Published 3 May 2018

Academic Editor: Xuebing Zhao

Soybean straw is a renewable resource in agricultural residues that can be used for lignocellulosic bioethanol production. To enhance enzymatic digestibility and fermentability, the biomass was prepared with an alkali-thermal pretreatment (sodium hydroxide, 121°C, 60 min). The delignification yield was 34.1~53%, in proportion to the amount of sodium hydroxide, from 0.5 to 3.0 M. The lignin and hemicellulose contents of the pretreated biomass were reduced by the pretreatment process, whereas the proportion of cellulose was increased. Under optimal condition, the pretreated biomass consisted of 74.0 ± 0.1% cellulose, 10.3 ± 0.1% hemicellulose, and 10.1 ± 0.6% lignin. During enzymatic saccharification using Cellic® CTec2 cellulase, 10% (w/v) of pretreated soybean straw was hydrolyzed completely and converted to 67.3 ± 2.1 g/L glucose and 9.4 ± 0.5 g/L xylose with a 90.9% yield efficiency. Simultaneous saccharification and fermentation of the pretreated biomass by *Saccharomyces cerevisiae* W303-1A produced 30.5 ± 1.2 g/L ethanol in 0.5 L fermented medium containing 10% (w/v) pretreated biomass after 72 h. The ethanol productivity was 0.305 g ethanol/g dry biomass and 0.45 g ethanol/g glucose after fermentation, with a low concentration of organic acid metabolites. Also, 82% of fermentable sugar was used by the yeast for ethanol fermentation. These results show that the combination of alkaline pretreatment and biomass hydrolysate is useful for enhancing bioethanol productivity using delignified soybean straw.

1. Introduction

The soybean (*Glycine max* L. Merr.) is an annual herbaceous plant in the species of legumes that originated in East Asia (including China, Japan, and Korea), widely grown for its edible bean as an important food resource. During soybean harvesting, the stalks, the husks, and the dry leaves remain as the agricultural residues. In Korean traditional agriculture farming, the dry leaves had been traditionally used as cattle feedstock, but the rest of residues had been consumed as biomass fuel for heating. However, the modern agriculture farm does not use these agricultural residues anymore and abandon the large volumes of the biomass [1].

Nevertheless, soybean straw, the residual part, has the potential to serve an inexpensive feedstock for the production of fermentable sugars, instead of food sources, such as corn, sugar cane, and other food stocks, for the production of bioethanol or other biorefinery products [1, 2]. Among various biomass sources, crop residues such as rice, wheat, barley straw, and corn stover have gained considerable interest and several studies have already been reported based on these feedstocks [3–5]. However, soybean straw, like other lignocellulosic biomaterials, consists of a rigid cellulose structure of strongly cross-linked amorphous hemicellulose and lignin [6–10]. These rigid biomass structures are too chemically complex and too resistant to enzymatic hydrolysis for the production of fermentable sugars. Thus, pretreatment is necessary to change the rigid lignocellulose structures into more enzymatically accessible and digestible forms [2–5].

Soybean straw contains a relatively low level of hemicellulose and lignin per gram biomass, compared with other lignocellulosic biomasses [6–10]. Thus, pretreatment is needed to increase the cellulose content and to decrease the hemicellulose and lignin contents in the biomass. The pretreatment processes should enhance the proportion of cellulose in soybean straw [7–10]. Acidic, alkali, and sequential acidic-alkali pretreatments, combined with high temperature or high pressure, have been applied in "conventional" chemical

treatment processes [3–5, 11–14]. Acidic pretreatments are known to be effective with lignocellulosic biomasses in reducing the hemicellulose content. Similarly, alkali pretreatments have been reported as simple processes for the delignification of biomass under mild conditions with minimal sugar degradation and without the formation of inhibitory compounds [14]. Thus, chemical pretreatments can reduce hemicellulose and lignin together to enhance the cellulose content of a biomass [11, 13, 14].

In this study, an alkali-pretreatment was carried out to decrease hemicellulose and lignin for high cellulose content in soybean straw. The biomass was pretreated under different concentration of sodium hydroxide at high temperature, that is, 121°C. The effectiveness of the alkali-pretreatment of the biomass was determined based on the degree of compositional change and enzymatic hydrolysis of pretreated solids. In addition, to evaluate the alkali-pretreatment process, the simultaneous saccharification and fermentation was also performed using an ethanologenic yeast strain of *Saccharomyces cerevisiae* and ethanol productivity was determined.

2. Materials and Methods

2.1. Materials. Soybean straws were obtained locally from a farm in Jeongeup, Jeonbuk, South Korea, at the end of November 2017. It was washed with water to eliminate soil and other particles and then dried at 105°C for 24 h. The straws were chopped into 5–10 cm lengths for chemical pretreatment. Cellic CTec2 cellulase was provided by Novozymes Korea (Seoul, Republic of Korea).

2.2. Chemical Pretreatment of Soybean Straws. Dried straws (20% w/v) with no physical treatment were soaked in sodium hydroxide (NaOH) solution in the concentration range of 0~3 M and heated in an autoclave (121°C, 15 psi, 60 min). The thermal-alkali-pretreated biomasses were removed from the black alkali solution and then washed with flowing tap water to remove NaOH from the biomass. This washing step was repeated several times until the washed water showed a pale brown color. The alkali-pretreated straws were dried at 105°C for 24 h to reduce the moisture content and then stored under anhydrous conditions. The composition of the pretreated biomass was analyzed based on the NREL chemical analysis and testing laboratory analytical procedures (LAPs) of the US Department of Energy (DOE). The lignin content of the biomass was analyzed according to the LAPs of the DOE (LAP-003 and LAP-004). The biomass pretreatment with different NaOH concentration was performed in triplicate.

2.3. Enzymatic Hydrolysis of the Alkali-Pretreated Soybean Straw. Enzymatic hydrolysis of the alkali-pretreated straw (2 M NOH-treated biomass) was carried out in a tube with a 30 ml reaction volume using Cellic CTec2 cellulase. 10% (w/v) pretreated biomass was soaked in phosphate buffer (pH 6.0) containing the cellulase with 10~50 FPU (filter paper unit) per gram of dry biomass. Enzymatic hydrolysis was performed at 42°C, 200 rpm, for 48 h. The biomass hydrolysate was withdrawn at each 12 h for 72 h. After centrifugation of the enzyme reactants, the hydrolyzed products were analyzed by high-performance liquid chromatography (HPLC) for the amount of monosaccharides generated in the enzymatic hydrolysis. The enzyme solution of Cellic CTec2 cellulase used for the enzymatic hydrolysis basically contains 206 ± 2.3 g/L glucose and 193.3 ± 0.2 g/L xylose. The calculation of the amount of monosaccharides (glucose and xylose) hydrolyzed from the pretreated biomass and the enzymatic saccharification yields excludes the amount of these sugars from the solution of the cellulase.

2.4. Ethanol Production Strain, Growth Conditions, and Fermentation. *Saccharomyces cerevisiae* W303-1A was used as an ethanol production strain [12]. The ethanologenic strain was cultivated in YPD broth (2% Bacto peptone, 1% Bacto yeast extract, and 2% glucose) at 30°C at 200 rpm for 24 h. To prepare a seed culture for ethanol fermentation, 1% (v/v) seed culture was inoculated in a medium containing enzymatic hydrolysis solution, in which 10% (w/v) pretreated soybean straw was hydrolyzed by the cellulase for 48 h as carbon sources, 2% Bacto peptone, and 1% Bacto yeast extract as nutrient sources. Then the seed culture was further cultivated at 30°C at 200 rpm for 24 h. 5% (v/v) preculture of the yeast strain was inoculated into a 1-L fermentor FMT ST-S (Fermentec, Cheongju, South Korea) with a 0.5 L working volume containing 10% (w/v) alkali-pretreated soybean straw, 2% Bacto peptone, and 1% Bacto yeast extract and then the fermentor was operated at 30°C with agitation at 300 rpm. The ethanol fermentation was performed in triplicate.

2.5. Analytical Procedures. Cell growth was monitored by measuring the optical density at 600 nm (OD600 nm) using a spectrophotometer. Total reducing sugars in the enzymatic saccharification reaction were measured using the 3,5-dinitrosalicylic acid method. The amounts of the released sugars in the enzymatic saccharification and the metabolites in fermentation were determined with a high-performance liquid chromatography (HPLC) system (Agilent Technologies, Santa Clara, CA, USA), equipped with a refractive index detector, an autosampler, and an Aminex HPX-87P column (7.8 × 300 mm; BioRad, Hercules, CA, USA) for monosaccharide analysis or a Rezex ROA-Organic Acid H^+ column (7.8 × 300 mm; Phenomenex, Torrance, CA, USA) for organic acid analysis. All samples were clarified by filtration with a 0.20-μm filter (Acrodisc LC PVDF Minispike; Pall Life Sciences, Ann Arbor, MI, USA) and then injected into the analytical HPLC column. The column temperature was kept at 65°C. The mobile phase was distilled water for monosaccharides and 2.5 mM sulfuric acid for organic acids, with a flow rate 0.5 mL/min under isocratic conditions. Under these conditions, cellobiose, glucose, xylose, ethanol, glycerol, and xylitol were detected at the retention times 9.93, 12.08, 13.14, 16.36, 18.96, and 34.33 min, respectively, in monosaccharide analyses. Succinic acid, lactic acid, acetic acid, and ethanol were detected at the retention times 13.14, 16.36, 18.96, and 34.33 min, respectively, in organic acid analyses. All analyses were performed in triplicate

Table 1: The chemical composition of soybean straws.

	Compositions (%) per 100 g soybean straw*					
Sample	1	2	3	4	5	6
Cellulose	44–83	25.0	34.1	39.8	35.3	44.2
Hemicellulose	-	11.9	16.1	22.6	16.9	5.9
Lignin(2)	5–14	17.6	21.6(1)	12.8	21.7(1)	19.2(1)
Ash	2–5	-	5.2	-	10.6	-
Reference	[6]	[7]	[8]	[9]	[10]	This study

*The percentage of composition in the biomass is based on the dry weight of soybean straw. (1)The amount of lignin contains acid-soluble and insoluble materials. (2)The lignin means acid-insoluble fraction.

3. Results and Discussion

3.1. Alkali Treatment of Soybean Straw and Its Composition. Prior to alkali-pretreatment, cellulose, hemicellulose, and lignin contents in the soy straw raw material were determined by using the methods of the US DOE. Dried soybean straw (100 g) consisted of 44.2% cellulose, 5.9% hemicellulose, and 19.2% lignin (Table 1). Compared to these contents in several different biomasses summarized in Table 1 [6–10], the soybean straw used in this study contained a relatively low amount of hemicellulose and a high content of lignin. It needs to reduce lignin content to enhance the enzymatic accessibility and digestibility to produce a fermentable sugar glucose and to enhance ethanol production yield using an ethanologenic strain [5].

To enhance a high-cellulose-content biomass, alkali-pretreatment was applied to reduce lignin in the soybean straw (Figure 1). After the biomass had dried completely, the chemical composition change in alkali-pretreated soybean straws was analyzed (Table 2). The concentration of sodium hydroxide affected the solubility of the biomass and the loss of cellulose, hemicellulose, and lignin contents. Alkali-thermal treatment within sodium hydroxide extracted up to 52~64.5% of the biomass into the soluble fraction, even though hot water without any alkali compound extracted 29.1% of the biomass. With 3 M sodium hydroxide pre-treatment, the insoluble residue fraction contained 72.9% cellulose, 9.1% hemicellulose, and 9.0% lignin per 100 g dry biomass. After alkali treatment, 9.0~12.6% lignin and 9.1~17.9% hemicellulose remained in the residual biomass. However, the pretreated biomass did not lose much cellulose content, from 66.4 g to 72.9 g per 100 g of dry soybean straw, with an increase in the sodium hydroxide concentration. The delignification yield with the alkali-thermal pretreatment was 34.1~53.0%, in proportion to the amount of sodium hydroxide, from 0.5 to 3.0 M. However, >47% of the lignin could not be removed from the biomass under the alkali-thermal pretreatment conditions, even with a high concentration of sodium hydroxide. Nevertheless, the alkali-thermal treatment of the biomass showed that sodium hydroxide reduces hemicellulose and lignin effectively and increases the cellulose content per gram biomass.

3.2. Enzymatic Hydrolysis of Soybean Straw. To assess the enzymatic hydrolysis of alkali-thermal-pretreated soybean straw with 2 M sodium hydroxide, the pretreated biomass (10% (w/v)) was digested with different enzyme dose of Cellic CTec2 cellulase, from 10 to 50 FPU per gram of dry biomass in phosphate buffer (pH 6.0) for 72 h. The pH in the reaction media for the enzymatic digestion could affect the growth, metabolism, and transport in an ethanologenic strain for further ethanol fermentation [15]. Thus pH was fixed at 6.0 for the enzymatic biomass saccharification. The amount of glucose produced by enzymatic hydrolysis increased with increasing amounts of cellulase per unit the alkali-pretreated soybean straw (Figure 2(a)). At 72 h, the cellulose generated 40.1~67.3 g/L glucose and 5.6~9.4 g/L xylose. The enzymatic digestibility at the enzyme loading ratio of 50 FPU cellulase per gram of dry biomass reached 54.2 ± 2.8%~90.9 ± 2.8% (Figure 2(b)). On the other hand, the nontreated biomass was hydrolyzed with less than 33% (data now shown). Compared with untreated soybean straw, the alkali-thermal-pretreated biomass contained higher amounts of glucose and lower amounts of xylose. Alkali-pretreatment with approximate

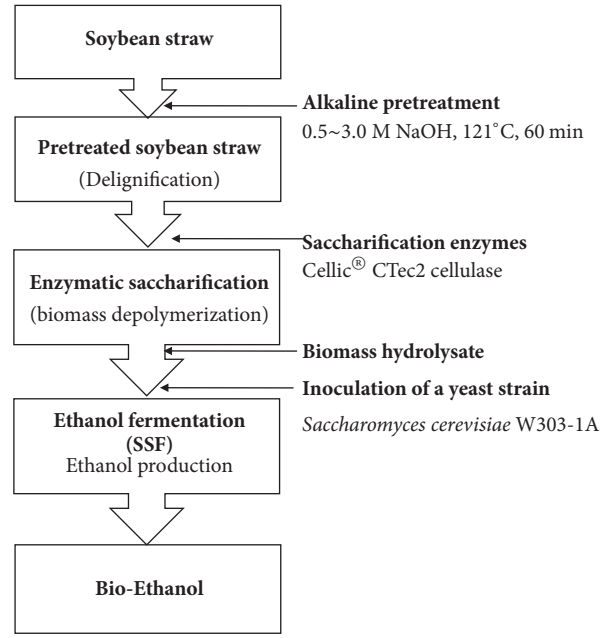

Figure 1: Overall procedure for the simultaneous saccharification and fermentation of the alkali-treated soybean straw for ethanol production.

Table 2: Effect of the concentration of sodium hydroxide for the alkali-pretreatment of the soybean straw and the efficiency of delignification.

NaOH	Compositions/100 g soybean straw[1]							Delignification[4]
	Soluble[2]	Insoluble[2]	Cellulose		Hemicellulose		Lignin[3]	
[M]	[g]	[g]	[g]	[%][5]	[g]	[%][5]	[g]	[%]
Untreated soybean straw	-	100.0 ± 0.8	44.2 ± 0.6	44.2	5.9 ± 0.5	5.9	19.2 ± 0.7	-
0.0 M	29.1 ± 0.5	70.9 ± 0.7	36.8 ± 0.8	51.9	5.7 ± 0.6	8.1	17.9 ± 0.5	6.9
0.5 M	52.0 ± 0.4	48.0 ± 0.5	31.9 ± 0.5	66.4	8.6 ± 0.7	17.9	12.6 ± 0.6	34.1
1.0 M	55.0 ± 0.3	45.0 ± 0.6	30.8 ± 0.7	68.6	6.9 ± 0.4	15.4	12.2 ± 0.5	36.5
1.5 M	57.5 ± 0.3	42.5 ± 0.5	30.0 ± 0.6	70.7	5.4 ± 0.2	12.7	11.9 ± 0.4	38.1
2.0 M	60.3 ± 0.6	39.7 ± 0.7	29.4 ± 0.6	74.0	4.1 ± 0.3	10.3	10.1 ± 0.6	47.4
2.5 M	62.8 ± 0.7	37.2 ± 1.2	27.4 ± 0.4	73.7	3.6 ± 0.2	9.7	10.1 ± 0.4	47.3
3.0 M	64.5 ± 1.2	35.5 ± 0.7	25.8 ± 0.5	72.9	3.2 ± 0.2	9.1	9.0 ± 0.4	50.0

[1]100 g soybean straw is the weight of the total solid without the moisture content. [2]Soluble and insoluble indicate soluble and insoluble solids in the total solids in soybean straw biomass. [3]The lignin content is the sum of acid-soluble and acid-insoluble lignin. [4]The percent of the relative delignification was calculated by the following formula: delignification (%) = $100 \times (1 - ([\text{lignin}]_{\text{treated soybean straw}}/[\text{lignin}]_{\text{untreated soybean straw}}))$. [5]The percent of each component means the relative amount in insoluble fraction.

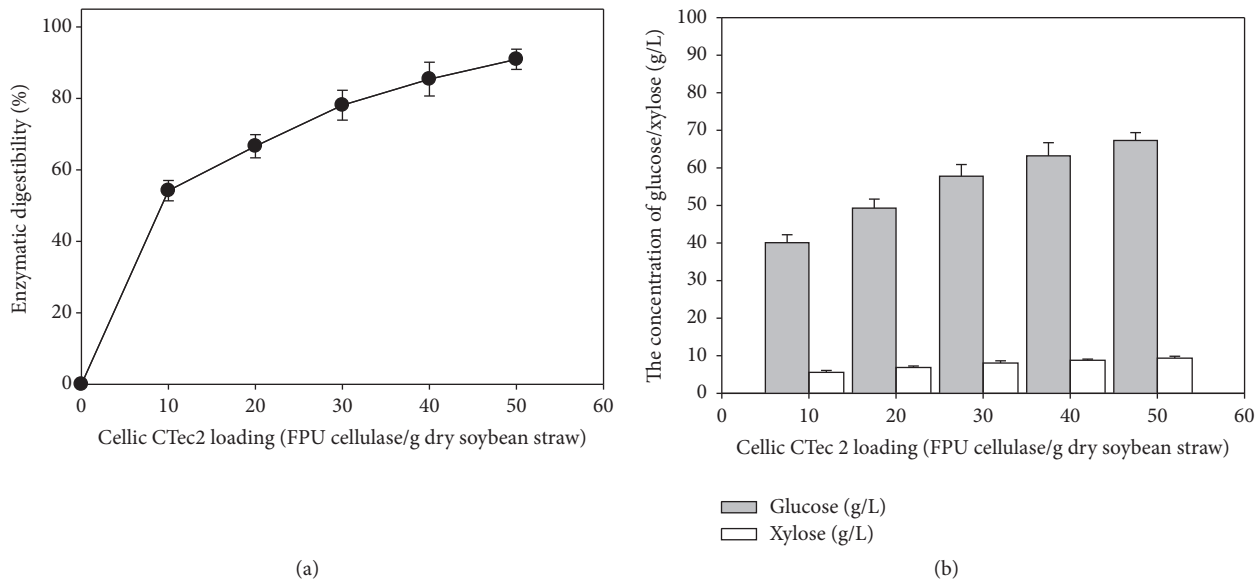

Figure 2: Enzymatic saccharification of the alkali-treated soybean straw with 50 FPU of Cellic CTec2 cellulase loading per gram of the dry biomass. The enzymatic digestibility was calculated by the relative amount of glucose released from the content of glucan in the pretreated biomasses after enzyme reaction.

47.4% delignification efficiency would affect the cellulase digestibility, resulting in a hydrolysis efficiency up to 90%. The chemical pretreatment also reduced the strong interactions in cellulose/hemicellulose/lignin complexes in the biomass structure, enhancing the enzyme reaction efficiency. An increase in the volume of enzymes used significantly affects the amount of fermentable sugar generation. At the final reaction time point, the amount of glucose increased up to 1.7 times depending on 5 enzyme loading ratios of Cellic CTec2 cellulase per biomass. Additionally, sugar production increased time-dependently, whereas enzymatic hydrolysis rates decreased exponentially due to product inhibition (data not shown). The generated glucose, xylose, and incompletely digested cellobiose may inhibit the hydrolysis reactions of the cellulase. These enzymatic saccharifications showed that alkali-pretreated soybean straw could be powerful to prepare a fermentable sugar glucose for bioethanol production.

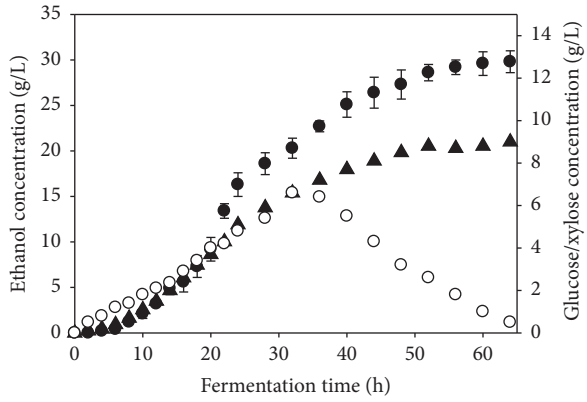

Figure 3: Batch simultaneous saccharification and fermentation of the alkali-pretreated soybean straw by *Saccharomyces cerevisiae* W303-1A in a 1-L jar fermenter. Profiles of ethanol (filled circle), glucose (open circle), and xylose (filled triangle) in the fermenter were analyzed by HPLC.

3.3. Separate Hydrolysis and Fermentation of Alkali-Pretreated Soybean Straw. To evaluate the fermentability of the sugars generated from the alkali-pretreated soybean straw, ethanol production was performed using *Saccharomyces cerevisiae* W303-1A [12]. Batch cultivation of the yeast strain was performed in a 50-mL culture volume in a 250-mL Erlenmeyer flask with 5 g of alkali-pretreated soybean straw, supplemented with a 50 FPU Cellic CTec2 cellulase. Before cell inoculation, prehydrolysis was performed at 42°C for 12 h. Then, 5% (v/v) yeast inoculum was added and cultured further (30°C, 180 rpm, 36 h) for ethanol fermentation. The prehydrolysis step generated ~12.1 ± 0.7 g/L glucose in the flask for yeast cell growth without the lag phase. At 36 h, the maximum ethanol concentration of 13.1 ± 0.7 g/L was observed in the culture broth. However, low ethanol production yield was observed in the flask culture. The enzymatic saccharification was not efficient in the flask culture.

3.4. Batch Simultaneous Saccharification and Fermentation (SSF) for Ethanol Production. To increase ethanol production, ethanol fermentation was performed in a 1-L jar fermentor. For batch SSF, 10% (w/v) pretreated biomass was enzymatically saccharified with 50 FPU of Cellic CTec2 cellulase per gram of dry biomass. The ethanol production proceeded gradually for 72 h (Figure 3). The amount of glucose was gradually increased by enzymatic hydrolysis. Although the ethanologenic yeast consumed glucose for cell growth, the

concentration of glucose generated exceeded the amount consumed. The yeast completely consumed all glucose enzymatically hydrolyzed from the biomass in the medium over 60 h. Nevertheless, the amount of xylose increased gradually to 9.1 ± 0.5 g/L, because the wild type *S. cerevisiae* W303-1A can not utilize the sugar. In a batch SSF, the maximum ethanol concentration was 30.5 ± 1.2 g/L at 72 h, giving an ethanol production yield of 0.305 g ethanol/g dry soybean straw and 0.45 g ethanol/g glucose at 72 h. Finally, 82% of the fermentable sugar hydrolyzed from the pretreated biomass was used by the yeast for ethanol production. In addition, the decrease of ethanol concentration was not observed until glucose was completely depleted in the fermentation (72 h).

In ethanol production of the alkali-pretreated soybean straw, the baker's *S. cerevisiae* W303-1A generated minor metabolites, including glycerol and organic acids such as acetic acid, lactic acid, and succinic acid (data not shown). These metabolites are less than 1.5 ± 0.4 g/L. These minor byproducts generated by the yeast were at lower concentrations than ethanol. Although these metabolites remained and were accumulated during the ethanol production, it did not affect the fermentation efficiency or the yeast cell growth.

In this study, an alkali-pretreatment was applied to an agricultural residue soybean straw as a potential bioresource to produce fermentable sugars by enzymatic saccharification. The soybean straw used in this pretreatment contained relatively high cellulose and lignin contents rather than hemicellulose. To reduce lignin and to enhance cellulose content, sodium hydroxide among chemical pretreatments was chosen for delignification of soybean straw. The maximum cellulose content of 74% was achieved with 2 M NaOH at 121°C after 60 min and, at this condition, delignification of 47.4% and hemicellulose content of 10.3% (Table 2).

In fact, the advantage of sodium hydroxide pretreatment can break down effectively the internal structure of lignocellulose component through degrading the ester and glycosidic chains. In addition, the alkali can alter the structure of lignin, causing cellulose swelling and partial decrystallization of cellulose [16]. Moreover the safer handling and the lower toxicity in the pretreatment, including lower operating temperatures and faster process times, make it an attractive alternative to ammonia pretreatment [17]. Relatively lower thermal-pretreatment condition also reduce sugar degradation products such as furfural, hydroxymethylfurfural, and organic acids, considering potential inhibitors for enzymatic saccharification as well as ethanol fermentation [18]. In enzymatic digestion and the fermentation process, these inhibitors were not detected in the biomass lysate. Moreover, the soybean straw pretreated with 2 M NaOH was effectively hydrolyzed with a hydrolysis efficiency up to 90% for production of the fermentable sugars (Figure 2(a)). Additionally, the simultaneous saccharification and fermentation converted the sugar of the biomass hydrolysate to 30.5 g/L of ethanol with ethanol conversion of more than 82% (Figure 3).

Although the concentration of sodium hydroxide for pretreatment of soybean straw was relatively higher than other alkali chemical compounds, sodium hydroxide solution could be recovered and reused several times for biomass pretreatment [19]. In addition, compared with other chemical pretreatments using aqueous ammonia, organosolv, and ionic liquids, the sodium hydroxide-treatment could be a simple and convenient process, because it does not require any special equipment or control systems for the pretreatment [19].

The utilization of soybean straw could offer several advantages for the sustainable development based on the biomass utilization. Sugar crops or alternative lignocellulosic biomass plants consumed nutrients in the soil leading to decreased nutrients levels. On the other hand, a legume plant soybean with symbiotic bacteria Rhizobia in the nodules of its root systems can fix nitrogen into ammonia and ammonium leading to nitrogen (N) enrichment in the soil, including CO_2 fixation by photosynthesis [20]. Considering the sustainability, the residual biomass from the soybean is a potential resource for production of fermentable sugar.

4. Conclusions

The alkali-pretreatment of soybean straw with sodium hydroxide effectively removed lignin and hemicellulose and enhanced enzyme digestibility. The alkali-pretreated biomass showed ~53% delignification efficiency. In the pretreated biomass, over 90% of the cellulose was hydrolyzed by Cellic CTec2 cellulase and was converted to fermentable sugars during enzymatic saccharification. In a flask-scale culture of separate hydrolysis and fermentation supplemented with the pretreated biomass, *S. cerevisiae* produced 13.1 g/L ethanol with 0.13 g ethanol/g biomass. In a batch of simultaneous hydrolysis and fermentation, the pretreated soybean straw was converted to 30.5 g/L of ethanol with the product yield of 0.305 g ethanol/g dry soybean straw and 0.45 g ethanol/g glucose. In the fermentation, 82% fermentable sugar was converted to ethanol within a low concentration of organic acid byproducts. These results clearly show that alkali-pretreatment for an agricultural byproduct soybean straw efficiently reduces lignin and hemicellulose components and increases enzymatic digestibility and ethanol productivity.

Conflicts of Interest

The author declares no conflicts of interest regarding the publication of this article.

Acknowledgments

This work was partially supported by Research Exchange Program under Memorandum of Understanding between the NRF-DAAD (NRF-2013K2A5A5079255) from Korea National Research Foundation (NRF), the New & Renewable Energy Technology Development Program of the Korea Institute of Energy Technology Evaluation and Planning (KETEP) granted financial resource from the Ministry of Trade, Industry & Energy, Republic of Korea (no. 20153030101580), and KRIBB Research Initiative Program grant.

References

[1] M. Caicedo, J. Barros, and B. Ordás, "Redefining agricultural residues as bioenergy feedstocks," *Materials*, vol. 9, no. 8, article no. E635, 2016.

[2] S. Brethauer and M. H. Studer, "Biochemical conversion processes of lignocellulosic biomass to fuels and chemicals - A review," *Chimia*, vol. 69, no. 10, pp. 572–581, 2015.

[3] L. Capolupo and V. Faraco, "Green methods of lignocellulose pretreatment for biorefinery development," *Applied Microbiology and Biotechnology*, vol. 100, no. 22, pp. 9451–9467, 2016.

[4] L. P. Devendra, M. Kiran Kumar, and A. Pandey, "Evaluation of hydrotropic pretreatment on lignocellulosic biomass," *Bioresource Technology*, vol. 213, pp. 350–358, 2016.

[5] M. H. L. Silveira, A. R. C. Morais, A. M. Da Costa Lopes et al., "Current Pretreatment Technologies for the Development of Cellulosic Ethanol and Biorefineries," *ChemSusChem*, vol. 8, no. 20, pp. 3366–3390, 2015.

[6] N. Reddy and Y. Yang, "Natural cellulose fibers from soybean straw," *Bioresource Technology*, vol. 100, no. 14, pp. 3593–3598, 2009.

[7] Z. Xu, Q. Wang, Z. Jiang, X.-X. Yang, and Y. Ji, "Enzymatic hydrolysis of pretreated soybean straw," *Biomass & Bioenergy*, vol. 31, no. 2-3, pp. 162–167, 2007.

[8] C. Wan, Y. Zhou, and Y. Li, "Liquid hot water and alkaline pretreatment of soybean straw for improving cellulose digestibility," *Bioresource Technology*, vol. 102, no. 10, pp. 6254–6259, 2011.

[9] M. Martelli-Tosi, O. B. G. Assis, N. C. Silva, B. S. Esposto, M. A. Martins, and D. R. Tapia-Blácido, "Chemical treatment and characterization of soybean straw and soybean protein isolate/straw composite films," *Carbohydrate Polymers*, vol. 157, pp. 512–520, 2017.

[10] E. Cabrera, M. J. Muñoz, R. Martín, I. Caro, C. Curbelo, and A. B. Díaz, "Comparison of industrially viable pretreatments to enhance soybean straw biodegradability," *Bioresource Technology*, vol. 194, pp. 1–6, 2015.

[11] S. Kim, J. M. Park, J.-W. Seo, and C. H. Kim, "Sequential acid-/alkali-pretreatment of empty palm fruit bunch fiber," *Bioresource Technology*, vol. 109, pp. 229–233, 2012.

[12] S. Kim and C. H. Kim, "Bioethanol production using the sequential acid/alkali-pretreated empty palm fruit bunch fiber," *Journal of Renewable Energy*, vol. 54, pp. 150–155, 2013.

[13] S. Kim, J. M. Park, and C. H. Kim, "Ethanol production using whole plant biomass of *Jerusalem artichoke* by *Kluyveromycs marxianus* CBS1555," *Applied Biochemistry and Biotechnology*, vol. 169, no. 5, pp. 1531–1545, 2013.

[14] S. Kim and C. H. Kim, "Evaluation of whole Jerusalem artichoke (*Helianthustuberosus* L.) for consolidated bioprocessing ethanol production," *Journal of Renewable Energy*, vol. 65, pp. 83–91, 2014.

[15] A. Peña, N. S. I. Sánchez, H. Álvarez, M. Calahorra, and J. Ramírez, "Effects of high medium pH on growth, metabolism and transport in *Saccharomyces cerevisiae*," *FEMS Yeast Research*, vol. 15, no. 2, pp. 1–13, 2015.

[16] Y. Jiang, X. Zeng, R. Luque et al., "Cooking with active oxygen and solid alkali: a promising alternative approach for lignocellulosic biorefineries," *ChemSusChem*, vol. 10, no. 20, pp. 3982–3993, 2017.

[17] A. D. Moreno, D. Ibarra, P. Alvira, E. Tomás-Pejó, and M. Ballesteros, "A review of biological delignification and detoxification methods for lignocellulosic bioethanol production," *Critical Reviews in Biotechnology*, vol. 35, no. 3, pp. 342–354, 2015.

[18] H. Rasmussen, H. R. Sørensen, and A. S. Meyer, "Formation of degradation compounds from lignocellulosic biomass in the biorefinery: Sugar reaction mechanisms," *Carbohydrate Research*, vol. 385, pp. 45–57, 2014.

[19] M. Vochozka, V. Stehel, and A. Maroušková, "Daphnia magna demonstrated sufficient sensitivity in techno-economic optimization of lignocellulose bioethanol production," *3 Biotech*, vol. 7, no. 3, article no. 162, 2017.

[20] P. M. Gresshoff, S. Hayashi, B. Biswas et al., "The value of biodiversity in legume symbiotic nitrogen fixation and nodulation for biofuel and food production," *Journal of Plant Physiology*, vol. 172, pp. 128–136, 2015.

Hindawi
International Journal of Polymer Science
Volume 2018, Article ID 2684962, 11 pages
https://doi.org/10.1155/2018/2684962

Research Article

Valorizing Rice Straw and Its Anaerobically Digested Residues for Biochar to Remove Pb(II) from Aqueous Solution

Jinyang Li,[1,2,3,4,5] Fei Shen,[1,2,3,4] Gang Yang,[3,4] Yanzong Zhang,[4] Shihuai Deng,[3,4] Jing Zhang,[3,4] Yongmei Zeng,[3,4] Tao Luo,[1,2] and Zili Mei[1,2]

[1]*Biogas Institute of Ministry of Agriculture, Chengdu 610041, China*
[2]*Key Laboratory of Development and Application of Rural Renewable Energy, Ministry of Agriculture, Chengdu 610041, China*
[3]*Institute of Ecological and Environmental Sciences, Sichuan Agricultural University, Chengdu, Sichuan 611130, China*
[4]*Rural Environment Protection Engineering & Technology Center of Sichuan Province, Sichuan Agricultural University, Chengdu, Sichuan 611130, China*
[5]*State Grid Sichuan Power Economic Research Institute, Chengdu, Sichuan 610041, China*

Correspondence should be addressed to Fei Shen; fishen@sicau.edu.cn

Received 2 November 2017; Accepted 1 February 2018; Published 20 March 2018

Academic Editor: Xuebing Zhao

To seek a new path to valorize rice straw (RS) and its anaerobically digested residues (DRS), biochar production at different temperatures for removing Pb(II) from aqueous solution and its basic physicochemical characteristics for elucidating potentially adsorption mechanisms were investigated. Overall, pH, electrical conductivity (EC), ash, specific surface area (SA), micronutrient content, and aromaticity of RS biochars (RSBCs) and DRS biochars (DRSBCs) increased with the promoted pyrolysis temperature, and opposite trends were found on the yield, volatile matter, H, N, and O. Lower pH and K content but higher yield, carbon stability, and N and P content were achieved by DRSBCs. Consequently, DRSBCs exhibited lower Pb(II) removal, which was 0.15–0.35 of RSBCs. Maximum adsorption capacities of 276.3 and 90.5 $mg \cdot g^{-1}$ were achieved by RSBC and DRSBC, respectively, at 500°C. However, distinct mechanisms dominated Pb(II) removal, in which carbonates and carboxylates were responsible for RSBCs, and phosphate silicate precipitation and complexation with carboxylate groups controlled DRSBCs.

1. Introduction

Rice is the staple food for over half the world's population. Approximately 480 million metric tons of milled rice is produced annually [1]. More than 90% rice are produced from Asian countries, in which China is the largest producer in the world; consequently, approximately 975 million metric tons of rice straw is generated annually in the fields [2]. It is reported that only 20% of rice straw produced in the world can be utilized, and the rest is left as waste [2, 3]. In most countries, the remaining rice straw is left undisturbed to serve as mulch, is ploughed into the ground as soil nutrients, or is directly disposed by open-burning in the fields, which leads to the serious air pollution and greenhouse gas emission in practice [4] and, thereby, is strictly prohibited in China. In addition, rice straw is also employed as part of the nutritional requirements of ruminant animals in most rice producing countries. However, low protein content, possession of phenolic properties, and high level of silica and lignin are negative to rice straw digestibility by ruminant animals [5]. Thus, seeking more paths for efficiently utilizing rice straw is meaningful to the sustainability of rice production. Recently, anaerobically digesting agricultural residues for biogas production, as an effective method, have been gradually popularized in all the world [6]. However, with the increased scale of anaerobic digestion, the disposal of digested residues has become an urgent issue to be solved.

At present, producing biochar, a carbon-containing material via pyrolyzing biomass in an oxygen-limited environment, has become one of the alternative ways to utilize the waste biomass, such as crop straw, forestry waste, and livestock manure [7, 8]. Its applications in sequestrating

carbon, remediating soil, improving soil quantity, and controlling pollutants make biochar more attractive and popularly investigated. Especially in pollutant control in water environment, many investigations indicate that the biochar can remove many types of organic and inorganic contaminants from the aqueous solutions [9]. Unlike most organic pollutants, inorganic pollutants, mainly heavy metals, are nonbiodegradable and may be transferred along the food chain via bioaccumulation [7]. Many studies have demonstrated that biochar has excellent performances to immobilize heavy metals in soil and water [10–12]. Thus, biochar is increasingly being considered as an alternative agent in water treatment technologies for removing heavy metals.

The mechanisms of removing heavy metals from aqueous solution by biochar are generally via precipitation, complexation, ion exchange, electrostatic interaction (chemisorption), and physical sorption [7]. The physical sorption is mainly depended on the surface areas and pore volumes. Although many biochars have been reported to have high surface area with well-distributed pore network, including micropores (<2 nm), mesopores (2–50 nm), and macropores (>50 nm) [13], it is well known that the pore development of biochar is not enough compared with the traditional activated char as biomass is carbonized directly for biochar without any activation processes [14]. Many biochars are reported as negatively charged surfaces, which can sorb positively charged metals through electrostatic attractions. However, prevalence of this mechanism in biochar-metal sorption process is dependent on the solution pH and point of zero charge (PZC) of biochar [13, 15]. Complexation (outer- and inner-sphere) involves the formation of multiatom structures (i.e., complexes) with specific metal-ligand interactions, which was mainly related to oxygen functional groups on the surface of biochar [16, 17]. Immobilizing heavy metals via ion exchange is another possible mechanism, which is closely related to the positively charged ions, such as Na, K, Ca, and Mg, on biochar surfaces and the cation exchange capacity (CEC) [18, 19]. By contrast, the precipitation has been widely accepted as one of the main mechanisms for removing heavy metals by biochar, which greatly related to the ash components of biomass, such as the elements of Ca, Mg, Fe, Cu, and Si [20, 21]. Obviously, the ash components in biomass may be potentially associated with the functions of ion exchange and precipitation and further affect the adsorption capacity to heavy metals. Rice straw, typically characterized by relatively higher ash content, thereby, can be potentially employed to immobilize heavy metals via precipitation or ion exchange. In addition, anaerobic digestion can convert part of organic matters, such as hemicellulose, cellulose, lignin, and other organic extractives into CH_4 and CO_2. Consequently, ash content of the anaerobically digested rice straw will be greatly promoted compared with the original rice straw. Considering the urgency for seeking the efficient paths of utilizing rice straw and its digested residues, their carbonization for producing biochar to remove heavy metals specially deserves being investigated in-depth.

Main sources of lead pollution in the environment are from lead-acid battery industry, mining, metal smelting, automobile exhaust, coal, and paint. At present, the main methods for treating lead pollution include chemical precipitation, redox, ion exchange, adsorption, reverse osmosis, and electrolysis. However, these technologies have some drawbacks, such as complex process, expensive chemical input, high running cost, inconvenient operation, and potential secondary pollution. In this context, the typical heavy metal ion of Pb(II) was selected as the model contaminant to investigate the adsorption performances of biochars derived from rice straw and its anaerobically digested residues. Meanwhile, different biochars from RS and DRS were obtained at an increasing pyrolytic temperature to seek their effects on Pb removal from aqueous solution. Correspondingly, the physical-chemical properties of biochars were discriminated by elemental analyses, scanning electron microscopy (SEM), Fourier transform infrared spectroscopy (FT-IR), and X-ray diffraction (XRD). The adsorption performances of biochars, concerning adsorption isotherm, kinetics, thermodynamics, and effects of solution pH were elaborated by batch experiments to discuss the possible adsorption mechanisms.

2. Materials and Methods

2.1. Rice Straw and Its Anaerobically Digested Residue. Rice straw (RS) was harvested from the local farm in Deyang, Sichuan province, and chopped in 2.0–3.0 cm for anaerobic digestion in a 100 L bioreactor. After 50 d batch digestion, the digested slurry was collected from outlet of the bioreactor. The solid residue of digested rice straw (DRS) was separated by filter, and it afterwards was air-dried for the following carbonization. Prior to pyrolysis, the RS and DRS were ground into powder (<0.45 mm, sieved) and dried at 105°C for 6.0 h to wipe off free moisture. The basic compositions of RS were analyzed for Klason insoluble lignin and carbohydrates as described in [22], and cellulose, hemicellulose, and lignin, were 14.0%, 30.8%, and 23.0%, and the corresponding compositions in DRS were 3.1%, 9.3%, and 44.4%, respectively.

2.2. Biochar Preparation. The dried RS and DRS were pyrolyzed in a tube furnace (OTL 1200, Nanjing Nanda Instrument Co., Ltd., China) under protective gas of N_2 (purity of 99.9%) with a flow rate of 0.1 $m^3 \cdot h^{-1}$. The heating rate of tube furnace was controlled at 10°C·min^{-1}, and the pyrolysis was maintained for 60 min after arriving at the designed temperature of 400°C, 500°C, 600°C, and 700°C. After pyrolysis, the furnace was cooled to room temperature for biochar collection. The derived biochar was weighted, and biochar yield was calculated according to the weights of biochar and the input RS and DRS. The obtained biochar from RS at different temperature was named as RS-400, RS-500, RS-600, and RS-700, respectively. The corresponding biochars from DRS were labeled as DRS-400, DRS-500, DRS-600, and DRS-700, respectively.

2.3. Characterization of Biochars. Proximate analysis, including ash, volatile matter, and fixed carbon, in RS, DRS, and their derived biochars, was performed according to the standard methods in the ASTM D 1762-84 [23]. The elemental compositions, including carbon, hydrogen, nitrogen, and oxygen, were determined using an elemental analyzer (EA112,

Thermo Finnigan, USA). pH and electric conductivity (EC) of biochars were measured by a pH meter (PHS-3C, LeiCi Instruments Co., Ltd., China) and a conductivity meter (DDS 12DW, BanTe Instruments Co., Ltd., China) with the ratio of 1 : 20 ($m \cdot v^{-1}$) for biochar to deionized water. The samples were digested in the concentrated HNO_3 and 30% H_2O_2 with the ratio of 3 : 1 for 24 h at 150°C to determinate the concentration of K, Na, Ca, Mg, and P. The elemental concentrations in the digested solution were determined by inductively coupled plasma spectroscopy (ICP-MS 7700s, Agilent, USA).

Thermal analysis of RS, DRS, and their corresponding biochars was conducted on a thermogravimetric analyzer (SDT Q600, TA instrument, USA) with the heating rate of 10°C·min^{-1} from 20°C to 700°C. The specific surface area (SA) of the biochars was measured by N_2 adsorption isotherms at 77 K (NOVA-2000E, Quantachrome Instruments, USA) with the Brunauer-Emmett-Teller (BET) method. The surface morphology of rice straw biochar (RSBC) and the digested rice straw biochar (DRSBC) were observed by a scanning electron microscopy (SU1510, Hitachi, Japan) to compare the apparent structure and surface characteristics. A Fourier transform infrared spectrometer (Nicolet 6700, Thermo Fisher Scientific, USA) was employed to identify the chemical functional groups of the original and Pb-loaded RSBC and DRSBC. The spectra were obtained by 64 scans of the sample in the range of 400–4000 cm^{-1} at a resolution of 4 cm^{-1}. In addition, the XRD analysis of RSBC, DRSBC, and Pb-loaded biochars were conducted on a computer-controlled diffractometer equipped with stepping motor and graphite crystal monochromator (I-2, Nicolet, Madison, WI, USA). The diffractometer was operated at 40 kV and 40 mA range from 5 to 70° with a scan speed of 1°·min^{-1}.

2.4. Adsorption. Pb(II) solution was prepared by dissolving analytic reagent grade $Pb(NO_3)_2$ in deionized water for batch adsorption with a concentration of 20–1200 mg·L^{-1} and 20 to 800 mg·L^{-1} for RSBC and DRSBC, respectively. 0.1000 g biochar was added to 150 mL screw-flasks filled with 50 mL Pb(II) solution and shaken at 120 r·min^{-1} for 24 h according to the kinetic result. After adsorption, the solutions were filtered through 0.45 μm filters and determined the residual Pb(II) concentration by an atomic adsorption spectrometer (FAAS-M6, Thermo, USA). As the thermodynamics were investigated, the batch adsorption was carried out at 15, 25, 35, and 45°C, respectively, with similar process. As the effects of pH were discussed, the Pb(II) solution was rapidly adjusted to the specified pH in equilibrium using 1.0 mol·L^{-1} HNO_3 or 1.0 mol·L^{-1} NaOH after 0.1 g biochar was added, and the batch adsorption was similar to the statement above. All runs for the adsorption were performed in triplicate, the presented data were the average of 3 reads.

3. Results and Discussion

3.1. Pyrolysis Behaviors and Biochar Yields of RS and DRS. Results of TG/DTG on RS and DRS are shown in Figure 1. The main mass loss stage of rice straw typically appeared in the range of 200–500°C with the maximum weigh loss at 340°C due to the decomposition of the typical fractions

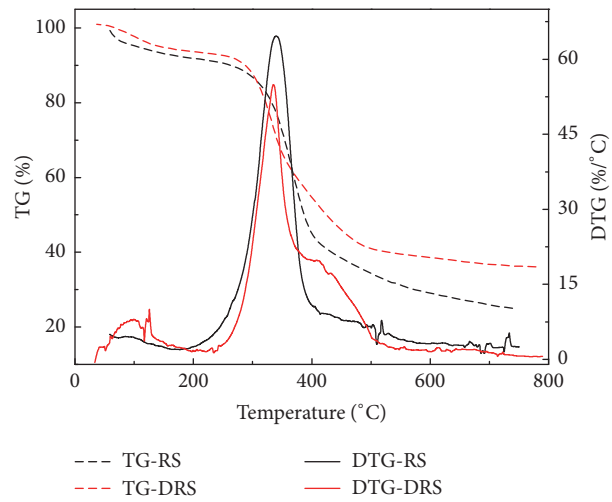

Figure 1: TG-DTG curves of RS and DRS.

of hemicellulose, cellulose, and lignin in the lignocellulosic biomass [24]. According to the DTG curve, the DRS was sharper than that of RS; however, the weight loss rate of DRS at 335°C was significantly lower than that of RS, indicating easier degradation via pyrolysis because most of hemicellulose and cellulose in the RS were degraded after anaerobic digestion, only 3.1% cellulose and 9.3% hemicellulose in DRS. An apparent peak at 408°C can be observed at DRS, because higher lignin remained to be undigested and the content of lignin increased from 23% to 44.4% after anaerobic digestion. Besides, the TG curves during final stage (400–750°C) indicated that more fix fraction will remain in DRS due to relatively higher ash content after anaerobic digestion. These results from TG/DTG basically responded to the composition change of RS after anaerobic digestion.

As shown in Table 1, the biochar yield decreased from 47.5% to 36.0% for the RS with the increase of pyrolysis temperature. By contrast, it was 74.9% to 57.5% for the DRS. The biochar yields of RS and DRS were both decreased rapidly from 400°C to 500°C but tended to be stable after 500°C. This was mainly because most organic matters were decomposed rapidly and only a few lignin dissociated in the pyrolysis process when the pyrolysis temperature over 500°C. Overall, the biochar yield from DRS was promoted by 21.5–27.4% compared with RS due to the relatively higher ash content in DRS, which was basically consistent with the results from TG/DTG.

3.2. Characterization of Biochar

3.2.1. Thermal Stability. Weight loss peaks appeared at 100°C in all biochars, mainly due to the dehydration of free water and bound water (see Figure S1). In contrast to the corresponding raw materials of RS and DRS, there was no obvious mass loss within 200–400°C because of the decomposition of hemicellulose, cellulose, and lignin during the pyrolysis process [25]. As RSBC was obtained at lower temperature of 400°C, 3 obvious weight loss peaks were detected at 335, 425, and 465°C, respectively, which was mainly due to the residual

Table 1: Physicochemical properties of biochars produced at different temperatures.

	Yield %	Ash %	FC[b] %	VM[c] %	EC (ms)	pH	SA ($m^2 \cdot g^{-1}$)	K ($g \cdot kg^{-1}$)	Na ($g \cdot kg^{-1}$)	Ca ($g \cdot kg^{-1}$)	Mg ($g \cdot kg^{-1}$)	P ($g \cdot kg^{-1}$)
RS	N.A.[a]	15.43	7.57	68.58	N.A.	N.A.	N.A.	17.60	0.28	8.34	1.81	0.88
RS-400	47.45	31.87	21.88	38.05	4.70	9.81	270.84	28.31	0.49	11.70	4.31	2.50
RS-500	39.25	35.01	33.30	24.73	5.32	10.89	314.86	38.80	0.69	11.37	5.82	3.22
RS-600	36.35	41.09	33.33	19.16	5.73	11.1	465.21	40.39	0.61	40.51	5.39	3.29
RS-700	36.00	42.16	34.65	17.20	5.77	11.18	404.97	40.69	0.71	11.33	4.90	3.06
DRS	N.A.	43.77	4.48	46.78	N.A.	N.A.	N.A.	5.01	1.21	40.47	5.54	13.74
DRS-400	74.85	57.36	8.07	31.13	0.57	8.6	117.42	6.75	1.62	51.82	7.34	20.19
DRS-500	63.16	64.18	13.95	18.04	0.74	9.12	137.50	6.50	1.57	52.07	7.66	21.03
DRS-600	59.70	69.01	12.46	14.97	0.69	9.52	162.00	8.62	2.04	256.91	9.61	25.38
DRS-700	57.52	70.82	14.76	11.04	0.79	9.73	213.27	8.60	2.12	174.85	8.96	25.61

Note. [a]N.A. means not applicable; [b]FC is fixed carbon; [c]VM is volatile matter.

cellulose and lignin after carbonization. Nevertheless, only one peak of lignin loss appeared at 470°C in DRS-400. A peak of weight loss still could be detected in DRS-500, but RS-500 peak could not be observed in the same area, which again implied the rich-lignin in DRS. With increasing pyrolysis temperature, the weight loss of RSBCs and DRSBCs were weakened within 400–550°C, which due to the carbonization was not complete during carbonization at middle temperature (400 and 500°C), and the residual cellulose and lignin were further pyrolyzed and released as volatile matters. By contrast, the biochars prepared at high temperatures (600 and 700°C) were relatively complete, suggesting relatively higher thermal stability. All biochars had a weak weight loss peak after 650°C, which was mainly due to the decomposition of mineral substances in the ash, for example, $CaCO_3 \rightarrow CaO$ [26]. Overall, DRSBCs have less mass loss compared with RSBCs being obtained at the investigated temperatures, implying relatively higher thermal stability.

3.2.2. Proximate Analysis on the Derived Biochars. As is known, fixed carbon (FC) and volatile matter (VM) can evaluate the biochar stability against the biological degradation [27]. Pyrolysis temperature exhibited a positive correlation with the FC content but negatively affected VM content in the biochar from both of RS and DRS, which were also observed in reference [28]. Overall, FC content decreased 13.8–20.9% in DRSBCs compared with the corresponding RSBCs at the investigated pyrolytic temperatures. Similarly, VM content in DRSBCs was reduced 4.2–6.9%. Ash content enhanced obviously as the pyrolysis temperature was increased, indicating more organic components in the RS and DRS were pyrolyzed at high temperature. Moreover, the ash in DRSBCs was 25.5–29.2% higher in contrast to the corresponding RSBCs, which was consistent to the biochar yield, suggesting biochar yields of RS and DRS were ash-dependent. High amounts of mineral elements, especially higher content of silicon, in rice straw, will lead to high ash content of the derived biochar (RSBCs) [29]. Relatively higher ash content in DRSBCs again indicated the organic fractions was decomposed and retained indigestibility mineral composition during anaerobic digestion process.

3.2.3. Ultimate Analysis. As expected, the elemental contents of H and O were reduced with increasing pyrolysis temperature (see Table S1). The C content in RSBCs was increased from 41.1% to 44.1% as the temperature was elevated from 400°C to 600°C, which was consistent with the biochar produced form traditional lignocellulosic biomass [8]. However, a slight decrease (43.8%) was observed at 700°C. Unlike the traditional lignocellulosic biomass with relatively lower ash content, the C content in DRSBCs exhibited obvious decrease with the increase of pyrolysis temperature. According to many reported works, it could be found that the biomass with lower ash content, and the increased C content with increasing pyrolytic temperature could be observed; however, the contrary results on C content will appear in the higher ash content biomass, such as swine manure, vermicompost, and sludge [19, 30, 31]. Obviously, the mineral fractions in ash-abundant biomass will function as the heat transmitter to intensify the release of volatile matters during pyrolysis [32]. Moreover, the relatively lower organic fraction (most of them were decomposed by biological process) in such substrates will more easily be pyrolyzed into low molecular weight compounds for rapid releasing. The decreased H/C and O/C ratios at higher pyrolysis temperature indicated more stability of RSBC and DRSBC [8]. As for the N content in biochars from RS and DRS, obvious decreases with increasing pyrolysis temperature can be observed, which was due to the volatilization in the form of NOx and NH_3 during the generation of waste gases [33]. However, significant increases also could be observed as the pyrolysis temperature kept increasing to 700°C, which was mainly related to the formation of stable N-derivatives or N-doping into complex structures at relatively higher temperatures [28, 34]. Relatively higher C content in DRSBCs suggested the stable N formation at higher temperature would be related to the ash content. However, the detailed production of stable N still required more investigations.

Besides, the contents of Na, Ca, Mg, and P in RS were all obviously lower than that of DRS. Correspondingly, their contents in the obtained biochars from RS were all lower than that of DRS. However, K content in RS was significantly higher than that of DRS, resulting in its relatively lower

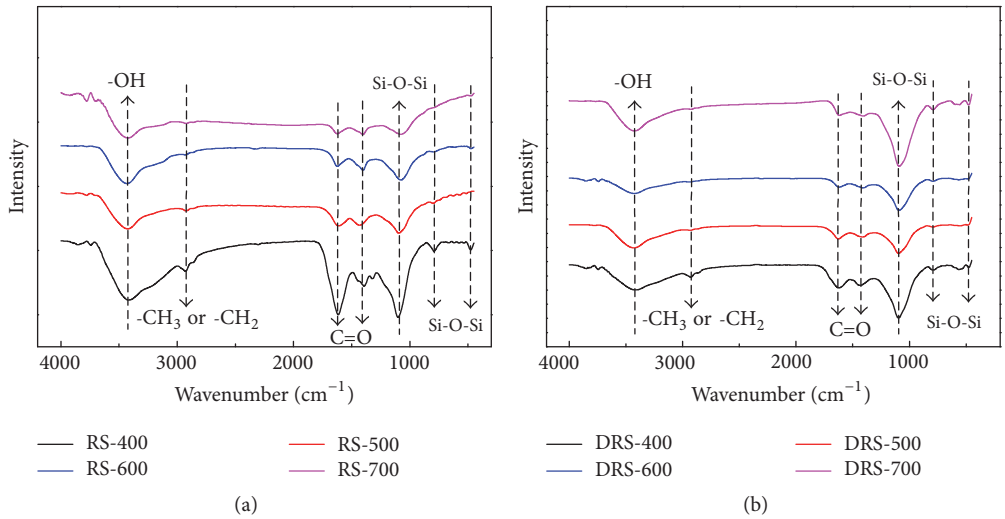

Figure 2: FT-IR spectra for RSBCs and DRSBCs. (a) RSBC; (b) DRSBC.

content in RSBCs correspondingly. These results indicated K in rice straw will be released more in the liquid fraction after anaerobic digestion, and the other investigated elements above will be kept more in the digested solid residue. K as a critical element for catalyzing the melting of silica in rice pyrolysis may affect the crystalline properties of the silicate particles and further the function of the produced biochars [35]. Overall, the content of K, Na, Ca, and Mg in biochar increased with the rising of temperature, indicating that the prepared biochars at high temperature can exhibit ion exchange capacity and can be potentially beneficial to the adsorption of heavy metals via ion exchange. However, the Ca and Mg content in both of RSBCs and DRSBCs reduced significantly at extra higher temperature of 700°C due to the volatilization via pyrolytic gas, and this result was consistent with the previous report on another kind of digested residue of vermicompost [19].

3.2.4. pH, EC, and Functional Groups. As expected, the investigated biochar is alkaline due to the abundance of alkali and alkaline earth metals. Moreover, the increased pH with increasing the pyrolysis temperature could be observed on RSBCs and DRSBCs as the mineral substances, especially the alkaline earth metals, could be decomposed into the corresponding oxides. The pH of DRSBCs was lower than that of RSBCs, which may relate to the relatively lower content of a main alkali metal of K in DRSBCs. In addition, some acid substances like humic acid, which produced in anaerobic fermentation, may also contribute to relatively lower pH in DRSBCs [36]. Overall, the EC enhanced with the increase of temperature, which was positively correlated with the soluble salt content in biochar. Overall, the SA of RSBCs and DRSBCs was increased with the increase of temperature, but a reduction appeared at high temperature (700°C) of RSBC, which was due to the rearrangement of the chemical structure and part of the pore size collapsed at high temperatures [37]. Furthermore, the RSBC produced at different temperatures exhibited typical higher SA compared with that of DRSBC, which may be attributed to the richer lignocellulosic faction in RS, and similar results were also reported in [38]. The scanning electron microscopy images (Figure S2) showed that RSBC had more multiple voids and micropores because of the dehydration of lignocellulose [29]. Conversely, the DRSBC images showed more crystalline and less porous structure, implying a relatively lower lignocellulosic fraction content.

According to the FT-IR spectra of RSBCs and DRSBCs in Figure 2, the band intensities at 3400–3430 cm^{-1} (-OH) and 2850–2950 cm^{-1} (aliphatic CH_2) decreased when the pyrolysis temperature was increased because of the thermal destruction of cellulose, hydroxyl groups, and aliphatic alkyl groups. Similarly, the features (C=O) between 1630 and 1580 cm^{-1} and between 1430 and 1390 cm^{-1} were decreased due to the thermal destruction of aliphatic matter and hydroxyl groups. The aromatic carbon remained after pyrolysis in high temperatures which is more inert than aliphatic carbon under oxidation conditions [39]. Therefore, the high-temperature derived biochars are more recalcitrant and may have lower adsorption capacity. The intensity of carboxylate groups (C=O stretching) are stronger in RSBCs, which can serve as adsorption sites for metals [40]. Thus, RSBCs may have better heavy metal adsorption ability than DRSBCs. 3 features at 1100, 800, and 470 cm^{-1} are assigned to the vibration of Si-O-Si. Si group in RSBCs became less intense with increasing pyrolytic temperature, implying the formation of silicon crystal at high temperature [40]. All biochars exhibit a strong Si-O-Si stretching band, which means RSBCs and DRSBCs could act as a novel silicon source due to its high silicon content [39].

3.3. Pb(II) Adsorption via the Derived Biochars from RS and DRS as Affected by Pyrolysis Temperature. Overall, the considerable Pb(II) removal from aqueous solution could be achieved by RSBCs. According to Figure 3, the adsorption of Pb(II) was promoted significantly as the pyrolysis

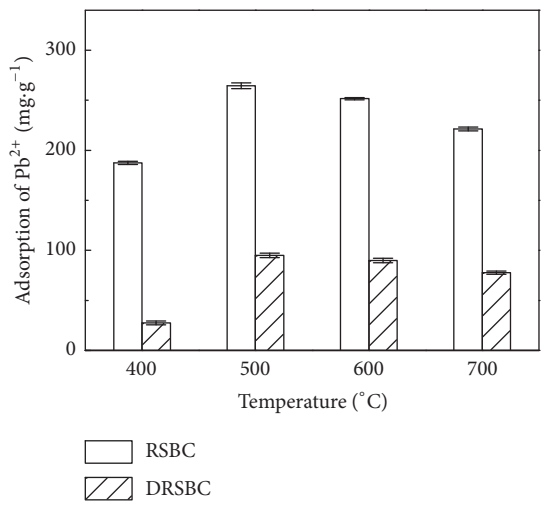

Figure 3: Pb(II) adsorption of biochars obtained at different pyrolysis temperatures.

temperature for producing biochar increased from 400°C to 500°C. The maximum adsorption capacity of 264.4 $mg \cdot g^{-1}$ appeared at RSBCs obtained from 500°C. Afterwards, the adsorption was reduced obviously to 221.3 $mg \cdot g^{-1}$ when pyrolysis temperature was increased to 700°C. Similar effects of pyrolysis temperature on the Pb(II) adsorption also happened on the biochar from DRS. Previous studies have shown the same result that biochar adsorption capacity improved as the pyrolytic temperature from 300°C to 500°C but did not increase when the pyrolysis temperature was kept increasing to 600°C [28]. In addition, the increased Pb(II) adsorption may be related to the increased SA as the pyrolysis temperature was lower than 500°C. Besides, the decreased Pb(II) adsorption was observed as the pyrolysis was higher than 500°C, indicating it may be affected negatively by another action. Previous studies have proved that the adsorption of heavy metals on biochar may be also mainly related to the interaction between surface functional groups and minerals [26]. The decreased oxygen functional groups on these biochars at higher pyrolysis temperature may partially decrease the Pb(II) adsorption (Figure 2). In addition, the Ca, Mg, P, and inorganic elements formed insoluble phosphate and carbonate crystals in high-temperature biochar which could slow the release rate of PO_4^{3-} and CO_3^{2-}, thereby reducing the reaction with Pb(II) via precipitation [41]. Based on these results, the adsorption of Pb(II) by RSBC and DRSBC may be related to the coactions of the development of SA, oxygen functional groups, and the anions involved in precipitation. Apparently, the Pb(II) removal from aqueous solution by DRSBCs was 0.15–0.35 of RSBCs, which may greatly be attributed to the loss of some surface functional groups and soluble salts during anaerobic digestion and the decreased SA as well [42].

3.4. Pb(II) Adsorption Behaviors of RSBC and DRSBC. According to the effects of pyrolysis temperature on Pb(II) adsorption, the biochar produced at 500°C from RS and DRS was selected to elucidate the adsorption behaviors via investigating the isotherms, kinetics, and thermodynamics. As presented in Figure S3a, the adsorption capacity of RSBC and DRSBC was elevated with the increase of initial Pb(II) concentration. The Pb(II) adsorption capacity of RS-500 and DRS-500 rapidly enhanced as the initial concentration of Pb(II) was lower than 500 $mg \cdot L^{-1}$ and 200 $mg \cdot L^{-1}$, respectively. Correspondingly, the Pb(II) could be almost removed completely at these concentrations. However, the adsorption tended to be balanced as Pb(II) initial concentrations kept increasing. This phenomenon was generally depended on the fact that the competitive adsorption for Pb(II) on RSBC and DRSBC surface sites was not obvious at the relatively lower concentrations, while their fiercely competition emerged as the Pb(II) concentration increased greatly. Langmuir (Eq. S1) and Freundlich (Eq. S2) isotherms have been widely accepted to describe the relationship between the concentration of adsorbate on adsorbent surface and in solution at equilibrium. In contrast to the Freundlich model (Figure 4(a) and Table S2), the higher correlation coefficient can be obtained by Langmuir model ($R^2 > 0.83$), demonstrating that the adsorptions of Pb(II) by RS-500 and DRS-500 were both based on monolayer homogeneous adsorption process. The maximum Pb(II) adsorption capacity of RS-500 and DRS-500 was determined as 276.3 and 90.5 $mg \cdot g^{-1}$, respectively, which was typically higher than most of the low cost adsorbents, such as anaerobically digested animal waste biochar (51.4 $mg \cdot g^{-1}$) and sludge biochar (30.9 $mg \cdot g^{-1}$) [43, 44]. This result implied that RSBC and DRSBC exhibited an excellent adsorption ability to remove Pb(II) from aqueous solution. Notably, the removal rate of RS-500 was very low as the initial Pb(II) concentration was less than 100 $mg \cdot L^{-1}$; however, almost no Pb(II) was detected in DRS-500 equilibrium solution even at initial Pb(II) concentration of 20 $mg \cdot L^{-1}$. Therefore, DRSBC should be more suitable for removing Pb(II) at low concentration compared with that of RSBC. The affinities between Pb(II) and biochar can be further predicted by using dimensionless separation factor R_L (Eq. S3). $1 > R_L > 0$, $R_L = 1$ and $R_L > 1$ indicate that the shape of isotherm is favorable, linear, and unfavorable, respectively. According to the RS-500 and DRS-500 parameters of Langmuir, the calculated R_L was 0.56 and 0.046, respectively, suggesting that the adsorption of Pb(II) on RS-500 and DRS-500 was favored.

Pb(II) adsorption of RS-500 was rapidly performed during the initial 2 h, and the removal of Pb(II) exceeded 215 $mg \cdot L^{-1}$ (Figure S3b). However, the adsorption gradually slowed down and reached equilibrium at 12 h. This could be regarded as large amount of vacant adsorption sites on the surface of RSBC were offered at initial stage, and the surface sites were progressive saturation and almost occupied as time was prolonged [43, 44]. Pb(II) adsorption of DRS-500 did not reach adsorption equilibrium in 48 hours, because DRS-500 is a relatively dense massive accumulation structure (Figure S2), which may lead to the adsorption sites be covered, resulting in slower reaction with Pb(II). Additionally, Pb(II) can be adsorbed by the precipitation of the anions released from biochar, and the reaction rate depends on the dissolution rate of the mineral components. Most of the minerals in RSBC are

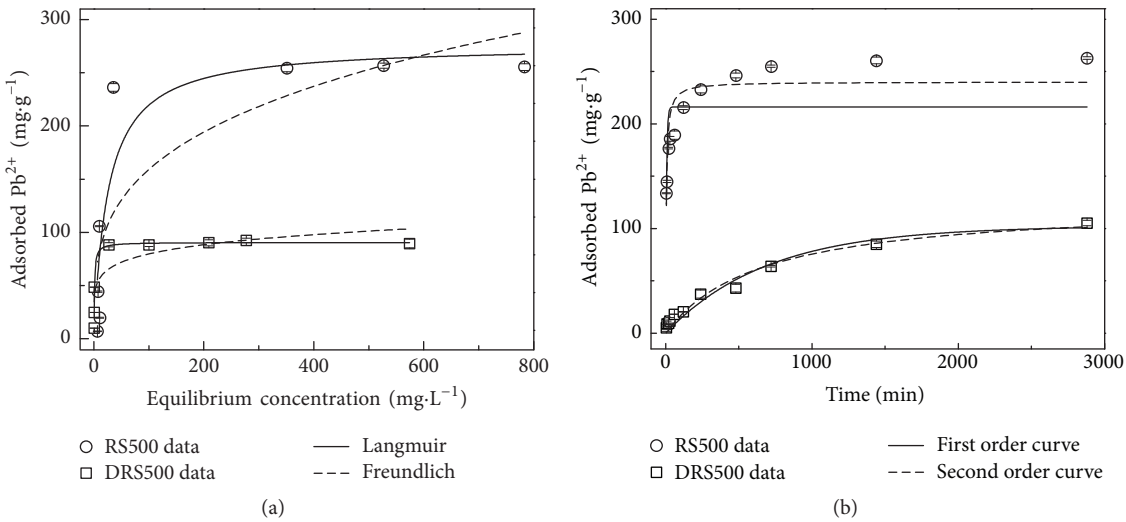

Figure 4: Adsorption isotherms and kinetics of Pb(II) adsorption on biochars: (a) adsorption isotherms of RS-500 and DRS-500; (b) adsorption kinetics of RS-500 and DRS-500.

amorphous and easily soluble mineral salts, which can release anions more easily and faster to precipitate with Pb(II) [41]. However, DRSBC formed more crystalline minerals, which was more difficult to dissolve. Even though a small amount of crystalline minerals can be dissolved, the dissolution rate is relatively slow; thereby the biochar adsorption of Pb(II) became slow. The kinetics of Pb(II) adsorption on RS-500 and DRS-500 were described by first-order (Eq. S4) and second-order (Eq. S5) model (Figure 4(b)), respectively. It can be known that the second-order model gives better simulation on both RS-500 and DRS-500 (Table S3), further confirming that the adsorption rate is greatly governed by chemisorption mechanism [45]. The second-order model (R^2 = 0.96) appeared to better describe adsorption of DRS-500 rather than RS-500 (R^2 = 0.87), partially suggesting that precipitation and inner-sphere surface complexation could also play an important role in Pb(II) adsorption by RS-500.

The Gibbs free energy (ΔG^0), enthalpy (ΔH^0), and entropy (ΔS^0) are generally considered to be important parameters to understand adsorption mechanisms. The equations were exhibited in Eq. S6–Eq. S8 and calculated results were given in Table S4. The values of ΔG^0 were negative to the adsorption temperatures, indicating that the adsorption process is spontaneous. The elevated ΔG^0 with the increasing temperature illustrated that the adsorption process of RS-500 and DRS-500 can be favored by temperature, which can be again proved in Figure S3d. As the temperature was elevated from 15 to 45°C, the Pb(II) adsorption capacity of RS-500 and DRS-500 can be increased from 245.1 $mg \cdot g^{-1}$ to 254.5 $mg \cdot g^{-1}$ and 63.0 $mg \cdot g^{-1}$ to 140.8 $mg \cdot g^{-1}$, respectively. This phenomenon could be attributed to the promoted occasion of collision between adsorption sites and Pb(II) ions at higher adsorption temperature [12]. The ΔH^0 values of RS-500 and DRS-500 were 0.244 $KJ \cdot mol^{-1}$ and 4.038 $KJ \cdot mol^{-1}$, suggesting the adsorption process was endothermic and the random thermal motion of ions in the aqueous solution has significant effects on Pb(II) adsorption of DRSBCs. The values of ΔS^0 were 5.9 and 18.0 $J \cdot mol^{-1} \cdot K^{-1}$, elucidating that RS-500, DRS-500, and Pb(II) were closely combined. In addition, increasing the adsorption temperature can increase the degree of freedom between adsorbate and adsorbed on solid-liquid interface [46]. DRS-500 had high activation entropy values, meaning that DRS-500 is far from its own thermodynamic equilibrium and the system can react faster to produce the activated complex [47]. Thus, complexation may play a more important role in DRSBCs than RSBCs.

Besides, as presented in Figure S3c, the adsorption of Pb(II) by RS-500 was enhanced by pH of solution, indicating that the lower pH resulted in the larger competition interaction between H^+ and Pb(II). Diversely, when the pH increased from 2.0 to 4.0, the DRS-500 adsorption capacity of Pb(II) was decreased from 115.1 $mg \cdot g^{-1}$ to 92.6 $mg \cdot g^{-1}$. In addition, SiO_2 is negatively charged at low pH (pH < 3.0) because its lower isoelectric point and the solution pH also can influence silicon dissolution from biochar [39, 48]. Therefore, the increase of DRS500 adsorption capacity at low pH value is mainly attributed to the contribution of SiO_2 components.

3.5. Potential Mechanisms for Pb(II) Adsorption by RSBC and DRSBC. As stated above, Pb(II) adsorption by RSBC and DRSBC was both decreased slightly as the SA was promoted greatly with the increased pyrolysis temperature. This result suggested the adsorption related to the increased surface area was not dominant. According to the FT-IR results on RSBC and DRSBC before/after Pb(II) adsorption (Figure S4), some bands shift after adsorption indicated the existing interactions between Pb(II) and the functional groups. For example, the shift of the COO- symmetric stretching to lower frequency (1433 → 1405 and 1420 → 1407 cm^{-1}) could be due to the low electron density induced by Pb(II) adsorption on RS-500 and DRS-500, respectively [49]. A

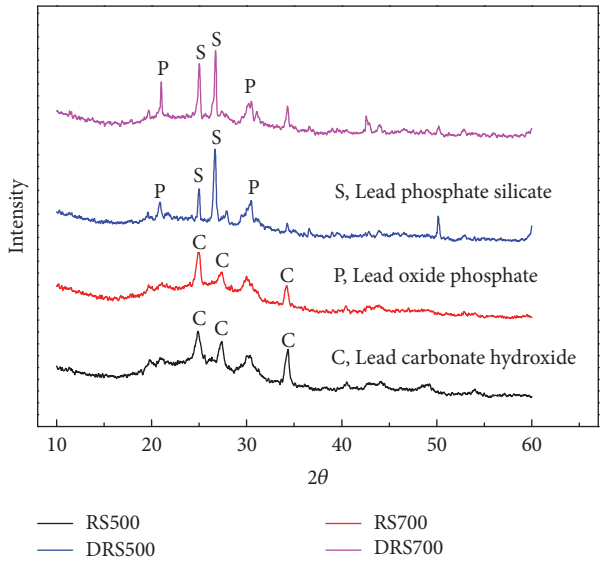

Figure 5: XRD diffraction patterns for RSBC-Pb and DRSBC-Pb.

shift of the COO- asymmetric stretching band to higher frequency (1611 → 1615 and 1622 → 1625 cm^{-1}) was also observed after Pb(II) adsorption on RS-500 and DRS-500, which likely resulted from the protonation of the carboxylate groups [49]. Thus, one possibility for Pb(II) adsorption by biochar from RS and DRS can be described as follows, revealing surface complexation via coordination between the carboxylate groups and Pb(II) is an important path (Eq. (1)).

$$\text{>C-COOH} + Pb^{2+} + H_2O \longrightarrow \text{>C-COOPb}^{+} + H_3O^{+} \quad (1)$$

In addition, the bands at 470, 800, and 1100 cm^{-1} were characteristic of Si-O-Si bend stretching, symmetric stretching, and asymmetric stretching, respectively [50]. After Pb(II) adsorption, these peaks were shifted and became less intense, which indicated that Pb(II) may relate to the existing structure of Si-O-Si; however, the substantial process deserved further investigations.

To further elucidate the interaction between minerals and Pb(II), XRD analysis was also conducted after Pb(II) adsorption as shown in Figure 5. Elemental analysis shows that DRSBC was rich in P, which was much higher than RSBC (Table 1). Previous research has shown that introducing P in biochar induced formation of insoluble lead phosphate minerals in Pb-polluted water [51]. XRD showed the precipitation of crystalline β-$Pb_9(PO_4)_6$ formation in DRS-500 after Pb(II) adsorption. Similarly, β-$Pb_9(PO_4)_6$ was also found in previous study on Pb(II) sorption on biochar converted from dairy manure [52]. The potential action process of the released phosphate from DRSBC with Pb(II) in aqueous solution can be deduced as the following equation to form stable minerals:

$$6HPO_4^{2-} + 9Pb^{2+} + 6OH^{-} \longrightarrow Pb_9(PO_4)_6 + 6H_2O \quad (2)$$

Besides, a sharp peak of $PbO{\cdot}P_2O_5{\cdot}SiO_2$ (lead phosphate silicate), with the typical 26.68 in the 2θ degree, was observed in Figure 5. The lead phosphate silicate precipitation was also reported by previous study [53]. The formation of lead phosphate silicate may be attributed to the reactions with lead and crystalline silica and phosphate on DRSBC, which may be the following reaction:

$$2HPO_4^{2-} + Pb^{2+} + SiO_2 \longrightarrow PbO{\cdot}P_2O_5{\cdot}SiO_2 + 2OH^{-} \quad (3)$$

However, only one lead precipitate $Pb_3(CO_3)_2(OH)_2$ (hydrocerussite) was found on the postsorption RSBC. We hypothesized that higher lead removal by RSBC may be attributed to formation of Pb-carbonate precipitate, which was confirmed by three hydrocerussite peaks in XRD. Contrary to DRSBC, higher pH (Table 1) and carbonate concentrations allowed for precipitation of hydrocerussite, which can be described as follows:

$$2HCO_3^{-} + 3Pb^{2+} + 4OH^{-} \longrightarrow Pb_3(CO_3)_2(OH)_2 + 2H_2O \quad (4)$$

Silica is also a major mineral component in rice straw [53], but there was no Pb-Si precipitation found on the postsorption RSBC. Based on these results, the interactions of Si-rich minerals with Pb(II) probably depend on Si crystallinity and the distinct crystalline substances in DRSBC, which may result from the elimination of K element [40]. Because K is a critical element to catalyze the melting of silica [35], the silicate particles in RSBC were more amorphous than DRSBC, which was potentially supported by the observations from SEM and XRD. In addition, the inferior removal rate of RS-500 at lower initial Pb(II) concentration (Figure S3a) is probably because solution calcium and magnesium remained unchanged till Pb > 0.5 mM [52]. Increased Ca^{2+} and Mg^{2+} are attributed to the dissolution of some Mg-substituted calcite [26], which also can provide more carbonate for hydrocerussite precipitation.

4. Conclusions

Biochars obtained from anaerobically digested rice straw (DRSBCs) showed lower pH value and potassium content, but higher yield, nitrogen, phosphorous content, and carbon stability compared with the biochars derived from rice straw (RSBCs). The biochars obtained at 500°C from both DRS and RS exhibited the highest performance for removing Pb(II) from aqueous solution. However, Pb(II) removal by RSBCs was typically higher than those of DRSBCs by 2.8–6.5-folds. As biochars produced at 500°C were selected, the maximum adsorption capacity of RSBC and DRSBC to Pb(II) arrived at 276.3 and 90.5 $mg{\cdot}g^{-1}$, respectively, according to the Langmuir model. Carbonates and carboxylates were contributed for the relatively higher adsorption capacity of RSBC. Pb(II) adsorption of DRSBC was dominated via forming phosphate silicates precipitation and complexing with carboxylate groups.

Conflicts of Interest

The authors declare that they have no conflicts of interest in this work.

Acknowledgments

This work is supported by the National Science & Technology Pillar Program (2015BAD21B03), the Special Fund for Agro-Scientific Research in the Public Interest (201403019), and the Agricultural Science and Technology Innovation Program (ASTIP) of Chinese Academy of Agricultural Sciences. Department of Science and Technology of Sichuan Province is also appreciated for funding supports (nos. 2017HH0047, 17ZDYF2972, and 2015NZ0100).

Supplementary Materials

(1) Supplementary Equation List: Supplementary Eq. 1: Langmuir model for Pb adsorption isotherm; Supplementary Eq. 2: Freundlich model for Pb adsorption isotherm; Supplementary Eq. 3: separation factor based on Langmuir model; Supplementary Eq. 4: the first-order model for Pb adsorption kinetics; Supplementary Eq. 5: the second-order model for Pb adsorption kinetics; Supplementary Eq. 6: model for Gibbs free energy; Supplementary Eq. 7: calculation for partition coefficient; Supplementary Eq. 8: linearized model for Gibbs free energy. (2) Supplementary Figures: Supplementary Figure 1: TG-DTG curves of biochars obtained at different temperatures; Supplementary Figure 2: the images of RSBCs and DRSBCs under the scope of SEM; Supplementary Figure 3: influences of reaction conditions, including initial concentration, temperature, duration, and pH, on Pb adsorption by RS-500 and DRS-500; Supplementary Figure 4: FT-IR spectra of the biochars of RS500 and DRS500 (after Pb adsorption). (2) Supplementary Tables: Supplementary Table 1: the results of elemental analysis of biochars produced at different temperatures; Supplementary Table 2: the calculated isotherm parameters of Pb adsorption on the biochars of RS-500 and DRS-500; Supplementary Table 3: the calculated kinetic parameters of Pb adsorption on the biochars of RS-500 and DRS-500; Supplementary Table 4: the calculated thermodynamic parameters of Pb adsorption on the biochars of RS-500 and DRS-500. *(Supplementary Materials)*

References

[1] S. Muthayya, J. D. Sugimoto, S. Montgomery, and G. F. Maberly, "An overview of global rice production, supply, trade, and consumption," *Annals of the New York Academy of Sciences*, vol. 1324, no. 1, pp. 7–14, 2014.

[2] R. Singh, M. Srivastava, and A. Shukla, "Environmental sustainability of bioethanol production from rice straw in India: A review," *Renewable & Sustainable Energy Reviews*, vol. 54, pp. 202–216, 2016.

[3] E. M. Hanafi, H. H. El Khadrawy, W. M. Ahmed, and M. M. Zaabal, "Some observations on rice straw with emphasis on updates of its management," *World Applied Sciences Journal*, vol. 16, no. 3, pp. 354–361, 2012.

[4] Y. Miura, T. Kanno, and Y. Miura, "Emissions of trace gases (co2, co, ch4, and n2o) resulting from rice straw burning," *Soil Science & Plant Nutrition*, vol. 43, no. 4, pp. 849–854, 1997.

[5] Y. Oladosu, M. Y. Rafii, N. Abdullah et al., "Fermentation quality and additives: a case of rice straw silage," *BioMed Research International*, vol. 2016, Article ID 7985167, 2016.

[6] C. M. Liu, A. C. Wachemo, H. R. Yuan et al., "Evaluation of methane yield using acidogenic effluent of NaOH pretreated corn stover in anaerobic digestion," *Journal of Renewable Energy*, vol. 116, pp. 224–233, 2017.

[7] M. I. Inyang, B. Gao, Y. Yao et al., "A review of biochar as a low-cost adsorbent for aqueous heavy metal removal," *Critical Reviews in Environmental Science and Technology*, vol. 46, no. 4, pp. 406–433, 2016.

[8] L. Ye, J. Zhang, J. Zhao, Z. Luo, S. Tu, and Y. Yin, "Properties of biochar obtained from pyrolysis of bamboo shoot shell," *Journal of Analytical and Applied Pyrolysis*, vol. 114, pp. 172–178, 2015.

[9] D. Mohan, A. Sarswat, Y. S. Ok, and C. U. Pittman, "Organic and inorganic contaminants removal from water with biochar, a renewable, low cost and sustainable adsorbent—a critical review," *Bioresource Technology*, vol. 160, pp. 191–202, 2014.

[10] Q. Cheng, Q. Huang, S. Khan et al., "Adsorption of Cd by peanut husks and peanut husk biochar from aqueous solutions," *Ecological Engineering*, vol. 87, pp. 240–245, 2016.

[11] J. H. Park, Y. S. Ok, S. H. Kim et al., "Competitive adsorption of heavy metals onto sesame straw biochar in aqueous solutions," *Chemosphere*, vol. 142, pp. 77–83, 2016.

[12] Z. Wang, F. Shen, D. Shen, Y. Jiang, and R. Xiao, "Immobilization of Cu2 + and Cd2 + by earthworm manure derived biochar in acidic circumstance," *Journal of Environmental Sciences*, vol. 53, pp. 293–300, 2017.

[13] A. Mukherjee, A. R. Zimmerman, and W. Harris, "Surface chemistry variations among a series of laboratory-produced biochars," *Geoderma*, vol. 163, no. 3-4, pp. 247–255, 2011.

[14] C. Kirbiyik, A. E. Putun, and E. Putun, "Comparative studies on adsorptive removal of heavy metal ions by biosorbent, biochar and activated carbon obtained from low cost agro-residue," *Water Science and Technology*, vol. 73, no. 2, pp. 423–436, 2016.

[15] X. L. Dong, L. Q. Ma, and Y. C. Li, "Characteristics and mechanisms of hexavalent chromium removal by biochar from sugar beet tailing," *Journal of Hazardous Materials*, vol. 190, no. 1–3, pp. 909–915, 2011.

[16] Z. Liu and F. Zhang, "Removal of lead from water using biochars prepared from hydrothermal liquefaction of biomass," *Journal of Hazardous Materials*, vol. 167, no. 1–3, pp. 933–939, 2009.

[17] D. Mohan, C. U. Pittman Jr., M. Bricka et al., "Sorption of arsenic, cadmium, and lead by chars produced from fast pyrolysis of wood and bark during bio-oil production," *Journal of Colloid and Interface Science*, vol. 310, no. 1, pp. 57–73, 2007.

[18] O. R. Harvey, B. E. Herbert, R. D. Rhue, and L. Kuo, "Metal interactions at the biochar-water interface: Energetics and structure-sorption relationships elucidated by flow adsorption microcalorimetry," *Environmental Science & Technology*, vol. 45, no. 13, pp. 5550–5556, 2011.

[19] G. Yang, Z. Wang, Q. Xian et al., "Effects of pyrolysis temperature on the physicochemical properties of biochar derived from vermicompost and its potential use as an environmental amendment," *RSC Advances*, vol. 5, no. 50, pp. 40117–40125, 2015.

[20] S. H. Ho, Y. D. Chen, Z. K. Yang, D. Nagarajan, J. S. Chang, and N. Q. Ren, "High-efficiency removal of lead from wastewater by

biochar derived from anaerobic digestion sludge," *Bioresource Technology*, 2017.

[21] D. Zhou, S. Ghosh, D. Zhang et al., "Role of Ash Content in Biochar for Copper Immobilization," *Environmental Engineering Science*, vol. 33, no. 12, pp. 962–969, 2016.

[22] R. Bura, S. D. Mansfield, J. N. Saddler, and R. J. Bothast, "SO2-catalyzed steam explosion of corn fiber for ethanol production," *Applied Biochemistry and Biotechnology - Part A Enzyme Engineering and Biotechnology*, vol. 98-100, pp. 59–72, 2002.

[23] C. M. Elsik, B. Devisetty, and S. W. Dean, "Round-Robin Evaluation of ASTM Standard Test Method E2798 for Spray Drift Reduction Adjuvants," *Journal of ASTM International*, vol. 8, no. 8, p. 103719, 2011.

[24] D. Chen, J. Zhou, and Q. Zhang, "Effects of heating rate on slow pyrolysis behavior, kinetic parameters and products properties of moso bamboo," *Bioresource Technology*, vol. 169, pp. 313–319, 2014.

[25] Y. Yao, B. Gao, M. Inyang et al., "Biochar derived from anaerobically digested sugar beet tailings: characterization and phosphate removal potential," *Bioresource Technology*, vol. 102, no. 10, pp. 6273–6278, 2011.

[26] X. Cao and W. Harris, "Properties of dairy-manure-derived biochar pertinent to its potential use in remediation," *Bioresource Technology*, vol. 101, no. 14, pp. 5222–5228, 2010.

[27] F. Ronsse, S. van Hecke, D. Dickinson, and W. Prins, "Production and characterization of slow pyrolysis biochar: influence of feedstock type and pyrolysis conditions," *GCB Bioenergy*, vol. 5, no. 2, pp. 104–115, 2013.

[28] Z. Wang, H. Guo, F. Shen et al., "Biochar produced from oak sawdust by Lanthanum (La)-involved pyrolysis for adsorption of ammonium (NH4+), nitrate (NO3-), and phosphate (PO43-)," *Chemosphere*, vol. 119, pp. 646–653, 2015.

[29] S. Kizito, S. Wu, W. Kipkemoi Kirui et al., "Evaluation of slow pyrolyzed wood and rice husks biochar for adsorption of ammonium nitrogen from piggery manure anaerobic digestate slurry," *Science of the Total Environment*, vol. 505, pp. 102–112, 2015.

[30] K. B. Cantrell, P. G. Hunt, M. Uchimiya, J. M. Novak, and K. S. Ro, "Impact of pyrolysis temperature and manure source on physicochemical characteristics of biochar," *Bioresource Technology*, vol. 107, pp. 419–428, 2012.

[31] Y. Sun, B. Gao, Y. Yao et al., "Effects of feedstock type, production method, and pyrolysis temperature on biochar and hydrochar properties," *Chemical Engineering Journal*, vol. 240, pp. 574–578, 2014.

[32] P. Devi and A. K. Saroha, "Simultaneous adsorption and dechlorination of pentachlorophenol from effluent by Ni-ZVI magnetic biochar composites synthesized from paper mill sludge," *Chemical Engineering Journal*, vol. 271, pp. 195–203, 2015.

[33] M. Stefaniuk and P. Oleszczuk, "Characterization of biochars produced from residues from biogas production," *Journal of Analytical and Applied Pyrolysis*, vol. 115, pp. 157–165, 2015.

[34] J. W. Gaskin, C. Steiner, K. Harris, K. C. Das, and B. Bibens, "Effect of low-temperature pyrolysis conditions on biochar for agricultural use," *Transactions of the ASABE*, vol. 51, no. 6, pp. 2061–2069, 2008.

[35] W. Wang, J. C. Martin, N. Zhang, C. Ma, A. Han, and L. Sun, "Harvesting silica nanoparticles from rice husks," *Journal of Nanoparticle Research*, vol. 13, no. 12, pp. 6981–6990, 2011.

[36] M. Ahmad, D. H. Moon, M. Vithanage et al., "Production and use of biochar from buffalo-weed (*Ambrosia trifida* L.) for trichloroethylene removal from water," *Journal of Chemical Technology and Biotechnology*, vol. 89, no. 1, pp. 150–157, 2014.

[37] T. J. Kinney, C. A. Masiello, B. Dugan et al., "Hydrologic properties of biochars produced at different temperatures," *Biomass & Bioenergy*, vol. 41, pp. 34–43, 2012.

[38] K. W. Jung, K. Kim, T. U. Jeong, and K. H. Ahn, "Influence of pyrolysis temperature on characteristics and phosphate adsorption capability of biochar derived from waste-marine macroalgae (Undaria pinnatifida roots)," *Bioresource Technology*, vol. 200, pp. 1024–1028, 2016.

[39] X. Xiao, B. Chen, and L. Zhu, "Transformation, morphology, and dissolution of silicon and carbon in rice straw-derived biochars under different pyrolytic temperatures," *Environmental Science & Technology*, vol. 48, no. 6, pp. 3411–3419, 2014.

[40] L. Qian and B. Chen, "Dual role of biochars as adsorbents for aluminum: The effects of oxygen-containing organic components and the scattering of silicate particles," *Environmental Science & Technology*, vol. 47, no. 15, pp. 8759–8768, 2013.

[41] H. Zheng, Z. Wang, X. Deng et al., "Characteristics and nutrient values of biochars produced from giant reed at different temperatures," *Bioresource Technology*, vol. 130, pp. 463–471, 2013.

[42] J. De Vrieze, A. M. Saunders, Y. He et al., "Ammonia and temperature determine potential clustering in the anaerobic digestion microbiome," *Water Research*, vol. 75, pp. 312–323, 2015.

[43] M. Inyang, B. Gao, Y. Yao et al., "Removal of heavy metals from aqueous solution by biochars derived from anaerobically digested biomass," *Bioresource Technology*, vol. 110, pp. 50–56, 2012.

[44] W. Zhang, S. Mao, H. Chen, L. Huang, and R. Qiu, "Pb(II) and Cr(VI) sorption by biochars pyrolyzed from the municipal wastewater sludge under different heating conditions," *Bioresource Technology*, vol. 147, pp. 545–552, 2013.

[45] S. A. Baig, J. Zhu, N. Muhammad, T. Sheng, and X. Xu, "Effect of synthesis methods on magnetic Kans grass biochar for enhanced As(III, V) adsorption from aqueous solutions," *Biomass & Bioenergy*, vol. 71, pp. 299–310, 2014.

[46] M. Kiliç, Ç. Kirbiyik, Ö. Çepelioğullar, and A. E. Pütün, "Adsorption of heavy metal ions from aqueous solutions by biochar, a by-product of pyrolysis," *Applied Surface Science*, vol. 283, pp. 856–862, 2013.

[47] Y. Xu and B. Chen, "Investigation of thermodynamic parameters in the pyrolysis conversion of biomass and manure to biochars using thermogravimetric analysis," *Bioresource Technology*, vol. 146, pp. 485–493, 2013.

[48] M. Waseem, S. Mustafa, A. Naeem, G. J. M. Koper, and Salah-Ud-Din, "Physiochemical properties of mixed oxides of iron and silicon," *Journal of Non-Crystalline Solids*, vol. 356, no. 50-51, pp. 2704–2708, 2010.

[49] Y. Xu and B. Chen, "Organic carbon and inorganic silicon speciation in rice-bran-derived biochars affect its capacity to adsorb cadmium in solution," *Journal of Soils and Sediments*, vol. 15, no. 1, pp. 60–70, 2014.

[50] P. Lu and Y. L. Hsieh, "Highly pure amorphous silica nano-disks from rice straw," *Powder Technology*, vol. 225, pp. 149–155, 2012.

[51] X. D. Cao, L. Q. Ma, M. Chen, S. P. Singh, and W. G. Harris, "Impacts of phosphate amendments on lead biogeochemistry at a contaminated site," *Environmental Science & Technology*, vol. 36, no. 24, pp. 5296–5304, 2002.

[52] X. Cao, L. Ma, B. Gao, and W. Harris, "Dairy-manure derived biochar effectively sorbs lead and atrazine," *Environmental Science & Technology*, vol. 43, no. 9, pp. 3285–3291, 2009.

[53] H. Lu, W. Zhang, Y. Yang, X. Huang, S. Wang, and R. Qiu, "Relative distribution of Pb^{2+} sorption mechanisms by sludge-derived biochar," *Water Research*, vol. 46, no. 3, pp. 854–862, 2012.

Hindawi
International Journal of Polymer Science
Volume 2017, Article ID 9850814, 9 pages
https://doi.org/10.1155/2017/9850814

Research Article

Preparation and Characterization of Nanofibrillated Cellulose from Bamboo Fiber via Ultrasonication Assisted by Repulsive Effect

Zhijun Hu, Rui Zhai, Jing Li, Yan Zhang, and Jiang Lin

Zhejiang Province Collaborative Innovation Center of Agricultural Biological Resources Biochemical Manufacturing, Zhejiang University of Science and Technology, Hangzhou 310023, China

Correspondence should be addressed to Zhijun Hu; huzhijun@zju.edu.cn

Received 7 September 2017; Accepted 19 November 2017; Published 26 December 2017

Academic Editor: Xiaofei Tian

Nanofibrillated celluloses (NFCs) have recently drawn much attention because of their exceptional physicochemical properties. However, the existing preparation procedures either produce low yields or severely degrade the cellulose and, moreover, are not energy efficient. The purpose of this study was to develop a novel process using ultrasonic homogenization to isolate fibrils from bamboo fiber (BF) with the assistance of negatively charged entities. The obtained samples were characterized by the degree of substitution (DS) of carboxymethyl, Fourier-transform infrared (FT-IR) spectroscopy, X-ray diffraction (XRD), thermogravimetric analysis, and transmission electron microscopy (TEM). The results showed that an NFC yield could be obtained above 70% through this route. The enzyme hydrolysis could enhance the surface charge of the fiber, and mechanical activation facilitates an increase in the DS. The disintegrating efficiency of the cellulose fibrils significantly depended on the input power of ultrasonication and the DS. FT-IR spectra confirmed the occurrence of the carboxymethylation reaction based on the appearance of the characteristic signal for the carboxyl group. From XRD analysis, it was observed that the presence of the carboxyl groups makes the isolation more efficient attributed to the ionic repulsion between the carboxylate groups of the cellulose chains.

1. Introduction

In recent years, much more attention has been paid to the sustainable, green, and environmental friendly materials because of the increasing public interest in environmental issues and the growing pressure from legislative institutions [1, 2]. Cellulose is the most abundant renewable natural biopolymer on earth and is present in a wide variety of living species such as plants, animals, and some bacteria. Cellulose is a multifunctional raw material which can self-assemble into well-defined architectures at multiple scales, from nano- to microsize, and is expected to be able to replace many nonrenewable materials [3]. Cellulose does not occur as an isolated individual molecule in nature, but it is found as assemblies of individual cellulose chain-forming fiber cell wall. Higher plants form highly crystalline cellulose microfibrils, each of which consists of 30–40 fully extended and linear cellulose chains and are the elements with the second smallest width (~3 nm) after single cellulose chains [4]. Plant cell walls are comprised of cellulose microfibrils filled with hemicelluloses and lignin. The microfibrils are so tightly hooked to one another by multiple hydrogen bonds, that their extraction has proven extremely difficult. By using harsh aqueous mechanical or chemical treatment, wood fiber can be degraded and opened into their substructural units giving a material such as microfiber and nanofiber.

The term "nanocellulose" generally refers to cellulosic materials having at least one dimension in the nanometer range. There are two major structures, namely, nanofibrillated cellulose (NFC) and nanocrystalline cellulose (NCC), as shown in Figure 1. The dissimilarity is related to their morphology. NCC can be regarded as the crystalline regions of the NFC. NCC, showing a short rod-like shape 100 to 200 nm in length and 4 to 25 nm in diameter, has been extensively

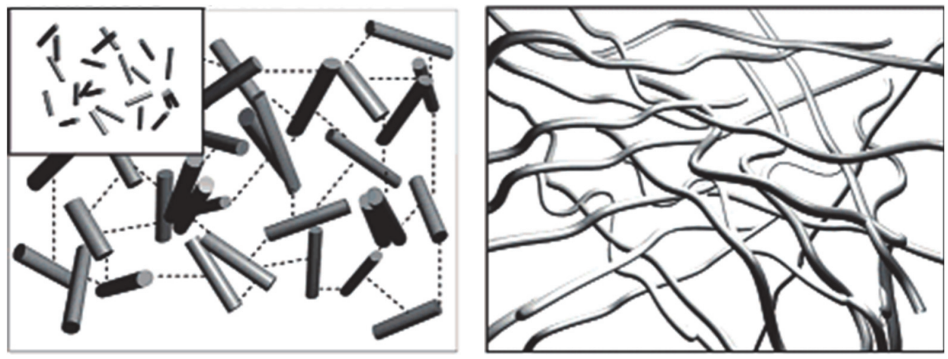

(a) Nanocrystalline cellulose (NCC) L = 100–300 nm (b) Nanofibrillated cellulose (NFC) L = several μm

Figure 1: Diagram of NCC and NFC.

isolated by acid hydrolysis treatment [5]. NFC has a diameter below 100 nm and a length of several microns, which can be isolated by mechanical processes [6].

NFCs consist of a long web-like structure displaying exceptional mechanical properties [7] including a high Young's modulus, a high strength, and a very low coefficient of thermal expansion. NFCs have attracted great interests for its combination with a suitable matrix polymer for high-quality specialty applications of bio-based composites. Therefore, the development of effective methods for extracting NFCs from biomass has received an arising interest.

NFCs were normally produced by mechanical disintegration using either super-grinders [8], high-pressure homogenizers [9], high-pressure microfluidizer [10], or through cryocrushing [11]. However, the mechanical disintegration of the fibers into nanofibers often involves several passes through the disintegration device leading to the high energy consumption. Single disintegrating method suffers from two major drawbacks. The first challenge is the relatively low yields. The second is hydrophilic nature of cellulose causing irreversible agglomeration during drying and compounding in nonpolar matrices.

Combination of two or more methods presents a promising approach to overcome the above drawbacks. Researchers have combined various pretreatments with some suitable mechanical fibrillation technique, including the use of refining [12], enzymes [13], alkaline-acid treatment [14], ionic liquid treatment [15], and chemical modification [16, 17]. Among these methods, chemical modification, involving the addition of negatively charged entities at the microfibril surface, has attained considerable interest in the scientific community including the 2,2,6,6-tetramethylpiperidine-1-oxyl (TEMPO) mediated oxidation [18] and carboxymethylation [19]. These are expected to result in NFC systems with smaller particle size distributions due to the high amount of charges as compared with other pretreatment processes [20, 21]. The charges and their repulsive effect can greatly enhance the ease of separation and dispersion of individual microfibrils at a lower power consumption rate. However, a critical drawback associated with TEMPO is the negative environmental impact due to the use of sodium hypochlorite and sodium bromide as catalyst. Carboxymethylation has been used for the commercial production of sodium carboxymethyl cellulose (CMC), so its impact on the environment can be easily controlled or eliminated. Hence, carboxymethylation is a relatively environmentally friendly pretreatment for carrying out the fibrillation of cellulose fibers at low energies. Accordingly, this study investigates the extraction of nanofibrillated cellulose (NFC) from natural bamboo fiber under pulsed carboxymethylation.

Recently, the ultrasonic technique has been applied to isolate cellulose nanofibers and it has attracted considerable attention [22, 23]. The effect of ultrasonication in degrading polysaccharide linkages has been well described [24]. Ultrasonication is the application of sound energy to physical and chemical systems. Ultrasound produces its effects mainly through cavitation, which can introduce much effect such as intense shear forces, shock waves, and microjets, and generates localized hot spots with very high temperatures, pressures, and heating/cooling rates [25, 26]. Such extreme environments provide a unique platform to break the strong cellulose interfibrillar hydrogen bonding, allowing nanofibers to be gradually disintegrated [24, 27].

Existing procedures for the production of NFC either result in low yields or severely degrade the cellulose and, moreover, are not environmentally friendly or energy efficient. In the present work, a novel route was developed for the preparation of water-redispersible NFC from bamboo fiber (BF). It consists of four steps including mechanical refining (R), enzyme treatment (E), carboxymethyl modification (CM), and ultrasonic homogenization (S). The bamboo fiber was disintegrated mainly by the effect of ultrasonication with the assistance of negative charges. The resulting samples were analyzed by charge titration, Fourier-transform infrared (FT-IR) spectroscopy, X-ray diffraction (XRD), thermogravimetric analysis (TGA), and transmission electron microscopy (TEM) to further investigate their chemical structure and morphology.

2. Materials and Methods

2.1. Materials. Raw bamboo was obtained from local farmers in Anji, Zhejiang province, China. Enzyme was obtained from Tianjin Changwei Biological Technology Co., Ltd.,

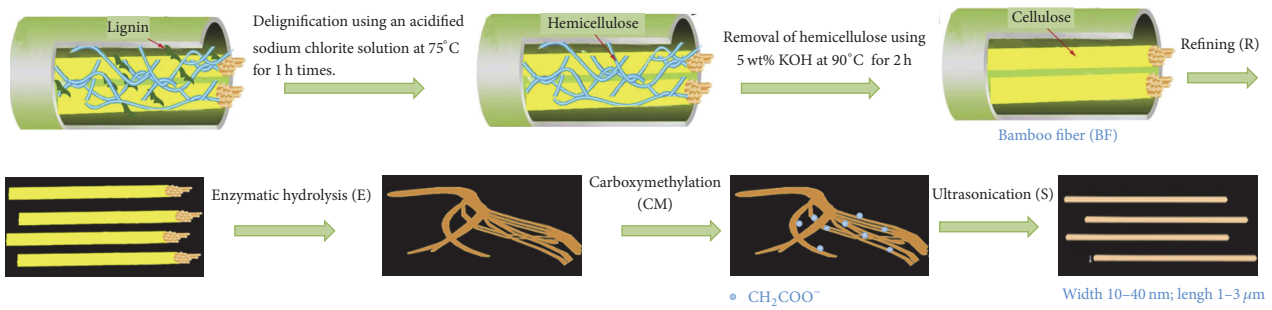

Figure 2: The individualization of bamboo fiber nanofibers from bamboo powders with typical laboratory-scale ultrasonication apparatus under neutral conditions.

and the cellulolytic activity was 1000 EGU/g (EGU means endoglucanase unit). Monochloroacetic acid (MCA) (sodium salt, purity ≥ 98%, M = 116.48 g/mol) was purchased from Aladdin. All other chemicals used were of ACS reagent grade and purchased from Hangzhou Huipu Co., Ltd. Deionized water was used for all the experiments.

2.2. Preparation of Bamboo Fibre (BF) and Nanocrystalline Cellulose (NFC). The process of isolating nanocrystalline cellulose (NFC) from bamboo fiber consists of a series of chemical treatments and high-intensity ultrasonication according to the flowchart shown in Figure 2. First, treatment with acidified sodium chlorite was carried out at 75°C for 1 hr, which was repeated five times until the product became white. The major lignin was then removed following the method of Abe and Yano [28]. Next, an alkaline treatment with potassium hydroxide (KOH) was conducted to remove the hemicelluloses, residual starch, and pectin. The obtained bleached bamboo fiber was labelled as BF.

The cell wall delamination of the BF was carried out in four steps: a refining (R) step to increase the accessibility of the cell wall to the subsequent endoglucanase treatment, an enzymatic treatment (E) step, a low degree of substitution carboxymethylation (CM) stage, and finally the treatment of the pulp slurry by ultrasonic homogenization (S). The above samples were labeled as BF-R, BF-E, BF-CM, and BF-S, respectively. In the enzymatic treatment, a total of 5 g BF, 200 mL acetate buffer solution (pH = 4.8), and enzyme were added into a conical flask. Enzymatic hydrolysis was performed at 50°C and continuously stirred using a water bath. Subsequently, the samples were carboxymethylated, under specific conditions which are detailed in the literature [20]. In brief, the fibers were first dispersed in deionized water at 10,000 revolutions in an ordinary laboratory disperser. The fibers were then solvent-exchanged with ethanol by washing the fibers in ethanol four times with an intermediate filtration step. The fibers were then impregnated in a solution of 2% MCA in 500 mL isopropanol for 30 min. This mixture was transferred to a 5 L reaction vessel equipped with reflux and containing a heated solution of 16.2 g NaOH in a mixture of 3/5 v/v ethanol/isopropanol. The carboxymethylation reaction was allowed to continue for 1 hr. Finally, the samples were further treated by ultrasonic homogenization (S), after dispersion in 500 ml of deionized water at a final concentration of 1.5% w/w. The ultrasonic treatment was carried out in an ice bath to avoid overheating of the sample. The input power of ultrasonication was varied from 400 to 1200 W. After ultrasonication, the suspension was concentrated by centrifugation at 5,000 rpm for 30 min [29]. The colloidal suspension of NFC was collected and freeze-dried for testing.

2.3. Determination of the Degree of Substitution (DS) of Carboxylate Group. Conductometric titration (CT) was used to determine the DS of carboxymethylated BF following the protocol [30]. 0.1 M aqueous hydrochloric acid (HCl) solution was added to the fiber suspension and stirred with a magnetic bar. The conductivity of the suspension was measured upon titration with 0.1 M aqueous NaOH solution, using a conductometer. The measurements were repeated three times for each sample. The titration curves showed the presence of a strong acid corresponding to the excess of HCl and a weak acid corresponding to the carboxylate content. The total amount of carboxymethyl (CM) groups and DS were calculated from

$$n_{\mathrm{CM}} = (V_1 - V_0)\, C_{\mathrm{NaOH}}, \tag{1}$$

$$\mathrm{DS} = \frac{162 \times n_{\mathrm{CM}}}{m - 58 n_{\mathrm{CM}}} \times 100\%, \tag{2}$$

where n_{CM} is the carboxymethyl content, V_1 and V_0 are the equivalent volumes of added NaOH solution, C_{NaOH} is the exact concentration of NaOH solution, and m is the weight of dried product.

2.4. Determination of NFC Yield. The ultrasonic sample was collected and washed with sufficient deionized water by repeating the centrifugation and dilution processes until its pH was neutral, and then the sample was freeze-dried for 48 hr. The yield of NFCs was calculated as follows:

$$Y = \frac{(m_1 - m_2)\, V_1}{m V_2} \times 100\%, \tag{3}$$

where Y is the yield of NFCs, m_1 is the total mass of vacuum freeze-dried NFC and weight bottle, m_2 is the mass of the weight bottle, and m is the mass of BF.

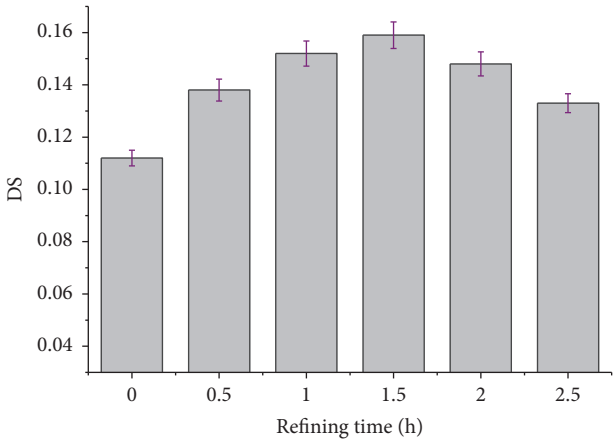

Figure 3: Effect of refining time on DS of cellulose.

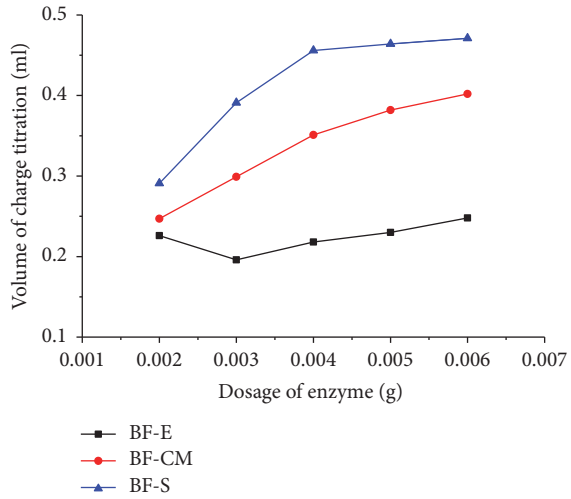

Figure 4: Effect of treatments on the surface charge.

2.5. X-Ray Diffraction (XRD). For each sample, three pellets were prepared by applying 3 t of weight to 750 mg of powder for 2 min. The pellets were measured in reflection mode, using an X'Pert Pro diffractometer from Panalytical (Almelo, Netherlands) with Cu Karadiation ($k = 1.5418$ A˚) in combination with a linear detector system (X'Celerator).

2.6. Fourier-Transform Infrared (FT-IR) Spectroscopy. The spectra were recorded using IRTracer-100 6000 Spectrometer in single reflection diamond ATR (Attenuated Total Reflectance) mode. The number of scans was 32 and the resolution was 4 cm^{-1}. The absorbance measurements were carried out within the range of 500 and 4000 cm^{-1}. They were all carried out in at least duplicate.

2.7. Thermogravimetry Analysis (TGA). Thermogravimetric analysis (TGA) was performed to compare the degradation characteristics of the cellulose fibers at each stage. The thermal stability of each sample was determined using a thermogravimetric analyzer (Pyris6, Perkin-Elmer, USA) with a heating rate of 5˚C/min.

2.8. TEM Observations. Dispersions of celluloses in water were observed using a photomicroscope (Olympus BX50). A 10 μL aliquot of the 0.01% (w/v) cellulose dispersion was mounted on a glow-discharged carbon-coated electron microscopy grid. The sample grid was observed at 100 kV using a JEOL electron microscope (JEM 2000-EXII).

3. Results and Discussion

3.1. Effect of Refining Time on the DS of Cellulose. Figure 3 showed the effect of the refining time of the pretreatment system on the degree of substitution (DS) of cellulose. The refining time was varied between 0 and 2.5 hr, while the other reaction parameters, molar ratio of monochloroacetic acid (MCA) to anhydroglucose units in cellulose of 3 : 5, liquid-solid ratio (volume/mass) of 10 mL/g, NaOH-MCA molar ratio of 1 : 1, temperature of 65˚C, and reaction time of 2 hr remained unchanged.

As can be seen from Figure 3, with an increase of refining time, the DS of the cellulose increased from 0.112 (without refining) to 0.159 (after a refining time of 1.5 hr). This provides direct evidence that refining would be beneficial for the etherification reaction of cellulose. As the refining time extended beyond this point, the DS exhibited a slow decline. This may be due to effects such as the degradation of cellulose materials, the reversibility of the etherification reaction, and alkaline degradation of the cellulose. However, the DS of the refined cellulose was always greater than that of unrefined cellulose. The results demonstrated that mechanical treatment of the fiber can significantly improve the reactivity of cellulose. This is because mechanical activation can change the crystalline structure of cellulose, thus reducing its crystallinity, allowing etherified reagent to more easily penetrate into the interior cellulose, which is consistent with Huang et al.'s study [31].

3.2. Influence of Different Pretreatment Methods on the Surface Charge. Three samples, named BF-E, BF-CM, and BF-S, were obtained following the route described in the Materials and Methods section (Section 2). The effect of the enzyme dosage on the surface charge is shown in Figure 4.

As can be seen in Figure 4, the surface charge of sample BF-E first decreased quickly and then increased slowly. The effect of the enzyme was first to hydrolyze the fibers and decrease the specific surface area of the fiber and hence reduce the number of exposed carboxyl groups on the fiber surface. With an increasing enzyme dosage, the enzyme hydrolyzed the fiber further, increasing the specific surface area of the fiber, and exposed more carboxyl groups, leading to an increase in the surface charge of the fibers. The surface charge of both BF-CM and BF-S first raised rapidly and then slowly with the increased dosage of enzyme. After carboxymethylation, the surface charge of the fibers increased significantly, indicating that the etherification enhanced the negative charge by increasing the number of carboxyl groups. Moreover, the final ultrasonic homogenization led to a

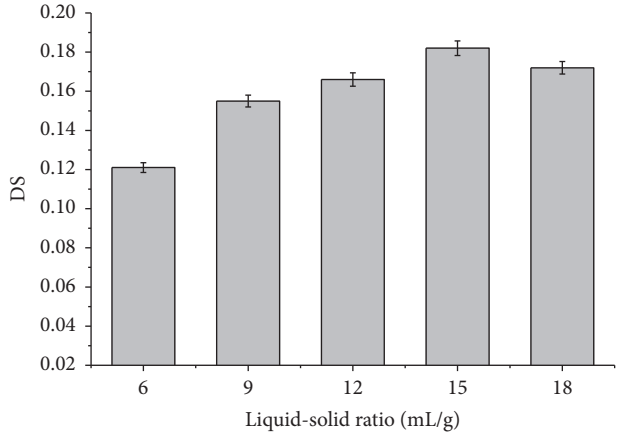

Figure 5: Effect of liquid-solid ratio on DS of cellulose.

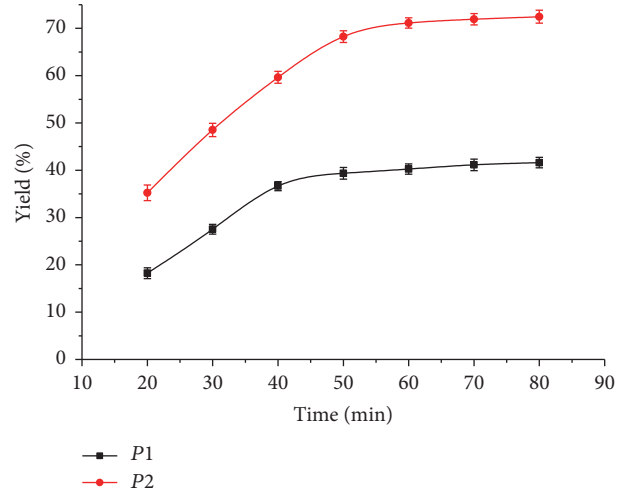

Figure 6: Effect of ultrasonic time on NFCs yield.

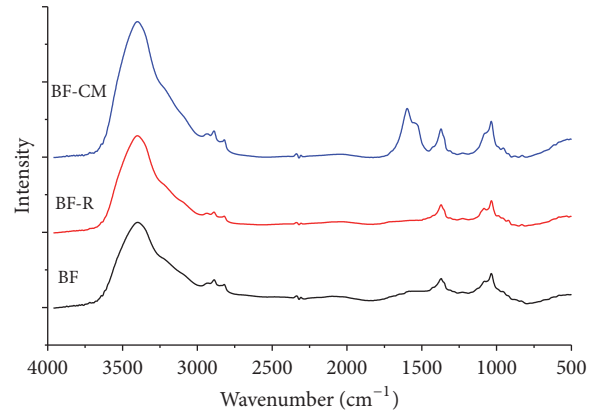

Figure 7: FT-IR of BF with different pretreatments.

further augmentation of the surface charge of the fibers. This can be explained by the fact that the ultrasonic treatment destroyed the crystal structure of cellulose, exposing more free carboxyl groups.

3.3. Effect of Liquid-Solid Ratio on DS of Cellulose. Figure 5 showed the effect of the liquid-solid ratio on the DS of cellulose. The DS value displayed a trend of first rising and then declining with an increase of the liquid-solid ratio. After increasing to 15 mL/g, the DS began to decrease. The reason is that when the liquid-solid ratio increased, the larger volume of liquid allowed the solid materials to disperse more evenly, improving the flow condition of the reaction system. Consequently, the etherifying agent made more frequent contact with the raw cellulose material, promoting the reaction and leading to an increase in the DS. The same phenomenon was also observed in Ye and Chen's study [32]. However, once the liquid-solid ratio was greater than 15 mL/g, an increase of the liquid-solid ratio only reduced the concentration of SCA, which did not benefit the flow state of the reaction system. Therefore, in the presence of low concentrations of SCA, the etherification of cellulose tended to decline.

3.4. Effect of Ultrasonication on the Yeild of NFCs. Ultrasonic homogenization is a crucial step affecting the defibrillation of the cellulose fiber. Ultrasonic treatment was conducted for time periods ranging from 20 min to 80 min, with a constant power of $P1$ (50% P_{max}) and $P2$ (70% P_{max}). The yield of the NFC was calculated according to (4), and the results are shown in Figure 6.

As shown in Figure 6, the ultrasonication time had a significant effect on the NFC yield; with increasing ultrasonication time, the yield of NFC significantly increased. An NFC yield above 65% could be obtained through the route in the optimum conditions. When the ultrasonic time increased from 20 min to 50 min, a significant increase in the NFC yield was observed. The yield reached a maximum of 72.46% with an ultrasonication time of 80 min and an input power of 70% P_{max}. The input power played an important role in the process of ultrasonic homogenization. The yield for 30 min with $P2$ was higher than that of 80 min with $P1$. This finding could be attributed to the breach of the inner crystallization area that needs sufficient power to be affected by ultrasonication. A similar result was reported in the literature [33].

3.5. FT-IR Analysis. To confirm successful carboxymethylation, the treated and untreated BF were characterized using FT-IR spectroscopy, and the results are shown in Figure 7.

The spectrum of the untreated BF showed the characteristic absorption bands of cellulose. A large band between 3,000 cm^{-1} and 3,800 cm^{-1} was attributed to the OH stretching vibrations, and the peak at 2,920 cm^{-1} was assigned to the CH stretching vibrations. A series of peaks between 1,300 and 1,500 cm^{-1} were associated with OCH deformation vibrations, CH_2 bending vibrations, and the CCH and COH bending vibrations. Finally, the band ranging from 900 to 1,100 cm^{-1} mainly contained signals from CC stretching vibrations and COH and CCH deformation vibrations. Refining disintegration of the BF (BF-R) did not lead to a change in the FT-IR spectrum. However, the absorption peak intensities displayed obvious changes, and the absorption

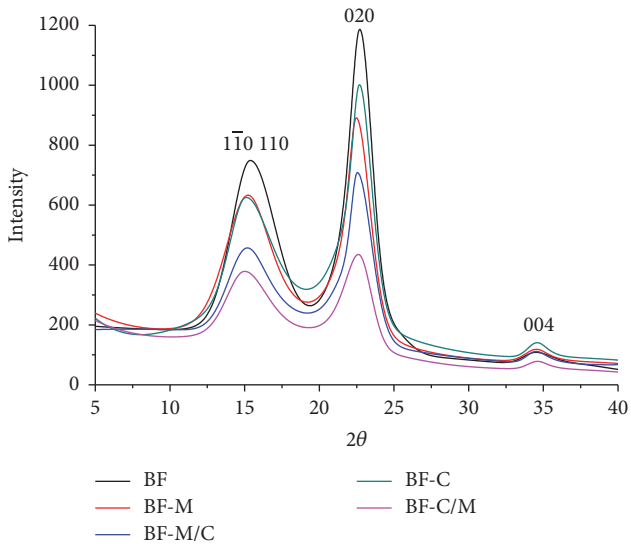

Figure 8: XRD diffractograms of BF samples.

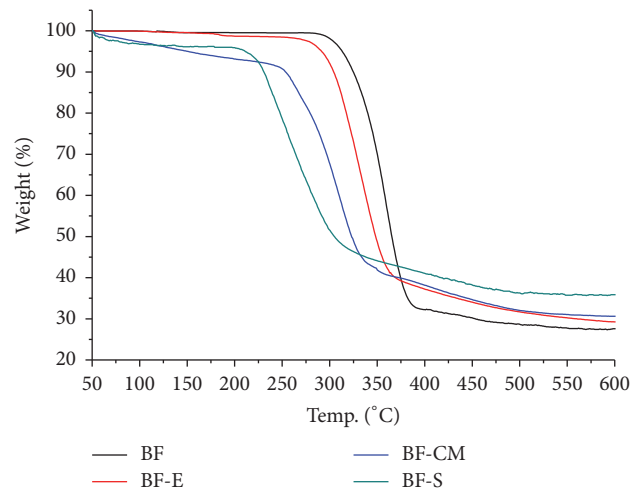

Figure 9: TGA of (a) BF (black curve), (b) BF-E (red curve), (c) BF-CM (blue curve), and (d) BF-S (green curve).

peak attributed to the OH stretching vibrations became wider, indicating that, under the action of mechanical activation, the intermolecular hydrogen bonding of cellulose was abated, and the amount of free hydroxyls increased. Carboxymethylation of the BF-R (BF-CM) led to the appearance of a new signal at 1,598 cm^{-1}, which was attributed to the asymmetric stretching vibration of the carboxylate group [34], confirming the successful carboxymethylation.

3.6. XRD Analysis. To investigate the effect of the sequence of chemical and mechanical treatments on the preparation of NFC, the crystallinities of the different samples were analyzed by X-ray diffraction. The samples were prepared through two routes. For route 1, the BF was first treated by mechanical disintegration (BF-M) and then by chemical modification (BF- M/C). For route 2, the BF was first treated by chemical modification (BF-C) and then by mechanical disintegration (BF-C/M). The results are shown in Figure 8.

The diffractogram of the untreated BF showed reflections of the cellulose lattice planes appearing at 2θ angles between 13° and 17° (110 and 110) and 22.3° (020) and 34.5° (004) [35]. The crystallinity χ_{cr} of the samples was estimated using (4) [36] with I_{020} being the intensity of the 020 peak (amorphous and crystalline reflections at 22.3°) and I_{am} being the intensity of the minimum between the 020 and 110 peaks.

$$\chi_{cr} = \frac{I_{020} - I_{am}}{I_{020}}. \quad (4)$$

According to (1), the highest value of crystallinity was obtained for raw BF (77.74%), followed by BF-M (69.02%), BF-M/C (66.99%), BF-C (63.19%), and BF-C/M (56.15%). As can be observed, mechanical disintegration of the BF (see curve of BF-M) strongly decrease its crystallinity, and the crystallinity was not significantly affected by postchemical modification (BF- M/C), implying that mechanical disintegration had a stronger effect on crystallinity than chemical modification. However, samples from route 2 (BF-C and BF-C/M) exhibited a more pronounced reduction in crystallinity compared to those from route 1. It can be concluded that the presence of the carboxylate groups made the mechanical isolation more efficient, as not only amorphous regions but also crystalline domains were affected by the treatment. The improved efficiency of the isolation of the fibrillated material could be attributed to the ionic repulsion between the carboxylate groups of the single cellulose chains [20].

3.7. Thermogravimetry Analysis (TGA). It is well-known that substituent groups have a significant influence on the thermal stabilities and derivatives of cellulose. Therefore, the native and treated samples were characterized by thermogravimetric analysis in order to obtain information about their thermal behaviors. Figure 9 presents TGA curves for the BF and differently treated samples. All the TGA curves showed a small initial weight loss between 50 and 150°C, which corresponds to a mass loss of absorbed moisture. For the original BF, a slight weight loss occurred at 300°C and a drastic loss at 300–390°C (see black curve), followed by slow weight losses up to 600°C. These results are similar to those reported in previous publications [37]. For BF-E, a significant weight loss started at approximately 285°C and ended at 374°C; the enzyme treatment slightly decreased the thermal stability. Carboxymethylation clearly reduced the thermal stability, showing a significant weight loss starting at approximately 245°C. This finding is in agreement with results obtained from the thermal degradation of partially carboxymethylated cellulose [38]. For BF-S, most weight loss occurred in the range of 210–500°C, and the degradation temperature was further decreased. Ultrasonication resulted in BF with a reduced molecular weight, an increased specific surface area, and more exposed active groups. Generally, the low molecular weight of cellulose fragments introduced into the outer surface of the cellulose crystals resulted in a decrease in thermal stability. These results were similar to those reported in previous publications [39].

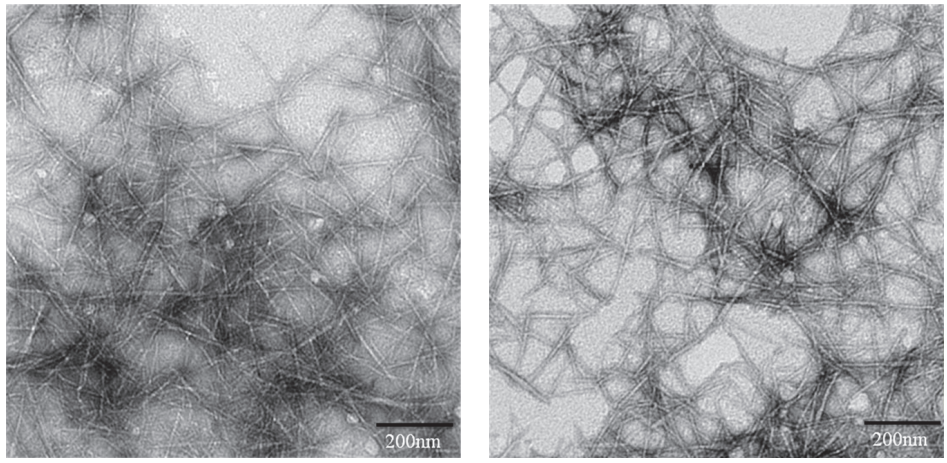

(a) (b)

Figure 10: TEM images of water-redispersed samples: (a) DS = 0.135 and (b) DS = 0.182.

3.8. Morphological Structures of NFCs. The TEM images of the water-redispersed samples with different DS values were shown in Figure 10. As can be seen in Figure 10, most of individualized cellulose nanofibers were dispersed in water, and the cellulose nanofibers obtained were mainly 10–40 nm in width and a few microns in length. The sample with DS = 0.182 (Figure 10(b)) presented better dispersion than that with DS = 0.135(Figure 10(a)). This revealed that the amount of negatively charged carboxyl groups played a critical role in the dispersion of NFC.

4. Conclusions

Nanofibrillated cellulose (NFC) from bamboo fiber was obtained by a combination of mechanical activation, enzyme treatment, carboxymethylation, and ultrasonic homogenization. It was encouraging that an NFC yield could be obtained above 70% through this route. Carboxymethylation was found to significantly increase the surface charge of the fibers. Ultrasonic homogenization led to a further augmentation of the surface charge by destroying the crystal structure of the fibers. Refining was able to activate the fiber by changing the crystalline structure of cellulose and allowing the etherified reagent to more easily penetrate into the cellulose interior, enhancing the efficiency of the etherification reaction of cellulose. The input power played a more significant role than the treating time in the process of ultrasonic homogenization attributed to the breach of the inner crystallization area requiring an adequate power of ultrasonication. FT-IR spectroscopy confirmed the occurrence of the carboxymethylation reaction in the modified BF by the appearance of characteristic signals at 1,598 cm^{-1}. Although carboxymethylation modification did not significantly affect crystallinity, the presence of carboxylate groups was beneficial for destroying crystallinity of the posttreatment samples. The chemical modification or physical treatment decreased the degradation temperature of the fiber. The number of carboxyl groups, leading to the addition of negative charge, played a critical role in the dispersion of NFC.

Conflicts of Interest

The authors declare that they have no conflicts of interest.

Authors' Contributions

Zhijun Hu, Rui Zhai, Yan Zhang, Jing Li, and Jiang Lin designed the project. Zhijun Hu, Yan Zhang, and Rui Zhai performed the experiments and analyzed the data; Jing Li and Jiang Lin assisted in data processing and the manuscript preparation; and all authors contributed to the manuscript.

Acknowledgments

The authors are grateful for the support of the China Natural Science Foundation under Grant no. 51376162, the Key Industrial Project of Special Major Science and Technology of Zhejiang Province (no. 2013C01082), and the Zhejiang Province Collaborative Innovation Center of Agricultural Biological Resources Biochemical Manufacturing Foundation under Grant no. 2016KF0019.

References

[1] D. G. Gray, "Recent advances in chiral nematic structure and iridescent color of cellulose nanocrystal films," *Nanomaterials*, vol. 6, no. 11, pp. 213–221, 2016.

[2] H. P. S. A. Khalil, N. A. S. Aprilia, A. H. Bhat, M. Jawaid, M. T. Paridah, and D. Rudi, "A Jatropha biomass as renewable materials for biocomposites and its applications," *Renewable & Sustainable Energy Reviews*, vol. 22, pp. 667–685, 2013.

[3] T. H. Wegner and P. E. Jones, "Advancing cellulose-based nanotechnology," *Cellulose*, vol. 13, pp. 115–118, 2014.

[4] A. Isogai, "Wood nanocelluloses: Fundamentals and applications as new bio-based nanomaterials," *Journal of Wood Science*, vol. 59, no. 6, pp. 449–459, 2013.

[5] B. Wang, M. Sain, and K. Oksman, "Study of structural morphology of hemp fiber from the micro to the nanoscale," *Applied Composite Materials*, vol. 14, no. 2, pp. 89–103, 2007.

[6] L. Du, J. Wang, Y. Zhang, C. Qi, M. P. Wolcott, and Z. Yu, "Preparation and Characterization of Cellulose Nanocrystals from the Bio-ethanol Residuals," *Journal of Synthetic Crystals*, vol. 7, pp. 593–605, 2009.

[7] G. Siqueira, J. Bras, and A. Dufresne, "Cellulosic bionanocomposites: a review of preparation, properties and applications," *Polymer*, vol. 2, no. 4, pp. 728–765, 2010.

[8] A. F. Turbak, F. W. Snyder, and K. R. Sandberg, "Microfibrillated cellulose, a new cellulose product: properties, uses and commercial potential," *Journal of Applied Polymer Science. Applied Polymer Symposium*, vol. 37, pp. 815–827, 1983.

[9] T. Taniguchi, "Microfibrillation of natural fibrous materials," *Journal of the Society of Materials Science Japan*, vol. 45, pp. 472-473, 1996.

[10] M. Pääkko, M. Ankerfors, H. Kosonen et al., "Enzymatic hydrolysis combined with mechanical shearing and high-pressure homogenization for nanoscale cellulose fibrils and strong gels," *Biomacromolecules*, vol. 8, no. 6, pp. 1934–1941, 2007.

[11] A. Chakraborty, M. Sain, and M. Kortschot, "Cellulose microfibrils: a novel method of preparation using high shear refining and cryocrushing," *Holzforschung*, vol. 59, no. 1, pp. 135-107, 2005.

[12] W. Stelte and A. R. Sanadi, "Preparation and characterization of cellulose nanofibers from two commercial hardwood and softwood pulps," *Industrial & Engineering Chemistry Research*, vol. 48, no. 24, pp. 11211–11219, 2009.

[13] M. Henriksson, G. Henriksson, L. A. Berglund, and T. Lindström, "An environmentally friendly method for enzyme-assisted preparation of microfibrillated cellulose (MFC) nanofibers," *European Polymer Journal*, vol. 43, no. 8, pp. 3434–3441, 2007.

[14] A. Alemdar and M. Sain, "Isolation and characterization of nanofibers from agricultural residues—wheat straw and soy hulls," *Bioresource Technology*, vol. 99, no. 6, pp. 1664–1671, 2008.

[15] M. I. Voronova, T. N. Lebedeva, M. V. Radugin, O. V. Surov, A. N. Prusov, and A. G. Zakharov, "Interactions of water-DMSO mixtures with cellulose," *Journal of Molecular Liquids*, vol. 126, no. 1-3, pp. 124–129, 2006.

[16] D. da Silva Perez, S. Montanari, and M. R. Vignon, "TEMPO-mediated oxidation of cellulose III," *Biomacromolecules*, vol. 4, no. 5, pp. 1417–1425, 2003.

[17] N. Siddiqui, R. H. Mills, D. J. Gardner, and D. Bousfield, "Production and characterization of cellulose nanofibers from wood pulp," *Journal of Adhesion Science and Technology*, vol. 25, no. 6-7, pp. 709–721, 2011.

[18] A. Benkaddour, K. Jradi, S. Robert, and C. Daneault, "Study of the effect of grafting method on surface polarity of tempo-oxidized nanocellulose using polycaprolactone as the modifying compound: esterificationversusclick-chemistry," *Nanomaterials*, vol. 3, no. 4, pp. 638–654, 2013.

[19] C. Eyholzer, A. Borges De Couraça, F. Duc et al., "Biocomposite hydrogels with carboxymethylated, nanofibrillated cellulose powder for replacement of the nucleus pulposus," *Biomacromolecules*, vol. 12, no. 5, pp. 1419–1427, 2011.

[20] L. Wågberg, G. Decher, M. Norgren, T. Lindström, M. Ankerfors, and K. Axnäs, "The build-up of polyelectrolyte multilayers of microfibrillated cellulose and cationic polyelectrolytes," *Langmuir*, vol. 24, no. 3, pp. 784–795, 2008.

[21] A. Tanaka, V. Seppänen, J. Houni, A. Sneck, and P. Pirkonen, "Nanocellulose characterization with mechanical fractionation," *Nordic Pulp & Paper Research Journal* , vol. 27, no. 4, pp. 689–694, 2012.

[22] S. Xiao, R. Gao, Y. Lu, J. Li, and Q. Sun, "Fabrication and characterization of nanofibrillated cellulose and its aerogels from natural pine needles," *Carbohydrate Polymers*, vol. 119, pp. 202–209, 2015.

[23] Q. Zhang, M. Benoit, K. De Oliveira Vigier et al., "Pretreatment of microcrystalline cellulose by ultrasounds: Effect of particle size in the heterogeneously-catalyzed hydrolysis of cellulose to glucose," *Green Chemistry*, vol. 15, no. 4, pp. 963–969, 2013.

[24] P. C. S. F. Tischer, M. R. Sierakowski, H. Westfahl Jr., and C. A. Tischer, "Nanostructural reorganization of bacterial cellulose by ultrasonic treatment," *Biomacromolecules*, vol. 11, no. 5, pp. 1217–1224, 2010.

[25] M. J. Bussemaker, F. Xu, and D. Zhang, "Manipulation of ultrasonic effects on lignocellulose by varying the frequency, particle size, loading and stirring," *Bioresource Technology*, vol. 148, pp. 15–23, 2013.

[26] K. S. Suslick, *Sonochemistry, Kirk-Othmer Encyclopedia of Chemical Technology*, John wiley & sons, New York, USA, 1998.

[27] B. W. Zeiger and K. S. Suslick, "Sonofragmentation of molecular crystals," *Journal of the American Chemical Society*, vol. 133, no. 37, pp. 14530–14533, 2011.

[28] K. Abe and H. Yano, "Comparison of the characteristics of cellulose microfibril aggregates of wood, rice straw and potato tuber," *Cellulose*, vol. 16, no. 6, pp. 1017–1023, 2009.

[29] C. Eyholzer, N. Bordeanu, F. Lopez-Suevos, D. Rentsch, T. Zimmermann, and K. Oksman, "Preparation and characterization of water-redispersible nanofibrillated cellulose in powder form," *Cellulose*, vol. 17, no. 1, pp. 19–30, 2010.

[30] R. W. Eyler, E. D. Klug, and F. Diephuis, "Determination of degree of substitution of sodium carboxymethylcellulose," *Analytical Chemistry*, vol. 19, no. 1, pp. 24–27, 1947.

[31] Z. Huang, X. Liang, L. Gao, H. Hu, and Z. Tong, "Graft copolymerization of mechanically activated sugarcane bagasse and acrylic acid (sodium acrylate)," *Journal of the Chemical Industry and Engineering Society of China*, vol. 60, pp. 1573–1580, 2009.

[32] Y. Ye and H. Chen, "Preparation of carboxymethylcellulose from steam exploded crop straw," *Journal of the Chemical Industry and Engineering Society of China*, vol. 60, pp. 1843–1849, 2009.

[33] S. Wang and Q. Cheng, "A novel process to isolate fibrils from cellulose fibers by high-intensity ultrasonication, part 1: process optimization," *Journal of Applied Polymer Science*, vol. 113, no. 2, pp. 1270–1275, 2010.

[34] L. T. Cuba-Chiem, L. Huynh, J. Ralston, and D. A. Beattie, "In situ particle film ATR FTIR spectroscopy of carboxymethyl cellulose adsorption on talc: Binding mechanism, pH effects, and adsorption kinetics," *Langmuir*, vol. 24, no. 15, pp. 8036–8044, 2008.

[35] J.-F. Sassi and H. Chanzy, "Ultrastructural aspects of the acetylation of cellulose," *Cellulose*, vol. 2, no. 2, pp. 111–127, 1995.

[36] L. Segal, J. Creely, A. Martin, and C. Conrad, "An empirical method for estimating the degree of crystallinity of native cellulose using the x-ray diffractometer," *Textile Research Journal*, vol. 29, no. 10, pp. 786–794, 1959.

[37] O. Ishida, D. Kim, S. Kuga, Y. Nishiyama, and R. M. Brown,, "Microfibrillar carbon from native cellulose," *Cellulose*, vol. 11, no. 3/4, pp. 475–480, 2004.

[38] M. L. Leza, M. Cortazar, I. Casinos, and G. M. Guzmán, "Thermal degradation of partially carboxymethylated cellulose grafted with 4-vinylpyridine," *Macromolecular Materials and Engineering*, vol. 168, no. 1, pp. 195–203, 1989.

[39] S. Cui, S. Zhang, S. Ge, L. Xiong, and Q. Sun, "Green preparation and characterization of size-controlled nanocrystalline cellulose via ultrasonic-assisted enzymatic hydrolysis," *Industrial Crops and Products*, vol. 83, pp. 346–352, 2016.

Hindawi
International Journal of Polymer Science
Volume 2017, Article ID 4915185, 9 pages
https://doi.org/10.1155/2017/4915185

Research Article

Lignin-Carbohydrate Complexes Based Spherical Biocarriers: Preparation, Characterization, and Biocompatibility

Houkuan Zhao,[1] Jinling Li,[1] Peng Wang,[1,2] Shaoqiong Zeng,[1] and Yimin Xie[1,2]

[1]*Research Institute of Pulp & Paper Engineering, Hubei University of Technology, Wuhan 430068, China*
[2]*Hubei Provincial Key Laboratory of Green Materials for Light Industry, Hubei University of Technology, Wuhan 430068, China*

Correspondence should be addressed to Yimin Xie; ppymxie@scut.edu.cn

Received 15 September 2017; Revised 22 October 2017; Accepted 30 October 2017; Published 13 December 2017

Academic Editor: Xiaofei Tian

Spherical biocarriers were prepared with lignin-carbohydrate complexes isolated from ginkgo (*Ginkgo biloba* L.) xylem. The specific surface and average pore size of the biocarriers were 17.15 $m^2 g^{-1}$ and 21.59 nm, respectively. The carriers were stable in solution at pH 4.0~9.5. Fourier transform infrared (FT-IR) spectrum indicated that the spherical carrier was composed of lignin and polysaccharides and had a typical lignin-carbohydrate complex (LCC) structure. The contents of galactose, lignin, and total sugar were 3.30%, 23.9%, and 64.62%, respectively, making the spherical biocarriers have good physical strength and compatible with hepatocytes. It was observed using a scanning electron microscopy (SEM) that liver cells adhered to the spherical biocarriers during culture. Cell counting indicated that the proliferation of liver cells in the experimental group was significantly higher than that of the control group. The albumin secretion (ALB) value and glucose consumption of the human hepatocytes were increased by 51.7% and 38.6%, respectively, by the fourth day when cultivated on the biocarriers. The results indicate that ginkgo LCC is very biocompatible and shows promise for the use as a biomaterial in the culture of human hepatocytes.

1. Introduction

Lignin is one of the most abundant natural products in the land-plant kingdom and is formed through phenolic oxidative coupling processes [1]. Lignin macromolecules are formed by the dehydrogenative polymerization of three monolignols: *p*-coumaryl, coniferyl, and sinapyl alcohols [2]. Some hemicellulose in the cell walls of lignified plants is linked to lignin to form lignin-carbohydrate complexes (LCC) [3]. With the development of analysis technology, more information has been reported in the literature describing the structure and properties of LCC, especially lignin-carbohydrate linkage (LC bond) [4–8]. As shown in Figure 1, (Galacto)glucomannan is the most common one in the softwood hemicelluloses, which is considered to be linked to lignin moieties by chemical bonds [9]. It is a branched heteropolysaccharide consisting of two glucose epimers, β-D-glucopyranose and β-D-mannopyranose, and galactose units which are bioactive for hepatocytes. Recently, LCC as a biological material has attracted attention. Many researchers have found that lignin-carbohydrate complexes are a good natural biodegradable material [10, 11]. In addition, LCC contains hydrophobic rigid lignin blocks and hydrophilic flexible polysaccharide blocks, making lignin-carbohydrate complexes have good amphipathy, biocompatibility, and mechanical strength [12]. The lignin and carbohydrate blocks in the LCC copolymer not only have an ideal structure for biomaterials, but also have good compatibility with animal cells [13]. The rigid lignin blocks can form lignin-protein complexes with membrane bound proteins in animal cells, enabling cells to grow [14]. Furthermore, the flexible polysaccharide blocks containing 2–5% galactan have the ability to recognize hepatocytes due to the presence of asialoglycoprotein receptors (ASGPR) on which galactose acts as a specific adhesive ligand on the hepatocytes [15–19] (Figure 2). Galactosylated substrates are useful biomaterials in the preparation of scaffolds for hepatocyte cultivation because of their specific interaction of the galactose moiety with the cell surface ASGPR [20].

In the literature describing lignin as a biomaterial, there have been two opinions which have been argued for many years. Some researchers think that although lignin has great strength, its hydrophobicity may affect animal cell adhesion

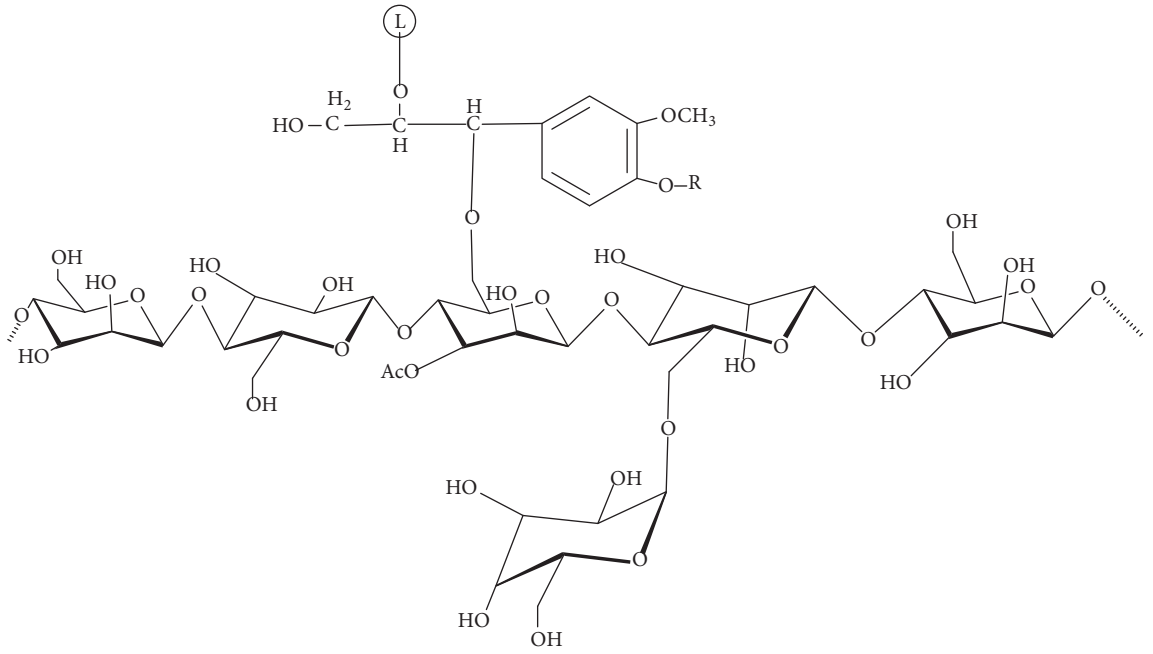

Figure 1: (Galacto)glucomannan in softwood hemicelluloses with linkage to lignin moieties (R = H or polylignol; L = polylignol).

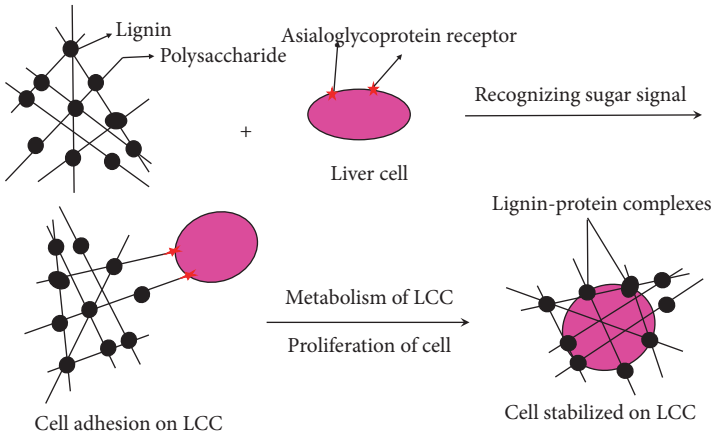

Figure 2: Binding of LCC material to hepatocyte.

on the lignin-based biocarriers. Other researchers suggest that lignin has many functional groups that possess physiological activity, such as methoxyl, phenolic hydroxyl, alcoholic hydroxyl, carboxyl, and carbonyl, which may promote normal metabolism of animal cells. Recently, Erakovic et al. studied the biocompatibility of modified lignin scaffold material and demonstrated that the lignin fragments in lignin-carbohydrate complexes not only have great strength, but also have good biocompatibility [21–23]. Moreover, Chung et al. [24] and Park et al. [25] demonstrated that the scaffolds immobilized by galactose retained a greater number of hepatocytes than those scaffolds which were unmodified or immobilized with galactose, due to specific interactions between hepatocytes and galactose moieties. Yang et al. [26] and Wang et al. [27] investigated the ability of hydrogels prepared with galactosylated acrylate (GAC) and poly (N-isopropylacrylamide) (NIPAAm) as scaffolds to proliferate hepatocytes and maintain the function of albumin and urea synthesis. They found that the cell adhesion and proliferation of hepatocytes occurred primarily on the surface of the hydrogels, suggesting that the incorporation of GAC containing galactose units could stimulate cell adsorption and growth, as compared with conventional PNIPAAm hydrogel. In our previous research, Wu et al. reported that hydrogel prepared from artificial LCC, that is, dehydrogenation polymer-(DHP-) galactose complex, has good biocompatibility with human hepatocytes [28]. However, the biocompatibility of natural LCC with hepatocytes is still open to investigation.

In order to understand the possibility of the application of natural LCC in the tissue engineering area, LCC

was isolated from ginkgo wood (*Ginkgo biloba* L.), in the group of gymnosperm. Spherical biological carriers were prepared using liquid nitrogen freeze-drying method. The spherical biocarriers with relative large specific surface area may provide more growth area for cell culture *in vitro*. Hepatocytes are difficult to proliferate in monolayer cultures and can be easily damaged by trypsin digestion and may be resolved using spherical biocarriers [29]. In this work, Fourier transform infrared spectroscopy (FT-IR), optical microscopy, high precision surface area, and pore size analyzer were used to characterize the structure and morphology of spherical biocarriers. The biocarriers were then used in the culture of human hepatocytes. The growth of the hepatocytes on the biocarriers was observed using an inverted biological microscope and scanning electron microscopy (SEM). The metabolic activities of the cells, including albumin secretion and glucose consumption, were also determined.

2. Materials and Methods

2.1. Materials. Gingko tree was obtained from Wuhan Botanical Garden. Human liver cells (L-02) were provided by Pricells Company (Wuhan, China).

2.2. Preparation of Gingko LCC. Gingko wood meal (40–60 mesh) was extracted using benzene/ethyl alcohol (2/1, V/V) followed by a hot water treatment and then dried in vacuo for 7 days. The extractives-free wood mill was further ground for 72 h in a vibration ball mill with water cooling. The gingko LCC was then extracted and purified using the Björkman method [30].

2.3. Posttreatment of the LCC. The LCC were further treated with hot water at 50°C in order to remove the water-soluble fraction which will cause the swelling of the LCC-based spherical biocarriers. The ginkgo LCC and distilled water were put into an Erlenmeyer flask. The mixture was stirred at 50°C for 8 h and then filtered. The water-insoluble LCC fraction was obtained by freeze-drying, yield: 21.7%.

2.4. Preparation of LCC-Based Spherical Biocarriers. The ginkgo LCC-based spherical biocarriers were obtained using the freeze-drying method, as shown in Figure 3. Firstly, 1 g water-insoluble ginkgo LCC was dissolved in 5 mL 90% (V/V) acetic acid under magnetic stirring. Secondly, the solution was dropped into liquid nitrogen using a 1 mL injector. Thirdly, the spherical biocarriers were obtained by drying the frozen beads using a freeze dryer (Labconco 195, USA). The morphology of spherical biocarriers was characterized using optical microscope and SEM.

2.5. FT-IR Spectroscopy. KBr pellets were prepared from 1 mg ground sample and 60 mg predried KBr. The spectrum was recorded in the range of 4000 cm^{-1}–400 cm^{-1} using a FT-IR spectrometer (Thermo Fisher 6700, USA).

2.6. Composition of the Spherical Biocarriers Material. Three-milligram spherical biocarrier samples were hydrolyzed using 3 mL 72% sulfuric acid at room temperature for 60 min. The sulfuric acid was then diluted to 4% using distilled water and sample hydrolyzed for 45 min at 121°C in an autoclave. The mixture was filtered through 1G4 glass filter. The filtrate was used to detect the sugar composition of the sample using HPLC (20AT, Shimadzu) equipped with a Aminex HPX-87P column at 85°C using water as the eluent at speed of 0.6 mL min^{-1}. The water-insoluble fraction was used to determine acid insoluble lignin [31].

2.6.1. SEM Observation of Spherical Biocarriers. The spherical biocarriers were put on a silicon wafer and sprayed with gold ions in vacuo. The morphological structures of surface and cross sections were observed using a JSM-6390LV SEM.

2.6.2. Diameter of the Spherical Biocarriers. The samples were examined using a stereomicroscopy (Olympus SZX16, Japan) equipped with a scale. The average diameter of the spherical biocarriers was calculated.

2.6.3. Pretreatment for Specific Surface Determination of Spherical Biocarriers. An empty tube was weighed and marked as m_0. The spherical biocarriers were put into the empty tube and treated at 120°C for 4.5 h. The dried spherical biocarriers were cooled to 25°C in a cooling bath. The tube containing the biocarriers was weighed and marked as m_1. The value of m_1 minus m_0 was the weight of the spherical biocarriers.

2.6.4. Determination of Specific Surface. The nitrogen adsorption method [32, 33] was used in the determination of the specific surface using a BELSORP-mini II type high precision surface area and pore size analyzer (Ankersmid, Netherland). The Brunauer–Emmett–Teller (BET) specific surface determination is based on the gas adsorption characteristics on a solid surface. In addition, corresponding to the defined pressure, the equilibrium adsorption was definite. The equilibrium adsorption determined was equivalent to the specific surface of the sample. The formulae to calculate these are

$$Sg = 4.36 \times \frac{V_m}{m},$$
$$\frac{P}{Va\left(P_0 - P\right)} = \frac{1}{V_m \bullet C} + \frac{C-1}{V_m \bullet C} \bullet \left(\frac{P}{P_0}\right), \quad (1)$$

where Sg is specific surface area of the sample ($m^2\ g^{-1}$); V_m is saturated nitrogen molecular monolayer adsorption (mL); Va is the actual adsorption of the sample (mL); m is the weight of the sample (g); C is constant related to adsorption capacity of the sample; P is adsorbent partial pressure; P_0 is adsorbent saturated vapor pressure.

2.6.5. Determination of the Pore Size. The pore size was also determined using a BELSORP-mini II type high precision surface area and pore size analyzer (Ankersmid, Netherland). The gas adsorption method was used to determine the pore size. This method is based on capillary condensation and the

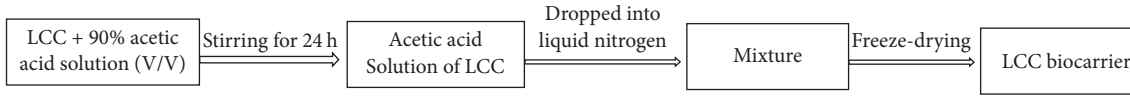

Figure 3: Preparation of LCC-based spherical biocarriers.

volume equivalent substitution. Corresponding to the ratio of P/P_0, there is a critical radius, Rk. The critical radius is calculated using the Kelvin equation as follows:

$$\mathrm{Rk} = \frac{-0.414}{\log\left(P/P_0\right)}. \quad (2)$$

2.6.6. Size Stability of Spherical Biocarriers. Five milligrams of spherical biocarriers was suspended in 5 ml of buffering solutions at various pH (acetate buffer pH 4~5, phosphate buffer pH 6.8~7.4, and sodium bicarbonate buffer pH 9.5). The size and morphology of spherical biocarriers in different buffering solutions were determined using a stereomicroscopy (Olympus SZX16, Japan) equipped with a scale after 15 days.

2.7. Culture of Human Hepatocytes. Human hepatocytes (L-02), obtained from Pricells Company (Wuhan, China), were rinsed with phosphate buffer. The hepatocytes were inoculated into 12-well culture plates at a density of 3×10^5 cells mL^{-1}. The spherical biocarriers were then sterilized at 120°C for 4 h. These were then added to the wells at a concentration of 2.5 mg mL^{-1}. The hepatocytes together with the spherical biocarriers were incubated at 37°C, 5% CO_2, and 100% relative humidity. The culture medium used was RPMI-1640 supplemented with 20% FBS, 1% penicillin, and streptomycin solution. The adhesion of human hepatocytes to the spherical biocarriers was observed daily using a XDS-1 inverted biological microscope. Cell-free supernatant was collected daily to detect the metabolic activity of the cells.

2.7.1. Cell Number Counting. On the 1~5th days of culture liquid media were collected every day. The cells were then washed twice with phosphate buffer, followed by 0.25% trypsin for 1~2 min. The media containing trypsin were then discarded. Then the new media were added to terminate the digestion. The cells were no longer adhered to the well but in a cell suspension. Two hundred mL of suspension liquid was taken and mixed with equal volume of 0.4% trypan blue staining solution. Some of the stained cells were put onto a blood cell counting plate. The number of stained cells was counted using a microscope.

2.7.2. Observation of the Cells Adhesion on the Carrier by SEM. On the 3rd day of cell culture, some spherical biocarriers were removed. The spherical biocarriers were fixed using 2.5% glutaraldehyde (GA) for 12 h at 4°C. The spherical biocarriers were then further fixed using 0.1% osmic acid for 30 min. After the spherical biocarriers were washed using phosphate buffer, a gradient dehydration was carried out using ethanol at concentrations of 30%, 50%, 70%, 80%, 90%, and 100%. The dried spherical biocarriers were put onto silicon wafer and sprayed with gold ions in vacuo. The hepatocytes adhered to the spherical biocarriers were observed using a JSM-6390LV SEM.

2.7.3. Detection of Metabolic Activity. The amount of albumin secreted was determined using the method according to the instructions of kit number A028 (provided by Nanjing Jiancheng Bioengineering Institute, China). Briefly, 10 μL distilled water, standard albumin, and cell-free supernatant were added to a test tube. After the addition of 2.5 mL bromocresol green buffer, the samples were shaken. After the reaction was carried out for 10 min at room temperature, the absorption values were monitored at 628 nm using a UV-Vis spectrophotometer (Shimadzu 2550, Japan).

$$\mathrm{ALB}\,(\mathrm{g/L}) = \frac{A_1 - A_2}{A_0 - A_2} \times C_0, \quad (3)$$

where ALB is the content (g L^{-1}) of albumin; A_0, A_1, and A_2 are the absorbance values of standard tubes, sample tubes, and control groups, respectively. C_0 (g L^{-1}) is the concentration of the standard.

The amount of glucose consumed by the hepatocytes was determined using the method according to the instruction of kit number CAT361500 (provided by Nanjing Jiancheng Bioengineering Institute, China). In test tubes, 10 μL distilled water, standard glucose, and cell-free supernatant were added. After the addition of 1 mL of a solution containing phosphate buffer (pH 7.0), phenol 10.6 mmol L^{-1}, and aminoantipyrine of 70 mmol L^{-1}, the samples were shaken. After the reaction was carried out for 15 min at 37°C, the absorption values were determined at 505 nm using a UV-VIS spectrophotometer.

$$C\,(\mathrm{mmol/L}) = \frac{A_1}{A_0} \times C_0, \quad (4)$$

where C is the content (mmol L^{-1}) of glucose. A_0 and A_1 are the absorbance values of standard tubes and sample tubes, respectively. C_0 (g L^{-1}) is the concentration of the standard.

3. Results and Discussion

3.1. FT-IR Analysis. A peak of 3419.2 cm^{-1} was assigned to the hydroxyl groups of gingko LCC, as shown in Figure 4. The strong absorption of C-O stretch at 1035.6 cm^{-1} indicated the presence of polysaccharides [34]. The peaks at 1510 cm^{-1} and 1423.2 cm^{-1} were related to the vibration of aromatic structures in the lignin moieties [35]. FT-IR analysis confirmed that the spherical biocarriers had a typical LCC structure composed of lignin and polysaccharides. Rigid hydrophobic lignin and flexible hydrophilic polysaccharide fragments gave

Table 1: Composition of ginkgo LCC-based biocarrier.

Composition	Lignin	Glucose	Xylose	Galactose	Arabinose	Mannose	Total sugars
Content %	25.5	22.30	10.93	3.30	6.15	21.94	64.62

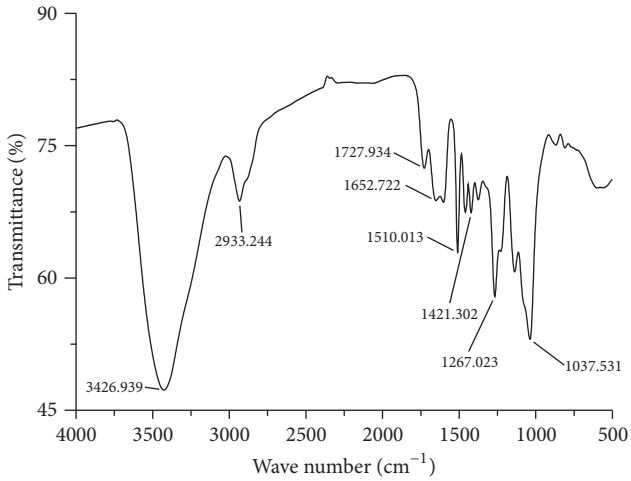

Figure 4: FT-IR spectroscopy of the LCC-based spherical biocarriers.

the spherical biocarriers good amphipathy properties and high strength, which are essential requirements of natural medical materials.

3.2. Composition Analysis. Galactose can be recognized by a receptor on hepatocytes and has a high physiological activity for hepatocytes [36]. Galactose was used to enhance the selective interactions between biocarriers and hepatocytes. As shown in Table 1, the content of galactose units in the LCC macromolecule was 3.30%. The contents of lignin and total sugars were 25.5% and 64.62%, respectively, which gave the spherical biocarriers good physical strength [37]. The results suggest that spherical biocarriers are suitable for use as biocarriers of human hepatocytes.

3.3. Morphology of the Spherical Biocarriers from Gingko LCC. The spherical biocarriers prepared with gingko LCC were porous material as observed by optical microscopy and SEM. As shown in Figure 5(a), the spherical biocarrier is seen in light gray. The morphology of the spherical biocarriers demonstrated that the LCC particles were porous and suitable for cell biocarriers under culture conditions as shown in Figure 5(b).

3.4. Diameter Determination and the Stability. As a biomaterial, the large diameter of the biocarriers will decrease the specific surface area, whereas small diameters will increase the density of biocarriers. Both could impact the growth of cells. Therefore the diameter of biocarriers must be in the appropriate range for the particular cells. In this study, the dry and wet diameters of the spherical biocarriers are 1.8–2.0 mm and 1.9–2.1 mm, respectively. There are some differences between dry and wet spherical biocarriers. The results indicated that the diameters of the spherical biocarriers were stable within a range that was suitable for cell culture. The stability of spherical biocarriers was determined when high concentrations of spherical biocarriers were suspended in a weak acid of pH 4-5, a neutral solution of pH 7.4, and an alkaline solution of pH 9.5. In Figure 6, it was found that the spherical biocarriers kept their intact diameter and style after 15 days in suspension. It was found that the spherical biocarriers had good stability and were suitable for cultivation at different pH.

3.5. Specific Surface Area and Average Pore Size of the Spherical Biocarriers. Specific surface area and average pore size of spherical biocarriers were measured using a high precision surface tester. The BET curve is shown in Figure 7. The V_m value can be calculated using the linear slope and intercept in Figure 7. According to (1) and Kelvin equation (2), the specific surface area and average pore size of spherical biocarriers were calculated to be 17.15 $m^2 g^{-1}$ and 21.59 nm, respectively. The results revealed that the spherical biocarriers had a high specific surface area. Thus, the spherical biocarriers can provide enough surface for cell growth and increase the cell density. When the monolayer of cells undergoes a trypsin digestion process, the damage to cells can be reduced by the cells being easily removed from the medium, compared with conventional monolayer cell culture, because of the 3D culture structure with the use of spherical biocarriers.

3.6. Cell Growth and Metabolic Activities of Hepatocytes Adhered to Spherical Biocarriers. In the presence of the biocarriers, human hepatocytes (L-02) were cultured statically. As shown in Figure 8, it was found that the majority of hepatocytes adhered to the spherical biocarriers, indicating that the LCC is nontoxic, biocompatible, and suitable for the hepatocyte culture. Using cell counting, the cell growth conditions of experimental and control groups in suspension during days 1 to 5 were observed in Figure 9. The cultured cells of the experimental and control groups during the first 3 days grew slowly. On the 4th day, the proliferation rate of the cells increased, which was greater in the experimental group compared to that of the control group.

In Figure 10, it was found that the content of albumin secretion (ALB) from the hepatocytes cultured on the porous biocarriers was significantly greater compared to the control group (without biocarriers). On the 4th day of cultivation the ALB value reached the highest level at 10.45 $g d^{-1} L^{-1}$, while the control group had a high value of 6.89 $g d^{-1} L^{-1}$. Therefore, The ALB value of the sample with the use of biocarriers was increased by 51.7% as compared with the control. As shown in Figure 11, the glucose consumption of the hepatocytes increased significantly with the use of

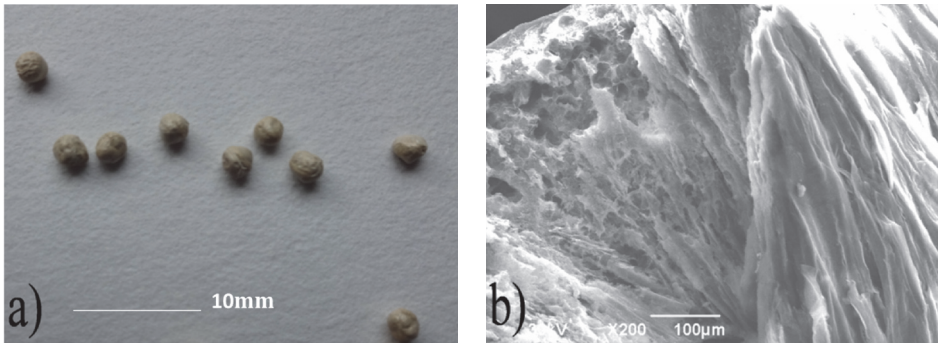

(a) (b)

Figure 5: Morphological observations by stereomicroscopy (a) and SEM (b) of the spherical biocarriers prepared from gingko LCC.

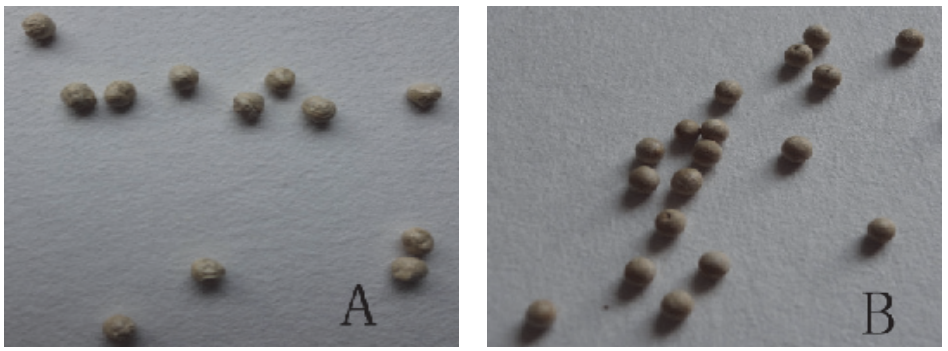

(a) (b)

Figure 6: The morphology of spherical biocarriers before (a) and after 15 days (b) suspended in pH 7.4.

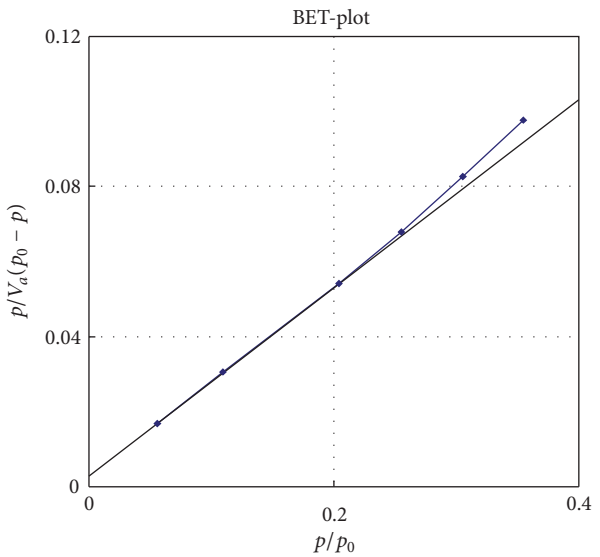

Figure 7: BET adsorption isotherm of the spherical biocarriers.

biocarriers when compared to the control experiment. In the 4th day of cultivation, glucose consumption reached the highest value of 14.0 mmol d^{-1} L^{-1}, while the highest value was 10.1 mmol d^{-1} L^{-1} in the control group. This suggests that the glucose consumption value of sample using biocarriers is enhanced by 38.6% as compared with the control. These results indicated that the biocarriers using ginkgo LCC had biocompatibility with human hepatocytes. The LCC are a promising biomedical polymers that could be used in the tissue engineering of culture hepatocytes to create hepatic organs.

4. Conclusions

(1) The spherical carriers were prepared using lignin-carbohydrate complexes from poplar wood with the liquid nitrogen freeze-drying method. It was found that the carriers were stable in aqueous solution. The specific surface area and average pore size were 17.154 m^2 g^{-1} and 21.59 nm, respectively. The specific surface analysis and SEM results indicated that the spherical carriers prepared from gingko LCC could provide a large cell growth platform.

(2) The FT-IR spectral analysis indicated that the spherical carriers were composed of lignin and polysaccharides. The spherical biocarriers had a typical LCC structure. The chemical analysis indicated that the contents of galactose, lignin, and total sugars were 3.30%, 23.90%, and 64.62%, respectively, giving good

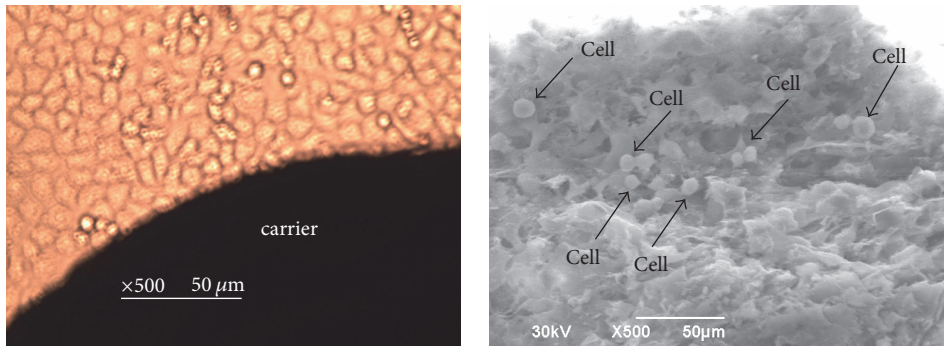

(a) (b)

Figure 8: An inverted microscope image (a) and SEM image (b) of the human hepatocytes L-02 cultured on the spherical biocarriers.

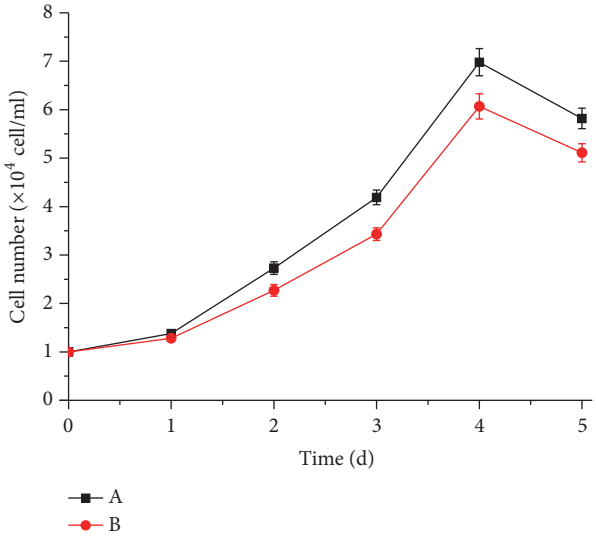

Figure 9: Cell counting of hepatocyte growth on spherical biocarriers (A) and control medium (B).

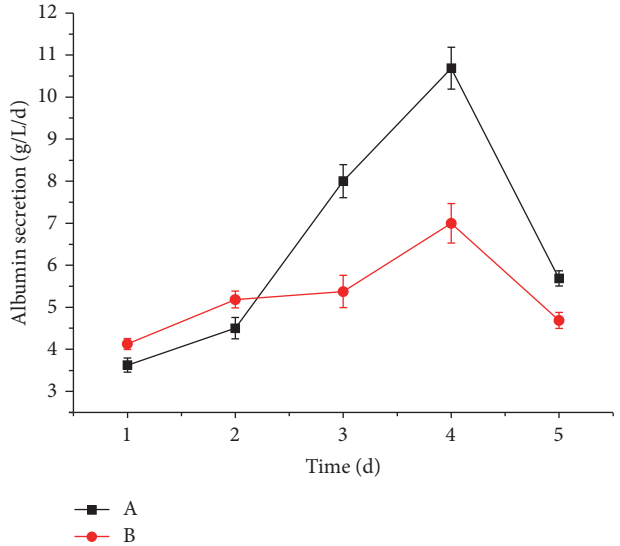

Figure 10: Albumin secretion by human hepatocytes cultured on biocarriers (A) and conventional media (B).

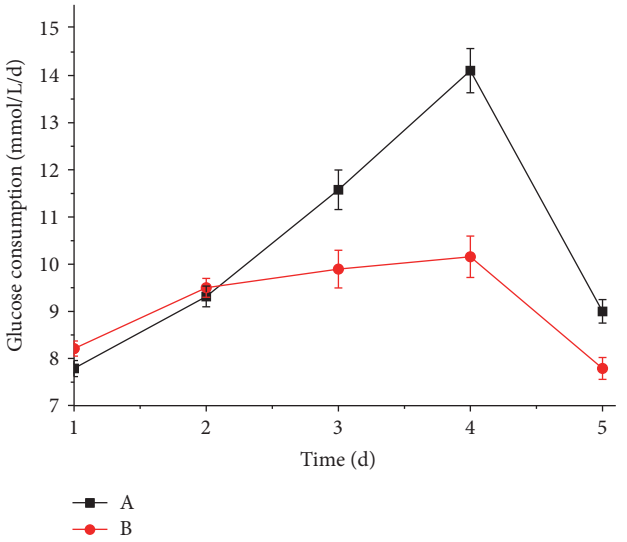

Figure 11: Glucose consumption of human hepatocytes cultured on biocarriers (A) and conventional media (B).

physical strength and compatibility of the biocarriers to hepatocytes.

(3) Cell counting showed that the cells increased faster than those of control group. It was also found that albumin secretion (ALB) value and glucose consumption of the human hepatocytes were enhanced by 51.7% and 38.6%, respectively, when cultivated on the biocarriers. The results indicate that material of ginkgo LCC is very biocompatible and shows promise for use as a biomaterial in the culture of human hepatocytes.

Conflicts of Interest

The authors declare that they have no conflicts of interest in this work.

Acknowledgments

The authors are grateful for the support of the National Natural Science Foundation of China (Grants no. 31370574 and no. 31300494) and Hubei Provincial Key Laboratory of Green Materials for Light Industry (Q20131402). The authors thank Professor Xue-Feng Li for his help in the preparation of the biocarriers.

References

[1] H. Sakagami, T. Kushida, and T. Oizumi, "Distribution of lignin-carbohydrate complex in plant kingdom and its functionality as alternative medicine," *Pharmacology & Therapeutics*, vol. 128, no. 1, pp. 91–105, 2010.

[2] N. G. Lewis and E. Yamamoto, "Lignin: occurrence, biogenesis and biodegradation," *Annual Review of Plant Biology*, vol. 41, no. 1, pp. 455–496, 1990.

[3] J.-I. Azuma and K. Tetsuo, "Lignin-carbohydrate complexes from various sources," *Methods in Enzymology*, vol. 161, no. 1, pp. 12–18, 1988.

[4] R. Singh, S. Singh, K. D. Trimukhe et al., "Lignin-carbohydrate complexes from sugarcane bagasse: preparation, purification, and characterization," *Carbohydrate Polymers*, vol. 62, no. 1, pp. 57–66, 2005.

[5] T.-Q. Yuan, S.-N. Sun, F. Xu, and R.-C. Sun, "Characterization of lignin structures and lignin-carbohydrate complex (LCC) linkages by quantitative 13C and 2D HSQC NMR spectroscopy," *Journal of Agricultural and Food Chemistry*, vol. 59, no. 19, pp. 10604–10614, 2011.

[6] X. Du, M. Pérez-Boada, C. Fernández et al., "Analysis of lignin–carbohydrate and lignin–lignin linkages after hydrolase treatment of xylan–lignin, glucomannan–lignin and glucan–lignin complexes from spruce wood," *Planta*, vol. 239, no. 5, pp. 1079–1090, 2014.

[7] M. H. Sipponen, C. Lapierre, V. Méchin, and S. Baumberger, "Isolation of structurally distinct lignin-carbohydrate fractions from maize stem by sequential alkaline extractions and endoglucanase treatment," *Bioresource Technology*, vol. 133, no. 4, pp. 522–528, 2013.

[8] Y. Xie, S. Yasuda, H. Wu, and H. Liu, "Analysis of the structure of lignin-carbohydrate complexes by the specific 13C tracer method," *Journal of Wood Science*, vol. 46, no. 2, pp. 130–136, 2000.

[9] A. Ghanem and M. L. Shuler, "Characterization of a perfusion reactor utilizing mammalian cells on microcarrier beads," *Biotechnology Progress*, vol. 16, no. 3, pp. 471–479, 2000.

[10] H. Sakagami, K. Hashimoto, F. Suzuki et al., "Molecular requirements of lignin-carbohydrate complexes for expression of unique biological activities," *Phytochemistry*, vol. 66, no. 17, pp. 2108–2120, 2005.

[11] H. Sakagami, M. Kawano, M. M. Thet et al., "Anti-HIV and immunomodulation activities of cacao mass lignin-carbohydrate complex," *In Vivo*, vol. 25, no. 2, pp. 229–236, 2011.

[12] H. Chung and N. R. Washburn, "Chemistry of lignin-based materials," *Green Materials*, vol. 1, no. 3, pp. 137–160, 2012.

[13] J.-B. Lee, C. Yamagishi, K. Hayashi, and T. Hayashi, "Antiviral and immunostimulating effects of lignin-carbohydrate-protein complexes from Pimpinella anisum," *Bioscience, Biotechnology, and Biochemistry*, vol. 75, no. 3, pp. 459–465, 2011.

[14] M. Zahedifar, F. B. Castro, and E. R. Ørskov, "Effect of hydrolytic lignin on formation of protein-lignin complexes and protein degradation by rumen microbes," *Animal Feed Science and Technology*, vol. 95, no. 1-2, pp. 83–92, 2002.

[15] C.-S. Cho, A. Kobayashi, R. Takei, T. Ishihara, A. Maruyama, and T. Akaike, "Receptor-mediated cell modulator delivery to hepatocyte using nanoparticles coated with carbohydrate-carrying polymers," *Biomaterials*, vol. 22, no. 1, pp. 45–51, 2001.

[16] C. S. Seo, S. J. Park, I. K. Kim, S. H. Kim, and T. H. Hoshibac, "Galactose-carrying polymers as extracellular matrices for liver tissue engineering," *Biomaterials*, vol. 27, no. 4, pp. 576–585, 2006.

[17] J. Yang, C.-S. Cho, and T. Akaike, "Galactosylated alginate as a scaffold for hepatocytes entrapment," *Biomaterials*, vol. 23, no. 2, pp. 471–479, 2002.

[18] S. M. Roopan, "An overview of natural renewable bio-polymer lignin towards nano and biotechnological applications," *International Journal of Biological Macromolecules*, vol. 103, no. 1, pp. 508–514, 2017.

[19] T.-T. You, L.-M. Zhang, S.-K. Zhou, and F. Xu, "Structural elucidation of lignin-carbohydrate complex (LCC) preparations and lignin from Arundo donax Linn," *Industrial Crops and Products*, vol. 71, no. 4, pp. 65–74, 2015.

[20] I. Geffen and M. Spiess, "Asialoglycoprotein receptor," *International Review of Cytology*, vol. 137, no. 137b, pp. 181–219, 1993.

[21] S. Erakovic, D. Veljovic, P. N. Diouf, T. Stevanovic, and M. Mitric, "Electrophoretic deposition of biocomposite lignin/hydroxyapatite coatings on titanium," *International Journal of Chemical Reactor Engineering*, vol. 7, no. 1, pp. 113–130, 2009.

[22] H. S. Mansur, A. A. P. Mansur, and S. M. C. M. Bicallho, "Lignin-hydroxyapatite/tricalcium phosphate biocomposites: SEM/EDX and FTIR characterization," *Key Engineering Materials*, vol. 284-286, pp. 745–748, 2005.

[23] M. Mastoby Martinez, B. Andrea Pacheco, and V. Marlene Vargas, "Histological evaluation of the biocompatibility and bioconduction of a hydroxyapatite-lignin compound inserted in rabbits' shinbones," *Revista MVZ Cordoba*, vol. 14, no. 1, pp. 1624–1632, 2009.

[24] T. W. Chung, J. Yang, T. Akaike et al., "Preparation of alginate/galactosylated chitosan scaffold for hepatocyte attachment," *Biomaterials*, vol. 23, no. 14, pp. 2827–2834, 2002.

[25] I.-K. Park, J. Yang, H.-J. Jeong et al., "Galactosylated chitosan as a synthetic extracellular matrix for hepatocytes attachment," *Biomaterials*, vol. 24, no. 13, pp. 2331–2337, 2003.

[26] N. Yang, L. Chen, M.-K. Yang et al., "In vitro study of the interactions of galactosylated thermo-responsive hydrogels with cells," *Carbohydrate Polymers*, vol. 88, no. 2, pp. 509–516, 2012.

[27] J.-Y. Wang, F. Xiao, Y.-P. Zhao, L. Chen, R. Zhang, and G. Guo, "Cell proliferation and thermally induced cell detachment of galactosylated thermo-responsive hydrogels," *Carbohydrate Polymers*, vol. 82, no. 3, pp. 578–584, 2010.

[28] M. H. Sipponen, C. Lapierre, V. Méchin, and S. Baumberger, "Isolation of structurally distinct lignin-carbohydrate fractions from maize stem by sequential alkaline extractions and endoglucanase treatment," *Bioresource Technology*, vol. 133, pp. 522–528, 2013.

[29] R. Chen, S. J. Curran, J. M. Curran, and J. A. Hunt, "The use of poly(l-lactide) and RGD modified microspheres as cell carriers in a flow intermittency bioreactor for tissue engineering cartilage," *Biomaterials*, vol. 27, no. 25, pp. 4453–4460, 2006.

[30] A. Björkman, "Studies on Findy Divided Wood Part 3. Extraction of Lignin-carbohydrate Complexes with Neutral Solvent," *Industrial and Engineering Chemistry Research*, vol. 60, pp. 243–251, 1957.

[31] C. Hansmann, M. Schwanninger, B. Stefke, B. Hinterstoisser, and W. Gindl, "UV-microscopic analysis of acetylated spruce and birch cell walls," *Holzforschung*, vol. 58, no. 5, pp. 483–488, 2004.

[32] J. Yan, Z. Fan, T. Wei, W. Qian, M. Zhang, and F. Wei, "Fast and reversible surface redox reaction of graphene-MnO_2 composites as supercapacitor electrodes," *Carbon*, vol. 48, no. 13, pp. 3825–3833, 2010.

[33] E. Raymundo-Piñero, V. Khomenko, E. Frackowiak, and F. Béguin, "Performance of manganese oxide/CNTs composites as electrode materials for electrochemical capacitors," *Journal of The Electrochemical Society*, vol. 142, no. 1, pp. 325–333, 2007.

[34] J. Chirkova, I. Andersone, I. Irbe, B. Spince, and B. Andersons, "Lignins as agents for bio-protection of wood," *Holzforschung*, vol. 65, no. 4, pp. 497–502, 2011.

[35] N. Wellner, M. Kačuráková, A. Malovíková, R. H. Wilson, and P. S. Belton, "FT-IR study of pectate and pectinate gels formed by divalent cations," *Carbohydrate Research*, vol. 308, no. 1-2, pp. 123–131, 1998.

[36] S.-J. Seo, T. Akaike, Y.-J. Choi, M. Shirakawa, I.-K. Kang, and C.-S. Cho, "Alginate microcapsules prepared with xyloglucan as a synthetic extracellular matrix for hepatocyte attachment," *Biomaterials*, vol. 26, no. 17, pp. 3607–3615, 2005.

[37] K. S. Vasanthan, A. Subramanian, U. M. Krishnan, and S. Sethuraman, "Role of biomaterials, therapeutic molecules and cells for hepatic tissue engineering," *Biotechnology Advances*, vol. 30, no. 3, pp. 742–752, 2012.